2020

Alkaline Pre-treatment of the Air Electrode in a Silicon-air Battery

Author	:	J.J.C. Prins
Date	:	27-08-2020
Student ID	:	4725174
Department	:	PVMD group, TU Delft
Supervisor	:	Dr. R.A.C.M.M. van Swaaij
Master's programme	:	Sustainable Energy Technology
Credits	:	45 EC

PVMD GROUP | TU DELFT
EEMCS FACULTY | MEKELWEG 4 | 2628 CD DELFT | THE NETHERLANDS

(Page intentionally left blank)

Abstract

The objective of this research is to evaluate the effect the air electrode has on the discharge performance of an alkaline silicon-air battery. Experiments are conducted to show that alkaline pre-treatment of the air electrode of up to eight hours leads to an increase in both discharge time and discharge potential of the battery. Furthermore, it is shown that alkaline pre-treatments of sixteen and 24 hours also increase the discharge time and discharge potential of the battery with respect to no pre-treatment. However, the increase in discharge time and discharge potential for these pre-treatments is much smaller than for pre-treatments between three and eight hours. A pre-treatment of 110.75 hours results in a discharge time and discharge potential similar to that of no pre-treatment. In the experiments it is also shown that pre-treating the air electrode with water only, instead of an alkaline solution, has no effect. Finally, the experiments show that discharging the battery at a current higher than 150 μA is not supported. A computer model is then used to evaluate the impact of some qualities of the air electrode on the discharge performance of the silicon-air battery. It is found that the electrical conductivity of the air electrode has very little impact, with a very large increase in electrical conductivity resulting in only a very small increase in discharge potential. The micro-pore surface area in the air electrode has slightly more influence on the discharge performance. Still, a relatively large increase in this parameter only results in an increase of approximately 0.2 V in discharge potential. Both of these parameters are found to have no effect on the discharge time of the battery. To explain the significant increase in both discharge potential and discharge time after alkaline pre-treatment found in the experiments two possible reasons are suggested. Firstly, the adsorption of OH^- ions contributing to the oxygen reduction reaction activity of the air electrode material. Secondly, other atmospheric gases besides oxygen might be suffocating the micro-pores of the air electrode. Increased micro-pore area as a result of alkaline pre-treatment could explain the extended time before the air electrode is fully suffocated.

Acknowledgements

First and foremost, I would like to thank Dr. René van Swaaij for his continuous support throughout this project. His availability and willingness to evaluate and discuss my findings have greatly helped me in designing my experiments and interpreting my results. Additionally, his feedback and critical view on my project allowed me to improve my work as well as my results.

Furthermore, I would like to thank Dr. Rudi Santbergen and Dr. Malte Vogt for helping me develop a computer model to perform simulations when conducting experiments had become unavailable. Their guidance and their knowledge on modelling have helped me to use simulations as a substitute for experimental results, allowing me to continue my research.

Additionally, I would like to thank Dr. Olindo Isabella and Dr. Marnix Wagemaker for taking time out of their busy schedules to be a part of the thesis defence committee.

I would also like to express my thanks to Gregory Pandraud, who guided me through the first period of this project, offering hands-on guidance and help in the lab when setting up experiments. His great experience in the lab allowed me to design and conduct battery experiments for the first time within the PVMD group. Additionally, I would like to thank Martijn Tijssen for designing the battery cell used in my experiments.

Finally, I would like to thank the other members of the silicon-air battery team: Shihao Wang and Nithin Jacob, for collaborating with me and helping me throughout my project.

Table of Contents

List of figures

List of tables

List of appendices

1. Introduction

Climate change can be considered as one of the great challenges of this generation. In order to combat the threat of climate change and global warming, it is generally accepted that a significant reduction in the emission of greenhouse gases such as carbon dioxide (CO_2), methane (CH_4), and other nitrogen or fluorine containing gases is required [1]. To this end, agreements have been made amongst countries over the past decades. Examples of these agreements include the Kyoto protocol in 1997 and more recently the Paris agreement in 2015 [2], [3]. Additionally, many countries have policies in place on a national level to prevent and deal with climate change [4], [5]. One way in which countries try to reduce their greenhouse gas emissions, is by steering electricity production away from carbon containing energy sources such as coal and natural gas and towards renewable energy sources. Perhaps two of the most well-known examples of renewable energy sources for electricity production are solar photovoltaics (PV) and wind. A problem with these energy sources, compared to their carbon containing counterparts, is the intermittent nature of the sun and the wind as an energy source. While some of the trends in solar and wind energy availability will counteract one another between solar and wind, an increasing share of electricity production from intermittent sources will inevitably put significant stress on the electricity grid, endangering the security of supply of countries that start to rely more and more on these sources. Add to this the increasing share of electric vehicles and other electrification, for example in the Netherlands in an effort to reduce the consumption of imported natural gas, and it becomes clear that there is an ever increasing need for means to store electrical energy at times of excess production to be used again at times when demand exceeds supply [6].

One type of technology that can be used to store electrical energy is the electric battery. Batteries typically consist of two half cells that are chemically separated, but electrically connected [7], [8]. Redox half-reactions take place on two electrodes. At the anode, an oxidation reaction takes place, while at the cathode, a reduction reaction takes place. During discharge, negatively charged electrons move from the anode to the cathode via an external circuit, generating an electric current. To compensate for these moving negative charge carriers, positively charged ions move from the anode to the cathode through the electrolyte, or negatively charged ions move from the cathode to the anode through the electrolyte, so that the overall system remains neutral.

A specific type of battery technology are metal-air batteries. The anodes in these batteries are made of metals that are readily available, like iron, aluminium or zinc [9]. At the anode side of the battery, these metals are oxidized, releasing electrons. The electrolyte in metal-air batteries is often potassium hydroxide (KOH) or some other agent that allows for easy hydroxide (OH^-) ion conduction. This electrolyte can be either a liquid or a solid polymer. At the cathode side of the battery, metal-air batteries use oxygen from the air. The cathode is often built up of some carbon structure that allows for good electron conduction.

One of the main reasons for the significant amount of research into metal-air batteries is the fact that they use oxygen from the air at the cathode [10]. This allows for reductions in both costs and weight, as no specific materials are needed in the cathodic reaction. Several different metals have been studied for use in metal-air batteries. Zinc-air batteries are already being used commercially in hearing-aids, while materials like aluminium and magnesium are used in metal-air batteries for military applications [11]. Additional research into the chemical rechargeability of these metal-air batteries is also being conducted extensively [12]–[14].

The use of aluminium in metal-air batteries can result in very high specific energies (amount of energy per unit weight of the battery). Specific energies reported in literature range from 190 Wh/kg up to 500 Wh/kg in 1999 [10]. More recent studies report design specific energies of 1300 Wh/kg, projecting up to 2000 Wh/kg in the future [15]. In comparison, Li-ion batteries will be able to provide between 350 and 450 Wh/kg according to projections [16]. However, the specific power (amount of power per unit weight of the battery) of aluminium-air batteries is unfortunately relatively low [10]. This means that this type of battery is unsuitable for applications where a larger amount of power is needed. Furthermore, problems with the long-term stability have hampered the further development of this type of battery [10]. Another type of metal-air battery that has been investigated in the past uses iron as anode. However, this resulted in low specific energy, as well as low specific power. This type of metal-air battery is therefore no longer receiving any significant amount of research attention [10]. A more promising type of metal-air battery uses zinc [17]–[19]. The open circuit voltage measured in such a cell ranges from 1.42 V to 1.52 V. This results in a specific energy of around 800 Wh/kg. Primary zinc-air batteries are already being used commercially for applications like medical devices and telecommunication. Other materials that could be used in metal-air batteries include lithium, germanium, calcium, magnesium, potassium, sodium, silicon and tin.

Silicon-air batteries are a type of metal-air batteries first proposed and studied in 2009 by Gil Cohn and Yair Ein-Eli at the Technion-Israel Institute of Technology [20]–[25]. The technology was also patented by Ein-Eli in 2011 [26]. Furthermore, the technology has been studied by Zhong et al. in 2012, by Park et al. in 2015 and more recently in 2017 by Durmus et al. [27]–[31]. A short communication by Garamoun et al. from 2014 details the use of amorphous, thin film silicon in flexible, rolled silicon-air batteries [32].

The theoretical specific energy for silicon-air batteries is 8470 Wh/kg, which is somewhat lower than lithium (11140 Wh/kg), but higher than iron (1200 Wh/kg), zinc (1350 Wh/kg) and aluminum (8100 Wh/kg) [30]. Nevertheless, silicon-air batteries have received only limited attention in previous research. Durmus et al. suggest that this might be partly due to the low electrical conductivity of silicon when it is not doped. Besides using silicon in silicon-air batteries, the use of silicon in lithium-ion and lithium-air batteries to reinforce or stabilize the electrode is also being actively investigated [33]–[36].

Silicon-air batteries face two distinct problems, that have to be solved for the technology to become commercially successful. Firstly, silicon-air batteries suffer from severe **corrosion** in alkaline electrolytes like KOH [28], [37]. Solutions suggested for this problem are lowering the concentration of the alkaline electrolyte or using a different electrolyte, like a room temperature ionic liquid (RTIL) [21], [28], [37]. Lowering the concentration of alkaline electrolytes has a slight negative influence on the open circuit potential and operating potential of the battery cell [27], [30]. This decrease in potential is attributed to decreased activity and ionic conductivity of the electrolyte as well as changes in surface reaction kinetics on the silicon anode. Using RTIL as electrolyte has been shown to significantly reduce the corrosion, prolonging the shelf-life of the silicon-air battery practically indefinitely [21]. However, using RTIL introduces new problems regarding chemical safety, in part due to the use of fluoride [27].

Secondly, continuous discharge of silicon-air batteries is limited by the build-up of **passivation** layers [27], [28]. In silicon-air battery cells using RTIL, reaction product builds up on the air cathode, suffocating the active material and blocking further oxygen reduction [20], [38], [39]. This effect is more pronounced when discharging at low current densities, forming finer reaction product particles that settle in the porous active material of the cathode [20]. In silicon-air battery cells using an alkaline electrolyte, a layer of solid silicon-oxide can form on the silicon anode surface [27], [28]. To prevent this from happening, the dissolution rate of reaction products into the electrolyte needs to be equal to or higher than the oxidation rate at which reaction product is being formed. This can be achieved in multiple ways. Continuously refreshing the electrolyte using a refill-type battery cell ensures that the reaction product can easily dissolve into the refreshed electrolyte at all times during operation [30]. Alternatively, texturing of the silicon anode surface allows for a larger effective area at which the reaction product can dissolve into the electrolyte [27], [28]. Thicker nanopores with smaller diameters maximize the effective area, yielding the best results [28]. Additionally, the build-up of a passivation layer can be further reduced by removing the native oxide layer present on the silicon anode prior to usage [28].

Besides texturing the silicon anode or flushing the electrolyte to prevent passivation and changing the concentration of the electrolyte or changing the electrolyte entirely to limit corrosion, this study introduces another way in which the performance of silicon-air batteries can be improved: **pre-treatment of the air cathode**.

In this study, an alkaline silicon air battery is developed and studied. A large electrolyte volume ensures that reaction product can dissolve into the electrolyte at a sufficient rate, even after relatively long discharge times of up to 70 hours at a discharge current density of 150 μA/cm^2. In the developed battery, passivation of the silicon anode is no longer the limiting factor in the initial discharge phase. This allows for the investigation of other factors that might limit the long-term performance of a silicon-air battery without passivation. It is found that pre-treating the air cathode with an alkaline solution before use in a discharge experiment can significantly improve the performance of the battery. Both the discharge potential and the discharge capacity of the battery can be increased by this pre-treatment. Furthermore, it is found that there is an optimal time for this pre-treatment step, where longer pre-treatment deteriorates the performance of the battery.

Several different reasons for the improved performance of the silicon-air battery after pre-treatment of the air cathode are suggested in this study. First of all, the oxygen reduction reaction at the air cathode takes place in so called ‘micro-pores’ in the cathode material [20]. It is noted by Wang et al. that the area/volume of these micro-pores is increased after an alkaline pre-treatment [40]. This increased reaction area allows for a higher rate of oxygen reduction, which is a possible explanation for the improved performance of the battery after alkaline pre-treatment. Furthermore, atmospheric air is used at the cathode. Other atmospheric gases such as nitrogen and carbon-dioxide might also be dissolving into the electrolyte and occupying micro-porous reaction sites. An increased micro-pore area then ensures that sufficient reaction sites are still available for oxygen reduction, even when a portion of the reaction sites are blocked by other molecules. Secondly, Wang et al. also note that alkaline pre-treatment of the air cathode leads to a decreased ohmic resistance of the air cathode [40]. Thirdly, alkaline pre-treatment of the air cathode leads to an increased oxygen reduction reaction rate, as a consequence of adsorbed hydroxide ions in the air cathode.

Since in this situation the performance of the silicon-air battery is limited by the oxygen reduction at the air cathode, the third issue with discharging silicon-air batteries besides **corrosion** and **passivation** is labelled **suffocation** in this study. This suffocation is the main topic of interest in this thesis. The main objective is to evaluate how different qualities of the air electrode influence the discharge performance of a silicon-air battery.

The first two chapters of this report discuss silicon-air batteries in detail. In the first chapter the mechanisms causing corrosion and passivation are investigated and explained. In the second chapter the performance of several different types of silicon-air batteries in previous literature is compared. From there, the experimental setup for the investigation of an alkaline silicon-air battery is described. The most important findings of these experiments are then discussed. In order to gain a better understanding of the results found in the experiments, computer modelling is used. Therefore, in the next chapter, the design of a computer model in COMSOL to model the performance of a silicon-air battery is explained. This computer model attempts to model the performance of the battery based on several processes such as the dissolution of oxygen into the electrolyte at the air cathode and the deposition of reaction product at the silicon anode. The results of the model and the experiments are then compared and differences between the two are explained using theory and previous literature. The report is completed with conclusions as well as recommendations for future research, both in the modelling and the experimental domains.

2. Silicon-air batteries

In this chapter alkaline silicon-air batteries are introduced and their working principles are described in detail. First, the growing interest in silicon for use in metal-air batteries is explained. After that, the discharge process of an alkaline silicon-air battery is explained. Other processes in the battery, like corrosion and passivation are then described and further detailed. These processes and the chemical reactions describing them will form the framework for the next chapters, where the design of the battery cell is detailed. The processes taking place in a silicon-air battery will then be used to justify several decisions made in the design of the battery cell.

2.1 Metal-air batteries

Metal-air batteries are an attractive option for the storage of electrical energy for several reasons. First of all, metal-air batteries only need atmospheric oxygen in their cathodic half-reactions. Secondly, the anode of a metal-air battery typically consists of an abundantly available metal. Other commonly used battery types, like lithium-ion batteries require anode and cathode materials in which the lithium ions are stored before and after discharge of the battery. Metal-air batteries only need the metal at the anode side and atmospheric oxygen at the cathode side. This allows for tremendous reduction in weight and cost for this type of battery, as no materials are needed, other than the materials actively taking part in the reaction. The fact that the metal being used in metal-air batteries is often non-scarce and readily available further contributes to the reduced cost of metal-air batteries compared to other battery types. The weight reduction in metal-air batteries compared to other battery types, allows for high theoretical gravimetric energy densities. Furthermore, the reduced use of materials not taking part in the reaction means that the theoretical volumetric energy density of metal-air batteries can often be many orders of magnitude higher than that of lithium-ion batteries. Figure 1 shows the theoretical energy densities of different materials when used in metal-air batteries, compared to lithium-ion batteries as well as gasoline [31].

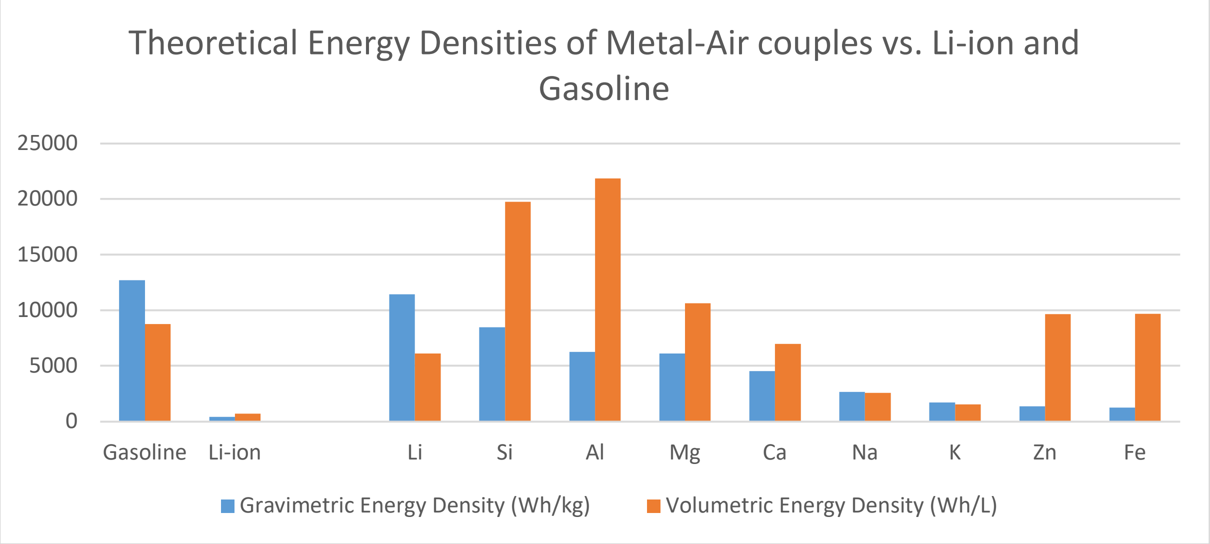

Figure 1: Theoretical gravimetric and volumetric energy densities of different materials when used in metal-air batteries, compared to lithium-ion batteries and gasoline. (Adapted from** [31]**)

From this graph it can be seen that theoretically, silicon-air batteries have one of the highest volumetric energy densities, only exceeded by aluminium-air batteries. Also, the theoretical gravimetric energy density of silicon-air batteries is only exceeded by lithium-air batteries and gasoline.

Using silicon as the anode, as opposed to other materials like lithium, puts less pressure on the environment as silicon is the eight most abundant element in the entire universe, and even the second most abundant element on earth, where it makes up 25.7% of the weight of the crust of the earth [41], [42]. This abundance of silicon is illustrated in Figure 2 [43]. In can be seen that silicon and oxygen are the two most abundant elements on earth. Significantly more abundant than the much scarcer lithium, which is commonly being used in batteries today. Not only is this beneficial for environmental reasons, it might also have economically beneficial consequences in later stages, should the technology reach mass production.

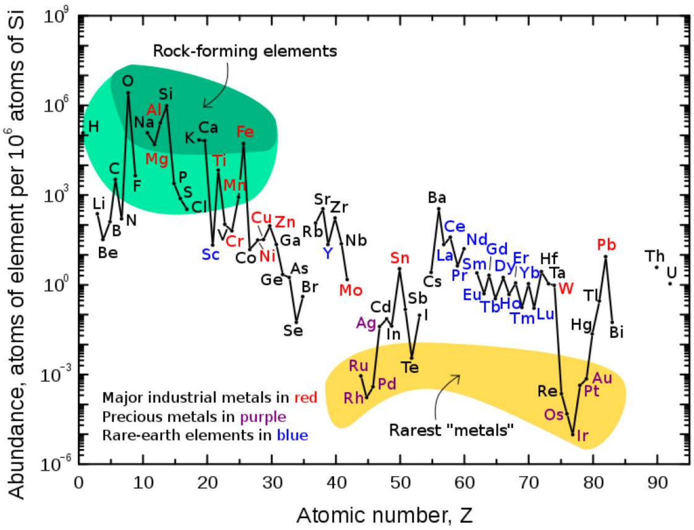

Figure 2: The abundance of elements on earth, relative to Silicon. Silicon is much more abundant than other materials used in batteries, like Lithium. (Image taken from [43]***)***

2.2 Discharge

In a silicon-air battery, silicon is oxidized in the anode half reaction, while oxygen is reduced in the cathode half reaction, during discharge. Depending on the chemical composition of the electrolyte, a positively charged molecule will move through the electrolyte from the anode to the cathode or a negatively charged molecule will move from the cathode to the anode, through the electrolyte, to compensate for the charge of the electrons moving from anode to cathode through the external circuit. In this study, KOH dissolved in water is used as the electrolyte of the silicon-air battery. This decision will be motivated in the next chapter. Figure 3 below graphically shows the working principle of an aqueous, alkaline silicon-air battery during discharge.

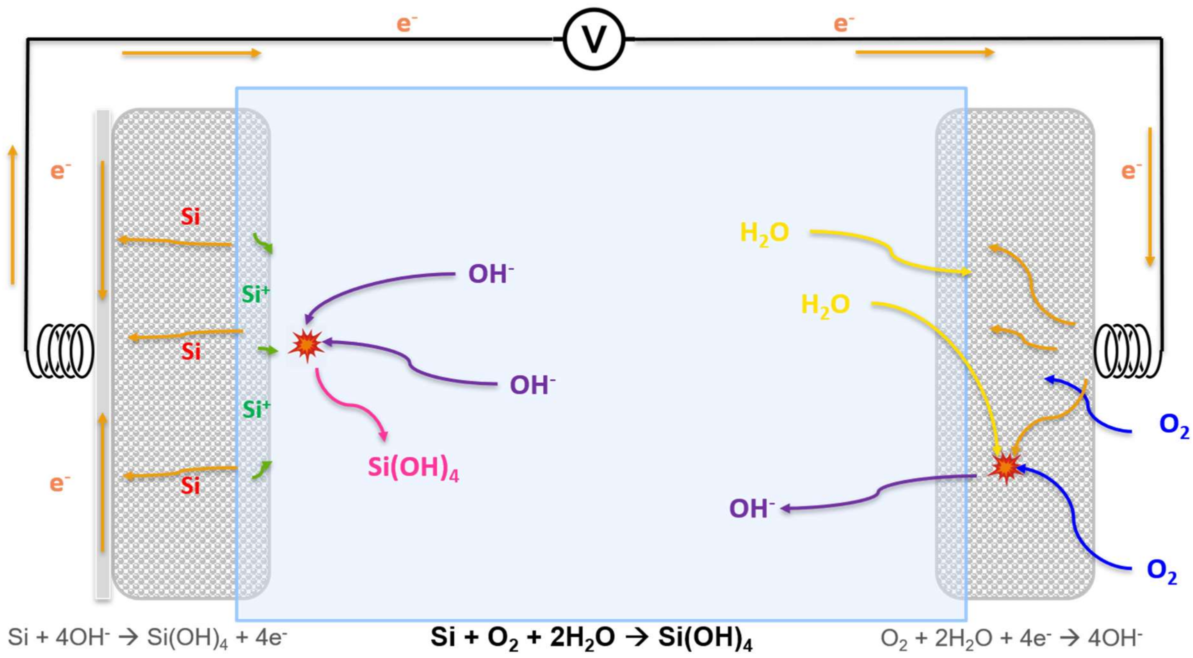

Figure 3: The working principle for an aqueous, alkaline silicon-air battery, with anodic and cathodic half-reactions and net reaction during discharge.

As can be seen in the image, silicon is oxidized at the anode. The electrons are collected in a current collector, while the positively charged silicon reacts with hydroxide from the electrolyte at the surface of the silicon anode. In this reaction, $Si(OH)_4$ or silicic acid is produced. Silicic acid is the main reaction product of the discharge reaction in this type of battery. At the cathode, electrons from the external circuit react with water from the electrolyte and oxygen from the air to form hydroxide. It is important for the performance of the battery that the electrolyte is able to diffuse into the air cathode, and that oxygen is able to dissolve into the electrolyte. In the overall reaction, silicon from the anode is consumed as well as oxygen from the atmospheric air. Furthermore, water is consumed from the electrolyte, to form silicic acid.

The reactions are thus as follows.

Anode: $Si + 4OH^- \rightarrow Si(OH)_4 + 4e^-$ ($E^0 = -1.69$ V) (1)

Cathode: $O_2 + 2H_2O + 4e^- \rightarrow 4OH^-$ ($E^0 = 0.40$ V) (2)

Overall: $Si + O_2 + 2H_2O \rightarrow Si(OH)_4$ ($E^0 = 2.09$ V) (3)

The standard potential of the battery cell is 2.09 V. In practice, this value will be significantly lower, due to different types of overpotential in the cell, such as:

- Electrolyte resistance
- Bubble formation on the surface of the electrodes
- Intrinsic catalytic overpotentials

2.3 Corrosion

Another process that takes place in alkaline silicon-air batteries besides the discharge process, is corrosion of the silicon anode. This process happens in several steps. Firstly, at so called anodic sites, the anodic half reaction takes place the same as it would during discharge. In the corrosion process however, the electrons do not move to the current collector and into the external circuit. Instead, they move to another site at the silicon anode surface [31]. These sites are called cathodic sites. Here, the electrons can react with water from the electrolyte, forming hydroxide and hydrogen gas. At the same time, the silicic acid formed in the anodic reaction, reacts with hydroxide in the bulk of the electrolyte, to form water and $SiO_2(OH)_2^{2-}$.

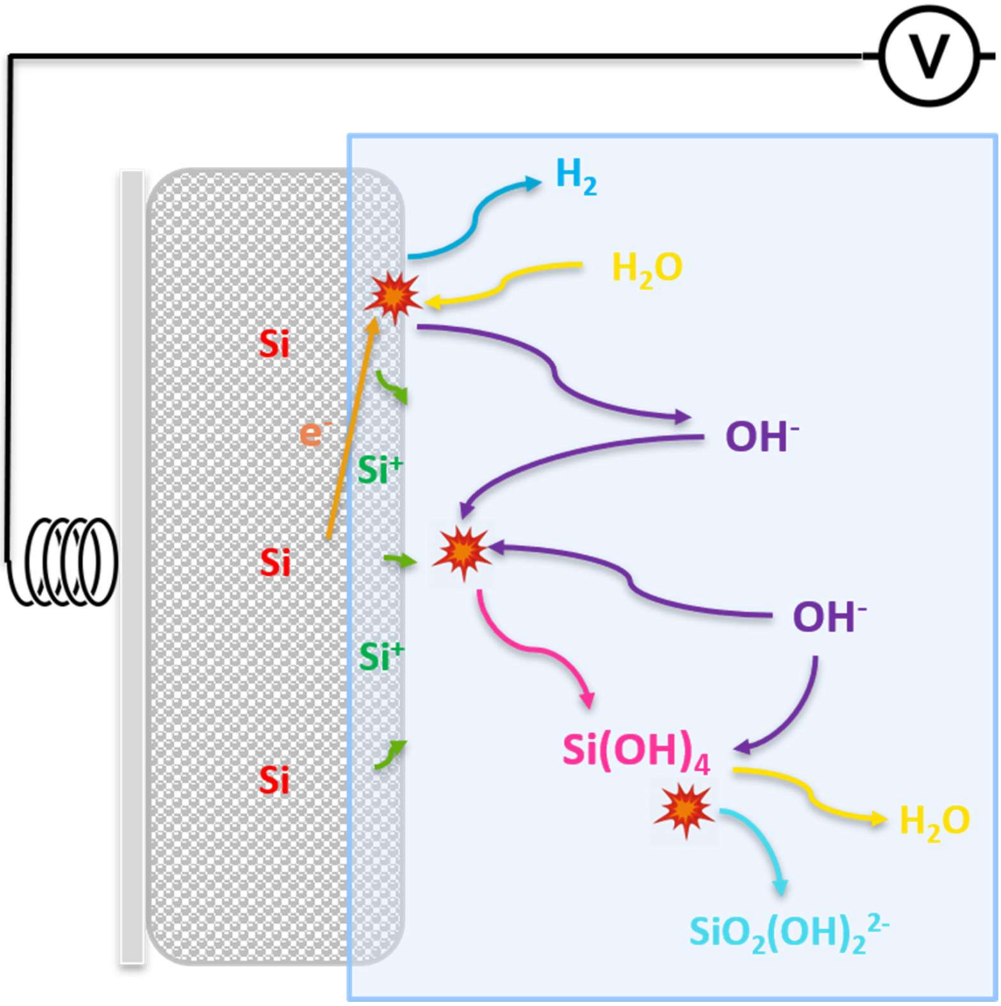

Figure 4: Schematic representation of the corrosion process at the silicon anode in alkaline silicon-air batteries.

The partial corrosion reactions and the overall corrosion reaction in alkaline silicon-air batteries are given below.

Anodic sites: $Si + 4OH^- \rightarrow Si(OH)_4 + 4e^-$ (4)

Cathodic sites: $4H_2O + 4e^- \rightarrow 4OH^- + 2H_2$ (5)

Bulk electrolyte: $Si(OH)_4 + 2OH^- \rightarrow SiO_2(OH)_2^{2-} + 2H_2O$ (6)

Overall corrosion: $Si + 2OH^- + 2H_20 \rightarrow SiO_2(OH)_2^{2-} + 2H_2$ (7)

2.3.1 Electrolyte stability window

The corrosion process and the extent to which it takes place can be explained by the so-called electrolyte stability window. In a battery, charge transfer takes places between the electrode and the electrolyte at the interface between the two [8], [44]. This process is shown in a simplified way in Figure 5. If the energy level of electrons in the electrode is higher than that of the lowest vacant molecular orbital of the electrolyte, this drives electrons from the electrode into that molecular orbital, resulting in a reduction of the electrolyte. Vice versa, if the energy level of electrons in the electrode is lower than that of the highest occupied molecular orbital of the electrolyte, this drives electrons from the electrolyte to the electrode, resulting in an oxidation of the electrolyte.

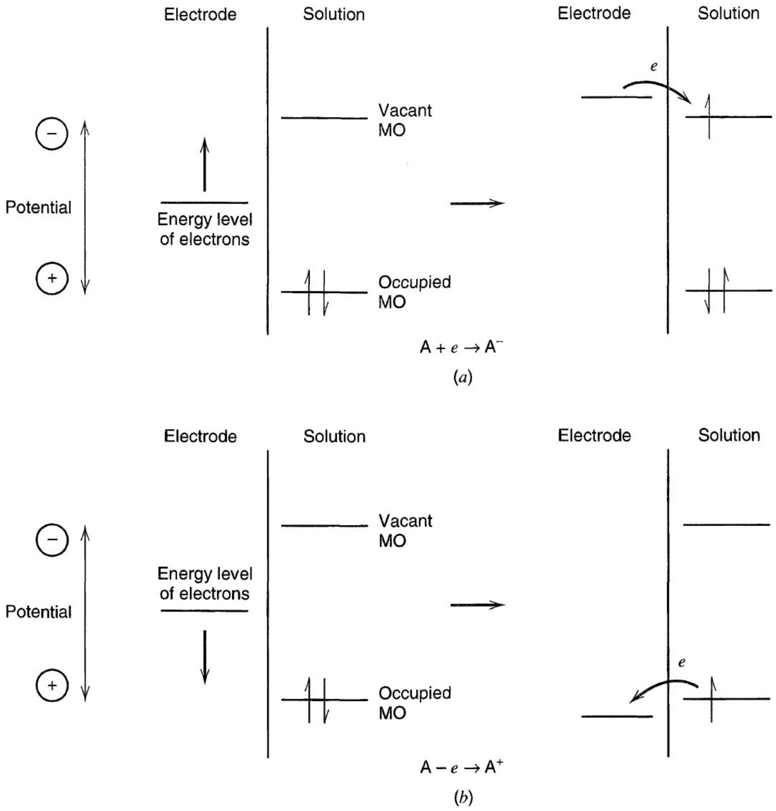

Figure 5: (a) Overview of reduction of a species A in the electrolyte solution by the electrode. By applying a more negative potential to the electrode, the energy level of electrons in the electrode is raised. At a certain point, this energy will be high enough for a transfer of electrons from the electrode to the species A in the electrolyte to be energetically favourable. (b) Overview of oxidation of a species A in the electrolyte solution by the electrode. By applying a more positive potential to the electrode, the energy level of electrons in the electrode is lowered to the point where electron transfer from species A in the electrolyte to the electrode is energetically favourable. (Image taken from** [44]**)

From this illustration, as well as from Figure 6 it can be seen that an anode with an electrochemical potential higher than the lowest unoccupied molecular orbital (LUMO) of the electrolyte will reduce the electrolyte. A cathode with an electrochemical potential lower than the highest occupied molecular orbital (HOMO) of the electrolyte will oxidize the electrolyte. This means that the potential difference between anode and cathode in an electrochemically stable battery cell is constrained by the energy difference between the HOMO and LUMO of the electrolyte. This energy difference between the HOMO and LUMO of the electrolyte species is referred to as the stability window of the electrolyte. If electrons in the electrodes have energy levels lower than the HOMO or higher than the LUMO, it will lead to oxidation or reduction of the electrolyte respectively. This is turns results in an unstable electrolyte.

In the case of an aqueous electrolyte, this means that the potential difference between anode and cathode is constrained by the stability window of water, for an electrochemically stable system. Figure 6 also shows how this stability window can be increased by the formation of a solid/electrolyte-interface (SEI) layer preventing the transfer of electrons between electrode and electrolyte.

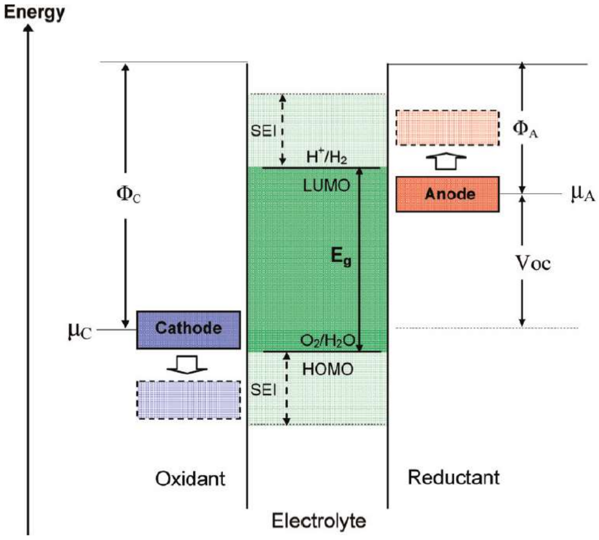

Figure 6: Illustration of energy levels for an electrochemically stable battery cell. (Image taken from** [45]**)

The stability of a species in aqueous electrolyte can be also be illustrated in a Pourbaix diagram [46], [47]. A Pourbaix diagram is a diagram that shows different possible equilibrium phases for species in an aqueous electrochemical system. In a Pourbaix diagram, these phases are shown as a function of the pH value as well as the potential. The lines in the Pourbaix diagram represent the transition from one phase to another. Besides pH value and potential, the different phases also depend on temperature, pressure and concentrations of different species. Pourbaix diagrams are therefore usually shown at room temperature, atmospheric pressure and concentrations of 10^{-6} for all species, as other conditions would yield different phase equilibria.

The Pourbaix diagram for silicon in aqueous electrolytes, as first published by Marcel Pourbaix, is shown in Figure 7. It is important to note that in this Pourbaix diagram, the vertical axis represents the potential, from negative to positive potentials. The energy level of electrons is inversely related to the potential. This means that the energy level of electrons in the Pourbaix diagram ranges from high to low over the vertical axis. In contrast, Figure 5 and Figure 6 show the potential from more positive to more negative over the vertical axis, which means that the energy level of electrons is shown from low energy to high energy in these figures.

In the Pourbaix diagram, dashed lines a and b show the stability window of water. These lines show the energy level of the LUMO and HOMO of water respectively, as a function of pH value. As explained above, a more negative potential means a higher energy level of electrons in a material. If this energy level exceeds the energy level of the LUMO of the electrolyte, this will warrant electron transfer from the electrode material to the

It can be seen that crystalline silicon is located at a more negative potential than the stability window of water in the Pourbaix diagram, meaning that silicon will readily reduce the aqueous electrolyte. In other words, electrons will readily be transferred from the silicon to the water in the electrolyte.

In a battery, any electrons that are lost to the electrolyte instead of transferred through the external circuit add to the loss in efficiency of the battery.

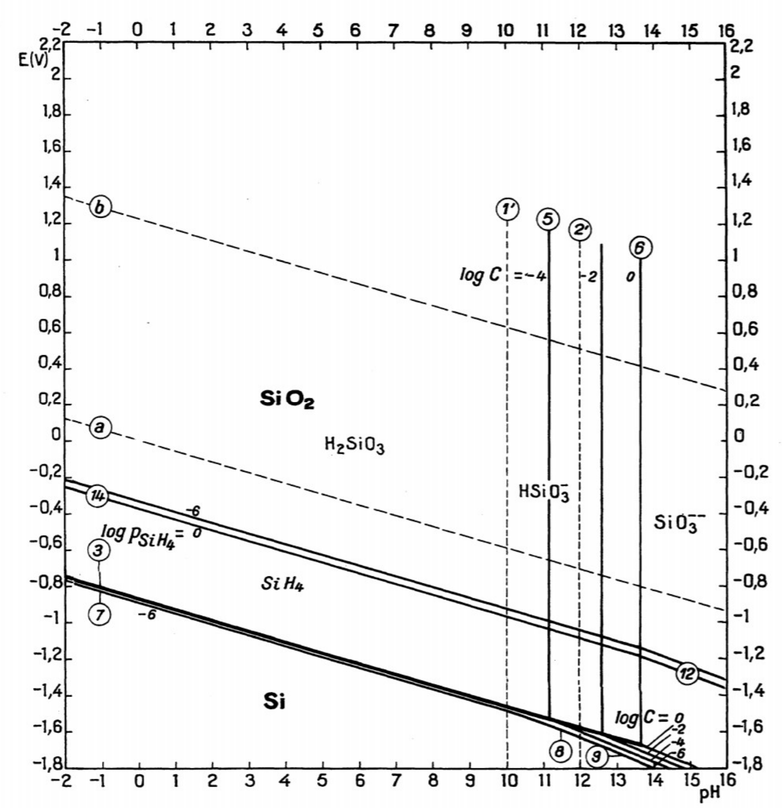

Figure 7: The Pourbaix diagram for silicon in aqueous solution. Dashed lines a and b show the stability window of water. Crystalline Si is well below the stability window, meaning it will readily be oxidized by water. (Image taken from [46]*)*

An adaptation of the Pourbaix diagram for silicon is shown in Figure 8 [48]. In this Pourbaix diagram, the corrosion area and passivation area are shown in red and green respectively. It becomes clear that solid crystalline silicon is unstable in aqueous solution; it will be readily oxidized. Formed SiO_2 is situated within the stability window of water, resulting in the formation of a solid SiO_2 passivation layer on solid crystalline silicon in aqueous solution.

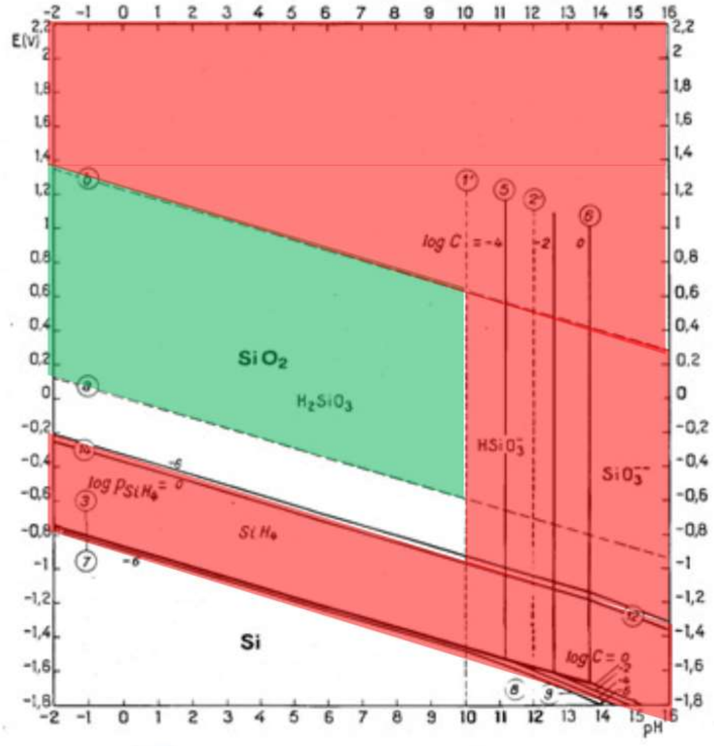

Figure 8: The Pourbaix diagram for silicon in an aqueous solution. The corrosion area is shown in red; the passivation area is shown in green. (Image taken from [48]*)*

From this Pourbaix diagram it can be understood that when using an aqueous electrolyte, an electrode consisting of crystalline silicon will face the problem of corrosion. Furthermore, SiO_2 is the stable reaction product in aqueous solution, meaning that this species has to be dealt with efficiently to reduce or prevent passivation of the silicon anode. Additionally, in order to develop a rechargeable silicon-air battery, silicon has to be recovered from the formed SiO_2. This can be done by reduction of the SiO_2. Reduction of SiO_2 is typically achieved by carbothermal reduction, a process that requires temperatures above 1700 °C [49]. Another option found for the electrochemical reduction of SiO_2 takes place in molten $CaCl_2$ at 850 °C, requiring at least 1.25 V negative potential [50]. For a rechargeable aqueous silicon-air battery, a new way to reduce SiO_2 is needed or the formation of SiO_2 should be prevented.

2.3.2 Energy band diagrams and the effect of doping

With this knowledge, the interaction between the electrolyte and a semiconductor electrode can also be illustrated using energy band diagrams. A typical energy band diagram of an undoped semi-conductor material is shown in Figure 9 (a) [51]. Where E_V indicates the top of the valence band, E_C indicates the bottom of the conduction band and E_G indicates the band gap. The energy level at which the value of the Fermi-Dirac distribution function is equal to ½ is called the Fermi-level, and can be interpreted as the electrochemical potential of electrons in the material.

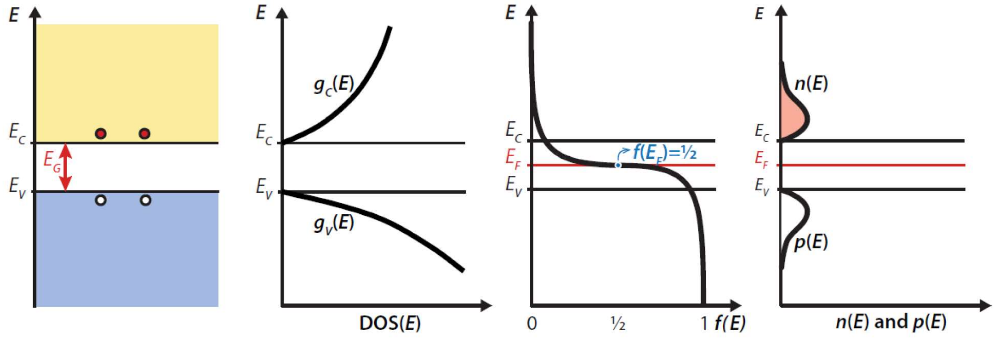

Figure 9: (a) Typical energy band diagram for semiconductor materials like silicon. (b) Energy density of states. (c) Fermi-Dirac distribution. (d) Charge carrier density. (Image taken from** [51]**)

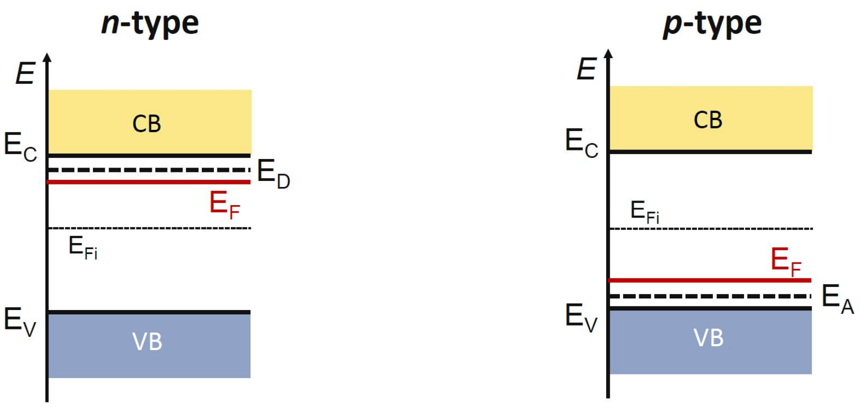

Figure 10: The effect of doping on the Fermi-level in semiconductor materials. N-type doping moves the Fermi-level up, while p-type doping moves the Fermi-level down. (Image taken from** [51]**)

In Figure 10 the effect of doping in semiconductor materials on the Fermi-level is shown. E_D and E_A indicate the energy levels of the donor and acceptor, respectively. E_F indicates the new Fermi-level, as a result of the doping. E_{Fi} indicates the Fermi-level in intrinsic material. N-type doping moves the Fermi-level up, closer to the conduction band, while p-type doping moves the Fermi-level down, closer to the valence band.

Figure 11 shows the density of states for an electrolyte material. D_{red} indicates the occupied states, while D_{ox} indicates the unoccupied states. D_{red} and D_{ox} follow Gaussian distributions around E_{red} and E_{ox} respectively. E_{red} and E_{ox} indicate the energy levels of the reduced and oxidized species of the electrolyte. E_{red} can be interpreted as the willingness or reluctance of the reduced species to donate its electrons. A low E_{red} means the species is more reluctant to donate electrons, while a high E_{red} indicates a higher willingness to donate electrons from the reduced species of the electrolyte. Similarly, E_{ox} can be interpreted as the willingness or reluctance of the oxidized species of the electrolyte to accept electrons. A higher E_{ox} means the oxidized species of the electrolyte is more reluctant to accept electrons, while a lower E_{ox} shows a higher willingness to accept electrons for the oxidized species of the electrolyte. E_{redox} is the mean of E_{ox} and E_{red} and indicates the overall willingness of the electrolyte to donate or accept electrons. E_{redox} is thus an indicator for the electrochemical potential of electrons in the electrolyte and can be seen as the 'Fermi-level' of the electrolyte [52].

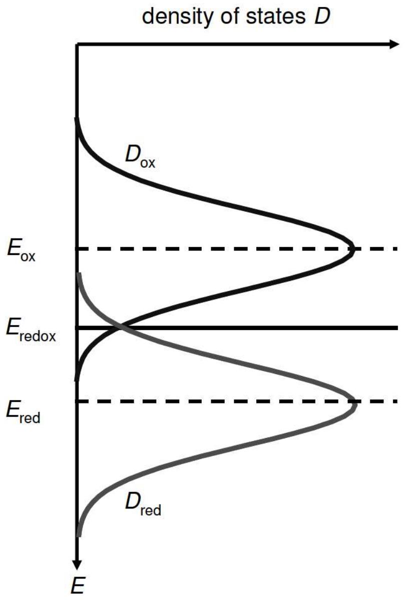

Figure 11: Different energy levels and the density of states D in the electrolyte. D_{red} indicates the occupied states, while D_{ox} indicates the unoccupied states. E_{redox} is the mean of E_{ox} and E_{red} and can be seen as the 'Fermi-level' of the electrolyte.

When the semiconductor material electrode comes into contact with the electrolyte, the Fermi-level of the semiconductor material will become equal to the 'Fermi-level' of the electrolyte at the interface, to achieve thermodynamic equilibrium[53], [54]. The resulting band diagrams are illustrated in Figure 12 and Figure 13, for p-type doped semiconductor material and n-type doped semiconductor material respectively. For the n-type doped semiconductor material in the figure, the Fermi-level of the semiconductor is higher than the redox-level of the electrolyte. For the system to reach equilibrium then requires the transfer of electrons from the semiconductor to the electrolyte. For the p-type doped semiconductor in the figure, the Fermi-level of the semiconductor is lower than the redox-level of the electrolyte. For the system to then reach thermodynamic equilibrium, electrons are transferred from the electrolyte to the p-type doped semiconductor material.

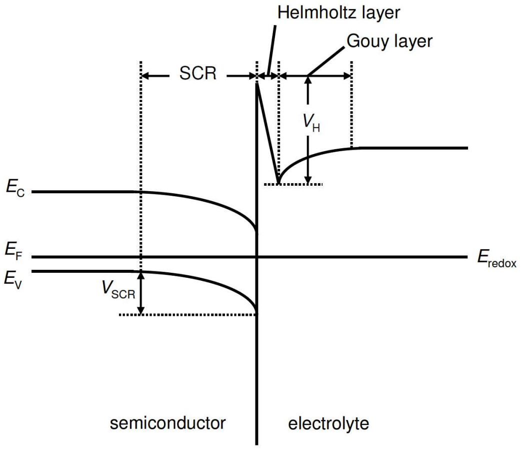

Figure 12: Energy band diagram for a semiconductor-electrolyte interface, with p-type doped silicon. (Image taken from [52]***)***

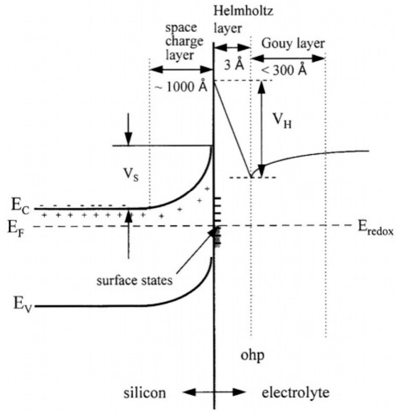

Figure 13: Energy band diagram for a semiconductor-electrolyte interface, with n-type doped silicon. (Image taken from [55]***)***

For silicon in aqueous electrolyte both p-type doped and n-type doped silicon have a Fermi-level higher than the redox-level of the electrolyte. However, due to the doping, the Fermi-level of n-type silicon exceeds the redox-level of the aqueous electrolyte to a larger extent than the p-type silicon. Therefore, electron transfer from the silicon to the electrolyte is more pronounced with n-type silicon, compared to p-type silicon. This electron transfer results in the oxidation of the silicon anode. From this it can thus be expected that n-type silicon is oxidized by the electrolyte in a silicon-air battery more heavily than p-type silicon. This oxidation of the silicon anode is also referred to as the corrosion of the silicon anode. Therefore, it can be expected that increased corrosion of the silicon anode occurs in silicon-air batteries using n-type doped silicon compared to p-type doped silicon. This was also found by Cohn and Ein-Eli [20].

Electron transfer from the electrolyte to the electrode is defined as the anodic current and electron transfer from the electrode to the electrolyte is defined as the cathodic current. Per definition, the current runs in the opposite direction of the electron flow. The anodic and cathodic currents can take place both via the conduction band and the valence band of the semiconductor material [52], [55]. The magnitude of the oxidation and reduction currents depend on the amount of overlap of the semiconductor bands and the bands in the electrolyte, as shown below in Figure 14.

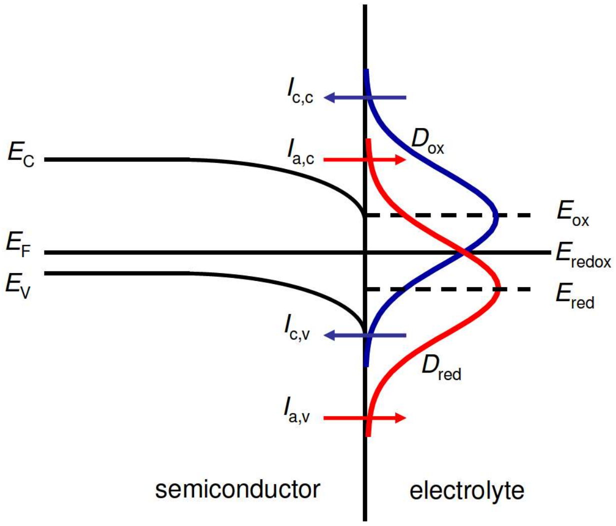

Figure 14: Anodic and cathodic current can take place through the conduction band as well as through the valence band of the semiconductor. The magnitude of the currents is dependent on the overlap of the semiconductor bands and the electrolyte bands.

In Figure 14 $I_{c,c}$ and $I_{c,v}$ represent the conduction band component and valence band component of the cathodic current respectively. As mentioned, the cathodic current is a result of electron transfer from the electrode to the electrolyte. $I_{a,c}$ and $I_{a,v}$ represent the conduction band component and the valence band component of the anodic current respectively. The anodic current results from electron transfer from the electrolyte to the electrode. Electron transfer from the electrolyte to the valence band of the electrode is only possible if there are holes at the surface of the electrode. The surface hole density of a semiconductor is dependent on the doping concentration of the semiconductor [52], [56].

A complete overview of the energy band diagrams of a semiconductor-electrolyte interface for both p-type and n-type semiconductors is also shown in Figure 15 [53].

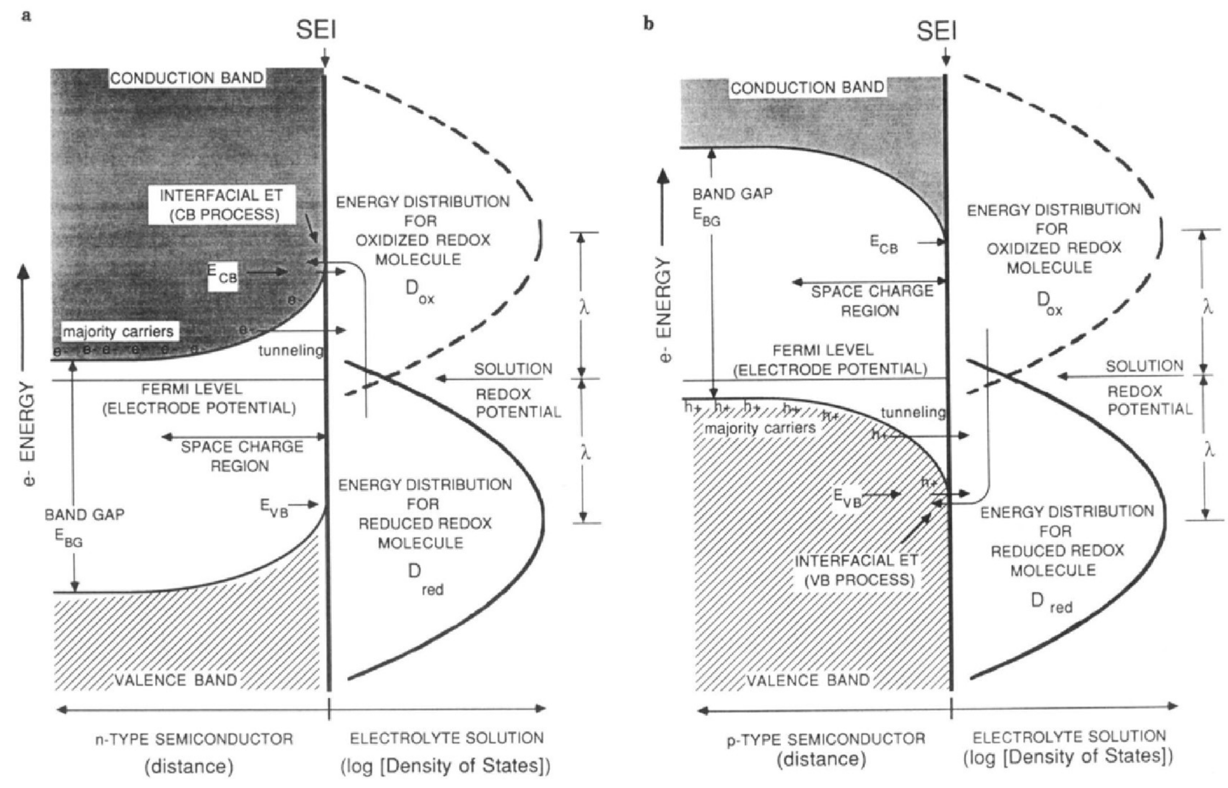

Figure 15: A complete overview of the energy band diagrams of n-type and p-type semiconductors in contact with an electrolyte. (Image taken from [53]***)***

As explained earlier in this section, the Fermi-level of a semiconductor can be interpreted as the electrochemical potential of electrons in the material. In n-type doped semiconductors, electrons have a higher electrochemical potential, compared to p-type doped semiconductors. This higher electrochemical potential of electrons corresponds to a more negative potential. The potential of a battery is determined by the difference between the potentials of the two electrodes. A more negative potential of the semiconductor electrode will increase this difference. Therefore, besides increased corrosion for n-type doped silicon, it can also be expected that using n-type doped silicon results in a higher battery potential [57], [58]. However, it has been found in multiple studies that this is only true for low discharge current densities [20], [58], [59]. At higher discharge current densities using p-type doped silicon results in a similar or higher potential, compared to n-type.

2.4 Passivation

Besides corrosion, the other main problem faced by silicon-air batteries, as identified in previous literature, is called passivation [27], [28]. During discharge, $Si(OH)_4$ is formed as the main reaction product. This compound dissolves into the electrolyte. However, this dissolution can only happen at a certain rate and to a certain extent. Once the rate of dissolution drops below the rate of production, the formed $Si(OH)_4$ splits into SiO_2 and water. SiO_2 is a solid compound which cannot dissolve into the electrolyte. Therefore, it deposits on the surface of the silicon anode. This forms a passivation layer, preventing the discharge reaction from taking place. This process is shown schematically in Figure 16.

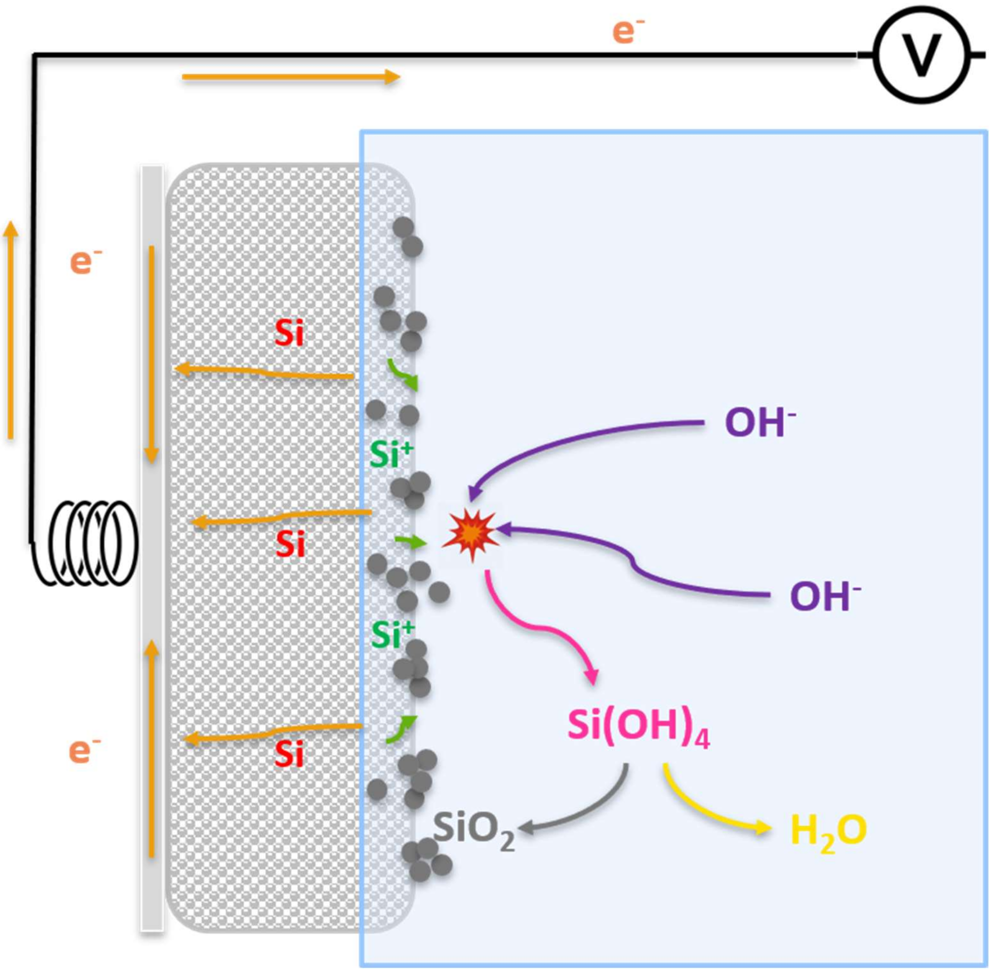

Figure 16: Schematic representation of the passivation process at the silicon anode in alkaline silicon-air batteries.

The passivation reaction is given below.

Passivation: $Si(OH)_4 \rightarrow SiO_2 + 2H_2O$ (8)

The rate at which the reaction product can dissolve into the electrolyte is a very important factor determining the performance of the battery. This dissolution rate is influenced by the concentration of discharge product that has already dissolved into the electrolyte. During discharge at a constant discharge current density, the rate at which reaction product is formed is constant over time. As the concentration of reaction product dissolved into the electrolyte increases, the rate at which new reaction product can dissolve into the electrolyte decreases. At some point the dissolution rate drops below the generation rate. At this point, the formation of a passivation layer will start. This is shown in Figure 17 below.

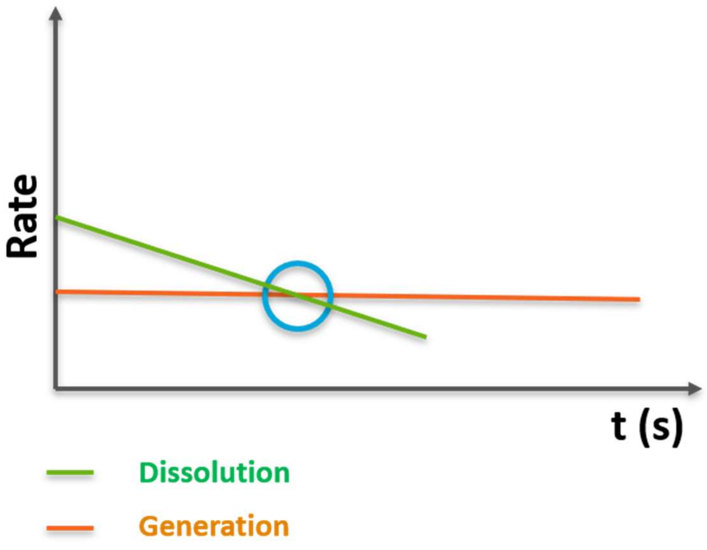

Figure 17: During discharge at a constant discharge current density, the rate at which reaction product is formed is constant over time. As the concentration of reaction product dissolved into the electrolyte increases, the rate at which new reaction product can dissolve into the electrolyte decreases. At some point the dissolution rate drops below the generation rate. At this point, the formation of a passivation layer will start.

From the image it can be inferred that the passivation process can be postponed in two ways; by increasing the overall dissolution rate (i.e. raising the green line) or by lowering the rate at which the dissolution rate decreases over time (i.e. decreasing the slope of the green line). This is illustrated in Figure 18.

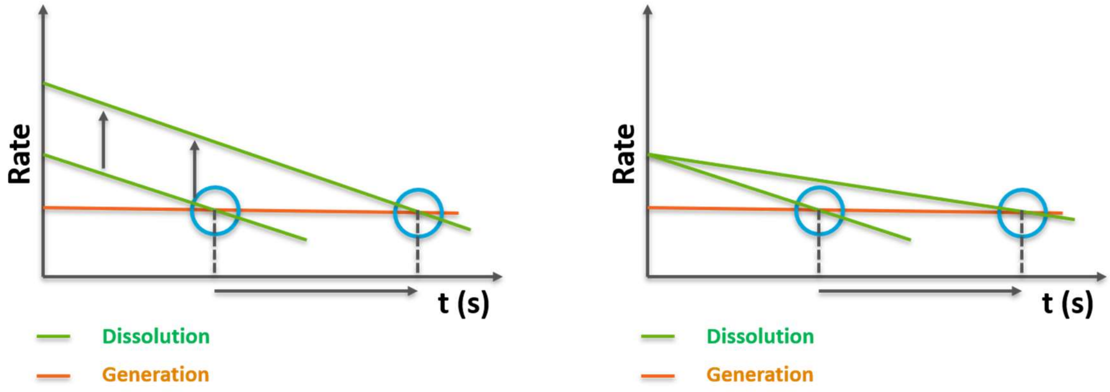

Figure 18: The passivation process can be postponed by raising the overall dissolution rate or by decreasing the slope of the dissolution rate.

One way in which the overall dissolution rate can be raised, is by texturing the silicon anode surface [27], [28]. By doing this, the contact surface area of silicon with the electrolyte is increased, which allows for the reaction product to dissolve more efficiently. Alternatively, decreasing the slope of the dissolution rate change can be achieved by constantly refreshing the electrolyte during discharge [30]. In this way, the concentration of reaction product in the electrolyte is kept to a minimum, which in turn keeps the dissolution rate of the reaction product as high as possible. Both of these approaches have already been investigated and will be discussed in the next chapter.

3. Cell design considerations

From previous literature, it is already known that there is a range of parameters in a silicon-air battery that can be altered to influence the performance of the battery. For the electrolyte, parameters such as the electrolyte salt concentration and the electrolyte volume can significantly affect the battery performance. Furthermore, the dopant type and dopant concentration of the silicon anode are important, as are other design choices, such as silicon crystal orientation and silicon anode texturing. This chapter describes some of the effects that certain design choices have on the performance silicon-air batteries, as described in previous literature. This chapter is only focussed on design choices regarding the electrolyte and silicon anode, as these two components of the battery have already been studied. The effect of design choices and treatment of the air cathode has not yet been extensively studied before and is the main topic of this thesis. These effects will therefore be discussed more comprehensively in later chapters. This chapter finishes with the evaluation of the performance of several silicon-air batteries from previous publications to provide a frame of reference for the results found in the experiments in this thesis work.

3.1 Electrolyte

Silicon exhibits very high self-discharge rates (corrosion) in alkaline electrolytes like KOH [60]–[62]. In an attempt to (partially) solve this persisting problem, the electrolyte used in the study by Cohn and Ein-Eli was hydrophilic 1-ethyl-3-methylimidazolium oligofluorohydrogenate [EMI·(HF)2.3F] room temperature ionic liquid electrolyte [63]. This electrolyte has many favourable qualities, like low flammability and low toxicity. Furthermore, the electrolyte has a wide electrochemical window, high conductivity and high stability, both chemically and thermally. Therefore, the electrolyte has recently also received attention for use in lithium based battery systems [64]–[66].

However, this fluoride-based electrolyte might introduce other problems related to chemical safety, particularly due to the fact that fluoride is used. Zhong et al. have therefore studied a silicon-air battery with an alkaline potassium hydroxide (KOH) electrolyte. The open circuit voltage of the silicon-air battery cell benefits from higher KOH concentration. However, higher KOH concentrations lead to increased corrosion of the silicon anode, and thus to lower specific capacities of the battery cell. This trade-off is addressed in the study by Zhong et al. It is found that at concentrations of 6 M, 2 M, and 0.6 M KOH the open circuit voltages are 1.32±0.01 V, 1.23±0.01 V, and 1.10±0.01 V for 24 h measurements respectively. This relationship between open circuit voltage and KOH concentration in the electrolyte is also shown in Figure 19. The operating voltages found by Zhong et al. at a discharge current of 0.05 mA/cm^2 are 1.01 V, 1.06 V and 1.18 V for 0.6 M, 2 M and 6 M KOH respectively. However, as mentioned above, KOH has a corroding effect on the silicon anode. This effect was also quantified by Zhong et al. The results are shown below in Table 1 below.

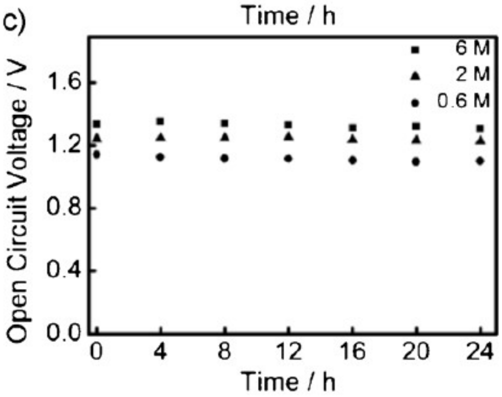

Figure 19: The open circuit voltage of the silicon-air battery at different KOH concentrations in the electrolyte, measured over 24 hours. higher KOH concentrations lead to higher open circuit voltages. (image taken from [27]***).***

Table 1: The specific capacity of the studied silicon anode for different concentrations of KOH in the electrolyte. Higher concentrations of KOH lead to increased corrosion and thus lower specific capacities. (Table taken from [27]***).***

Discharge current density [$mA\,cm^{-2}$]	KOH concentration [M]	Mass of silicon [mg]	Specific capacity [$mA\,h\,g^{-1}$]
0.05	6	2.26	154.8
0.05	2	1.63	214.7
0.05	0.6	0.49	715.7
0.1	0.6	0.58	1206.0

From these findings it is calculated that the corrosion rates at different concentrations KOH are 1.34 µm/h, 0.95 µm/h and 0.24 µm/h for 6 M, 2 M and 0.6 M respectively, at a discharge current of 0.05 mA/cm^2 [55]. From these corrosion rates it can be expected that a 500 µm thick silicon wafer lasts up to 2000 hours at a low KOH concentration. It becomes clear from this study that using KOH as the electrolyte in a silicon-air battery requires careful consideration of the used concentration.

The study by Durmus et al. uses KOH electrolyte as well. In this study, the molarity of KOH is also varied to investigate the effect of different concentrations of KOH on the cell potential as well as on the corrosion of the silicon electrode. Figure 20 the relationship found between the cell potential and the KOH concentration.

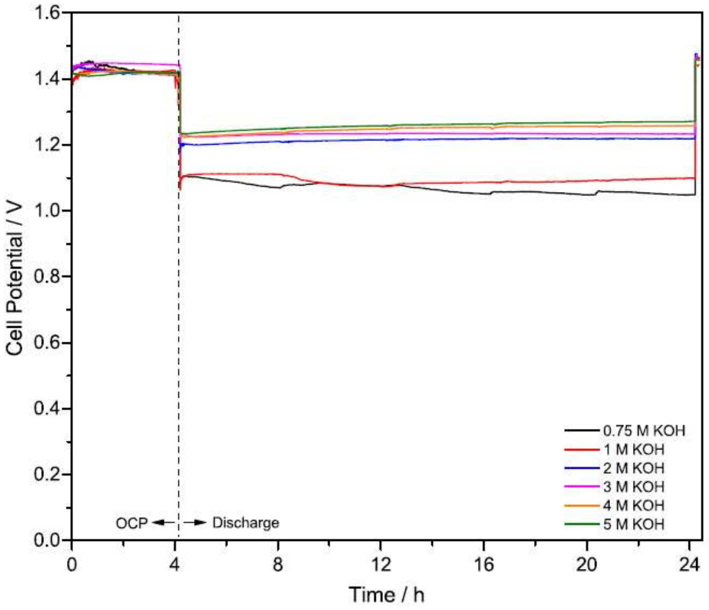

Figure 20: The open circuit potential and discharge potential profiles of a silicon-air battery for different KOH concentrations, discharged at 0.05 mA/cm^2. (Image taken from* [30]*)

The open circuit potential in the study by Durmus et al is found to be around 1.4 V and is not significantly influenced by the KOH concentration. The discharge potentials are found to be around 1.1 V for low concentrations of KOH (up to 1 M), while the discharge potentials for high KOH concentrations (2 M and up) are found to be around 1.2 V for 2 M up to 1.27 V for 5 M. Durmus et al. suggest that this increased discharge potential can be partially attributed to the increased conductivity and activity of the electrolyte at higher KOH concentrations. However, the discharge current used in the experiment by Durmus et al. is relatively low, therefore the change in conductivity of the electrolyte should not result in a 100 mV change in discharge potential. It is suggested that the change in discharge potential can also be partly attributed to surface reaction kinetics on the silicon anode surface. Faster surface reaction kinetics cause lower overpotentials, leading to a higher discharge potential.

3.2 Anode

The technology studied by Cohn and Ein-Eli uses a single-crystal heavily doped n-type silicon wafer as an anode. As can be seen below in Figure 21 the voltage gap between the tested anode and the air cathode at low current densities is biggest for n-type doped silicon. However, at higher current densities, p-type silicon results in a bigger potential difference. Furthermore, the corrosion rate is higher for n-type doped silicon than it is for p-type, as can be seen in Table 2. Nevertheless, heavily n-type doped silicon was selected in the study by Cohn and Ein-Eli, since a high cell potential is deemed essential in optimizing cell performance. The dopant molecule as well as the orientation of the silicon are found to have little impact on the performance.

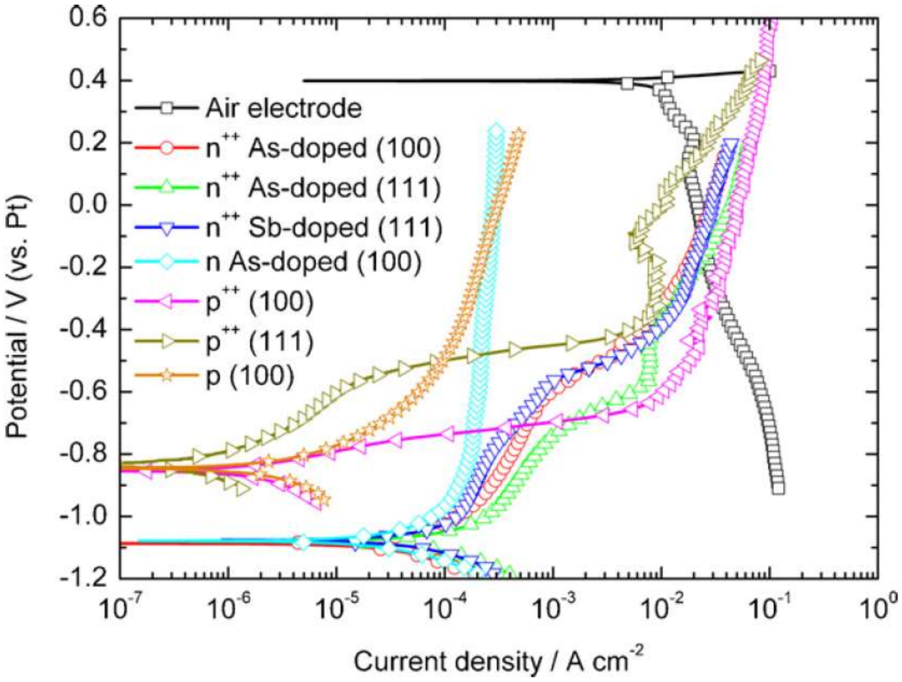

Figure 21: The potential of the different tested electrodes versus the platinum reference electrode at different current densities. The potential gap between anode and air cathode is bigger for n-type doped silicon at low current densities. At higher current densities p-type silicon results in a bigger potential difference. (Image taken from [20]***)***

Table 2: Corrosion rate in the used electrolyte for the different tested silicon anode wafers. N-type doped silicon corrodes faster than p-type doped silicon in hydrophilic 1-ethyl-3-methylimidazolium oligofluorohydrogenate [EMI·(HF)2.3F] room temperature ionic liquid electrolyte. (Table taken from [20]***)***

Silicon type	Corrosion current (μA/cm^2)	Corrosion rate (nm/min)
n 1 0 0 (As)	8.71	0.16
n^{++} 1 0 0 (As)	4.23	0.08
n^{++} 1 1 1 (As)	4.22	0.08
n^{++} 1 1 1 (Sb)	3.71	0.07
p 1 0 0	1.29	0.02
p^{++} 1 0 0	0.54	0.01
p^{++} 1 1 1	0.42	<0.01

++ is designated for heavily doped silicon wafers.

The anode used in the study of Zhong et al. is also made of n-type doped silicon. This study also concludes that a higher dopant concentration in the silicon wafer is beneficial for the performance of the cell. This improved cell performance for highly doped silicon is attributed to the decreased internal resistivity in the silicon wafer as a result of the doping. Figure 22 shows Galvanostatic discharge curves for differently doped, surface modified silicon wafers, at different discharge current densities.

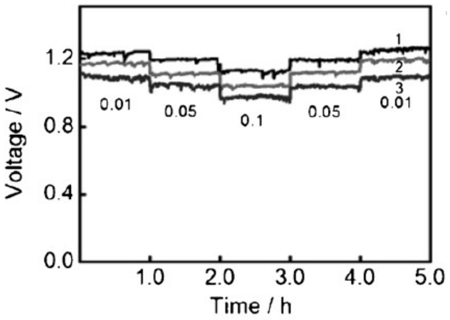

Figure 22: Galvanostatic discharge curves for surface modified silicon wafers with different doping levels. Higher doping levels result in higher discharge potentials. (1) 0.001-0.002 Ω cm (2) 0.008-0.01 Ω cm (3) 0.3-0.8 Ω cm. (Image taken from [27]***)***

The main focus of the study by Zhong et al. is the effect of nano structuring of the silicon anode. Using metal-assisted electroless chemical etching, a layer of microporous nanowire bundles of around 1.5 µm thick are created on top of the silicon surface. This causes a significant increase in the roughness of the silicon surface. The effects of this increased roughness can be seen below in Figure 23. The unmodified wafer can only be discharged for less than 10 minutes, while the modified wafer can be discharged until the silicon is completely used up. Only the first 30 hours of this process are shown in the figure. The discharge potential is also slightly higher for the modified wafer.

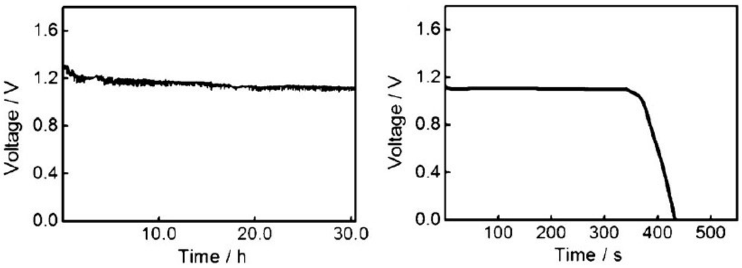

Figure 23: Galvanostatic discharge curves at 0.05 mA/cm^2 for a surface modified silicon wafer on the left versus an unmodified wafer on the right. (Image taken from [27]***)***

It is thus clear that the surface modification in the study by Zhong et al. plays a crucial role in the continuous discharge of the battery cell.

Park et al. use p-type boron-doped silicon as anode material. The silicon is (100) oriented and the internal resistivity is <0.005 Ω cm. The decision for p-type silicon over n-type silicon is not explicitly motivated. Like Zhong et al., the study of Park et al. is focused on the effects of nano structures on the silicon surface to improve the performance of the battery cell. Electrochemical etching was used to realize different surface morphologies, with different pore diameters and thickness. In accordance with the findings of Zhong et al., the electrochemically etched silicon wafer can be discharged for a longer time and at a higher voltage, as shown in Figure 24.

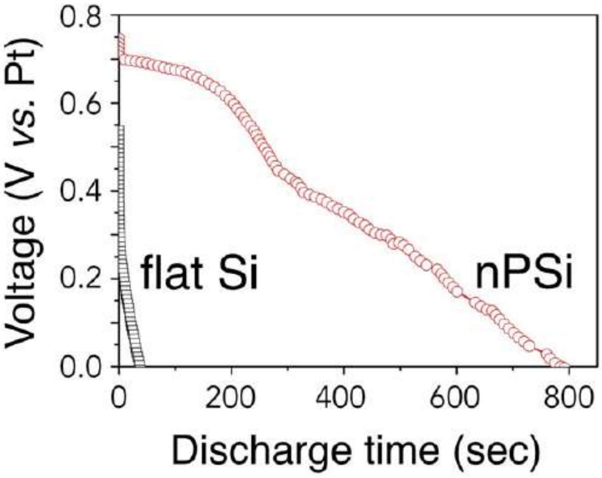

Figure 24: Galvanostatic discharge curves for a flat silicon wafer verses a nano porous silicon (nPSi) wafer at 5µA/cm^2. The nano porous silicon anode can be discharged for a longer time at a higher voltage. (Image taken from [28]***)***

While the effect of different types of doping at different doping levels is not explicitly investigated in the study by Durmus et al., n-type arsenic-doped silicon is again used as the anode. In this study, the limited research interest in undoped silicon as anode material is also explained by the low electronic conductivity of the undoped material. The surface of the silicon wafer used in this study is unmodified. As can be seen in the corrosion reaction above, water from the electrolyte is being used up during the corrosion process. To ensure that the battery can be continuously discharged until the anode material is completely used up, the electrolyte is constantly being refreshed.

The study by Garamoun also uses n-type doped silicon. However, the silicon in this study is amorphous and is compared with silicon carbide as fuel for the battery cell. No surface modification is performed prior to discharging the battery. In this research, it is found that a higher specific capacity can be achieved by using silicon-carbide instead of silicon as fuel for the silicon-air battery.

3.3 Cell performance

In the study by Cohn and Ein-Eli it is concluded that heavily doped n-type silicon has the best performance as anode material. An average working potential of 0.8-1.2 V is found. This voltage decreases slightly over a discharge cycle, due to build-up of reaction products. Most importantly, silicon dioxide (SiO_2) builds up on the air electrode, blocking the further reduction of oxygen at this site. This voltage behaviour can be seen in Figure 25. Due to the use of the novel electrolyte, the shelf life of the battery is very long, while the self-discharge rate is low. Relatively high current densities of up to 0.3 mA/cm^2 can be supported by the studied silicon-air battery.

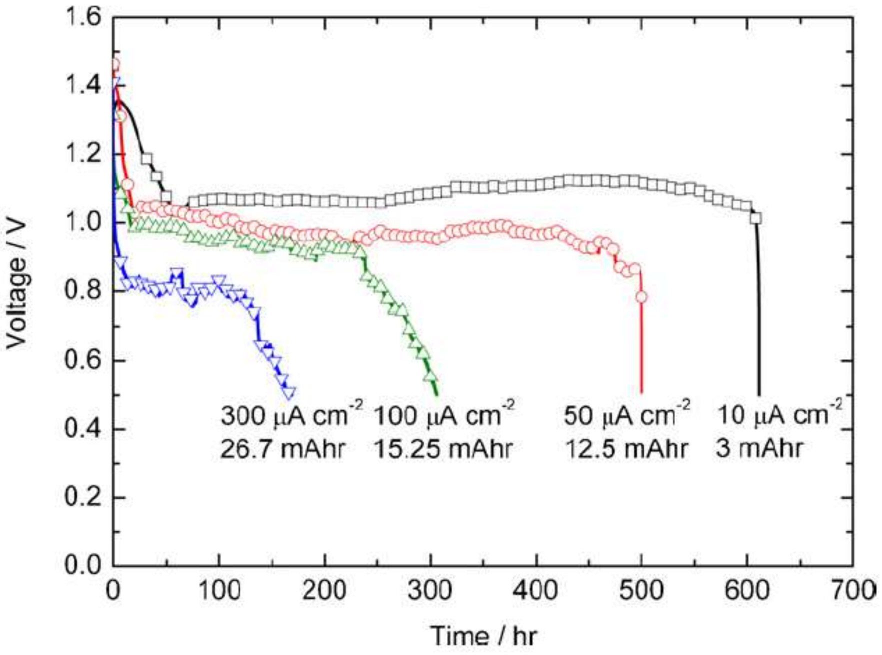

Figure 25: The cell voltage as a function of time when discharging at different constant discharge rates. The working voltage depends on the C-rate, with a higher C-rate resulting in a lower working voltage, most likely due to increased overpotentials. The total capacity also depends on the C-rate, with a higher C-rate resulting in a higher capacity. (Image taken from** [20]**)

Surprisingly, the total capacity of the battery increases at higher discharge rates, indicating that the battery operates more efficiently at higher discharge rates. An explanation for this unique behaviour is offered in the study by Cohn and Ein-Eli. It was found that at the most, no more than ~10% of all the available silicon in the anode was used up, when the battery operation stopped. Since silicon wafers were being used as fuel, it was expected that battery operation would continue until all or most of the silicon fuel was used up. However, it was found that over the course of a discharge cycle, the reaction product (SiO_2) is deposited on the air cathode, blocking further reaction and terminating battery operation. The activated carbon in the air cathode of the battery has a porous structure with pores of different sizes, ranging from 0.7 nm micro-scale pores to >50 nm macro-scale pores. The actual reduction of oxygen takes place in the micro-scale pores, with the fraction and distribution of these micro-pores determining the active surface area of the cathode. As illustrated below in Figure 26, the reaction product can be deposited on the activated carbon in the micro-pores or in the macro-pores depending on the size of the deposited particles. At low discharge current densities, small particles of SiO_2 are being formed, which are deposited on the micro-pores of the activated carbon. This blocks oxygen diffusion, suffocating the cathode and ending battery operation. In contrast, high discharge current densities lead to larger SiO_2 particles being produced. These are deposited on the macro-pores, instead of on the micro-pores. The micro-pores then remain free for longer, allowing oxygen diffusion and continuing the battery operation, until the activated carbon surface area is completely blocked off by the larger SiO_2 particles.

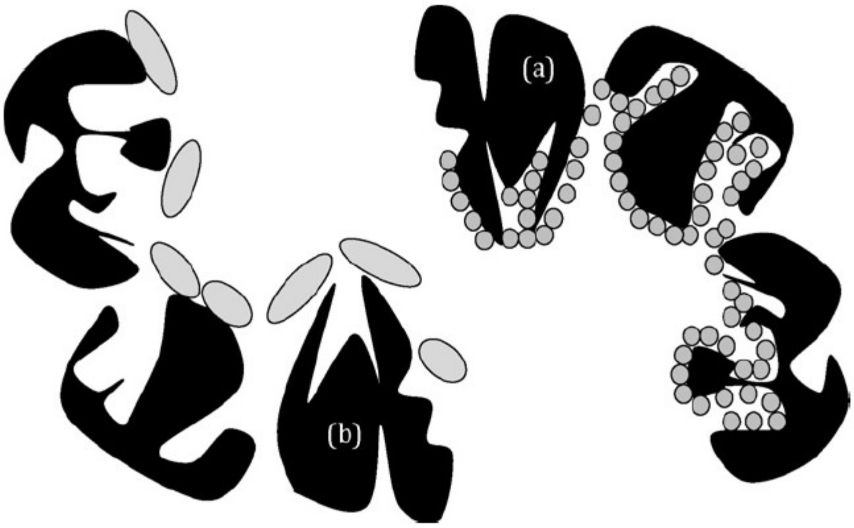

Figure 26: Illustration of SiO_2 reaction product being deposited on the activated carbon in the air cathode. (a) At low discharge current densities, the reaction product is deposited in the micro-pores. (b) At higher discharge current densities, the reaction product is deposited on the macro-pores. (Image taken from [20]***)***

A similar, yet slightly different problem is identified in the other studies, using KOH as electrolyte. As mentioned earlier, according to the passivation reaction, the reaction product ($Si(OH)_4$) can react at the anode surface, forming solid silicon dioxide and water. This solid silicon dioxide can form a layer on the anode surface, blocking further reaction and preventing continuous discharge of the battery. It is therefore crucial for the silicon-air battery operation that the reaction product can dissolve into the electrolyte at rates similar to or higher than the oxidation rate.

In the study by Zhong et al. this problem is addressed, as mentioned before, by creating microporous nano structures on top of the silicon wafer surface. These nano structures can increase the total surface area, in some cases by several orders of magnitude. The KOH electrolyte can easily diffuse into the pores. This increases the overall dissolution rate and enables continuous operation. The oxidation rate found in the study by Zhong et al. is 50-100 nm/h for a smooth planar wafer at a discharge current density of 0.05 mA/cm^2. The dissolution rate for an unmodified silicon wafer is found to be only 1-2 nm/h. This results in a passivation layer that quickly builds up on the anode. The surface modification allowed the dissolution rate to surpass the oxidation (passivation) rate, enabling continuous discharge. In this way, specific capacities up to 1206 mAh/g were realized.

Park et al. adopt a similar approach to ensure that continuous discharge is possible in their silicon-air battery cell. Electrochemical etching is used to create pores of various diameters and thicknesses. The influence of pore diameter and thickness is then evaluated. The results of these experiments are shown below in Figure 27 and Figure 28.

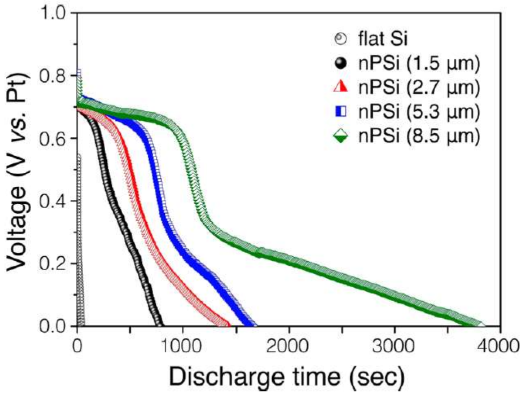

Figure 27: Galvanostatic discharge curves of nano porous silicon wafers with pores of different thicknesses. Higher thickness results in longer discharge time at higher voltage and thus higher capacity. (Image taken from** [28]**)

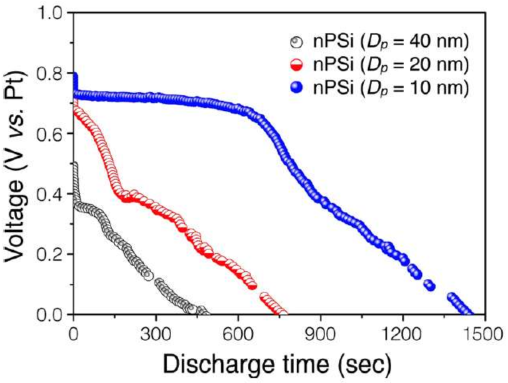

Figure 28: Galvanostatic discharge curve of nano porous silicon wafers with pores of different diameters. Larger diameter results in shorter discharge time at lower voltage and thus lower capacity. (Image taken from** [28]**)

As can be seen in the figures above, thicker pores with smaller diameters lead to increased discharge times, voltages and capacities. It was found that an optimal pore layer had a uniform thickness of 20 µm and pore diameters of 10 nm. This was created by etching the wafer in 15 wt % ethanolic HF for 2 hours. In an attempt to increase the thickness even further, the etching time was extended beyond 2 hours. However, this resulted in severe dissolution of the already formed pore layer.

The optimized anode was discharged at 10 µA/cm^2 as well as at 1 µA/cm^2. The results are shown below in Figure 29. It was found that the anode performs better at lower discharge current density. This is most likely due to higher overpotentials at higher discharge current densities.

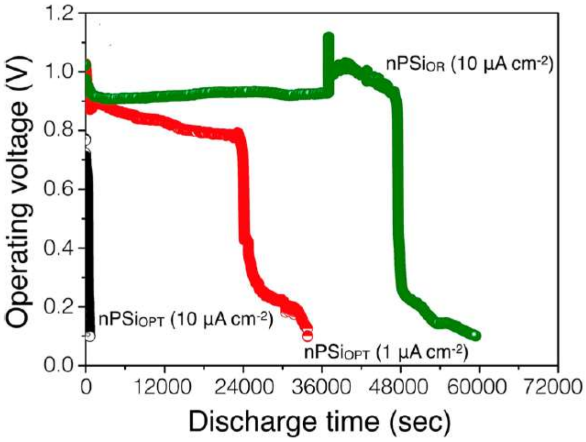

Figure 29: Galvanostatic discharge curves for the optimized anode nPSi$_{OPT}$ at different discharge current densities, in 1.0 M KOH. The anode performs better at lower current densities. The performance of the anode can be further optimized by removing oxygen from the surface (nPSi$_{OR}$). (Image taken from** [28]**)

Furthermore, oxygen at the anode surface is detrimental to the performance of the battery at high current densities as it amplifies the passivation. Therefore, the optimized anode was tested again, after removing oxygen from the surface. This anode of which the oxygen was removed performed well, even at high discharge current densities. It could be discharged at a stable voltage above 0.9 V for over 48 000 seconds.

Durmus et al. deal with the passivation problem in a different way. By continuously refreshing the electrolyte at the anode surface, the reaction product is essentially transported away before it can form a solid layer on the anode. A schematic representation of such a device is shown in Figure 30.

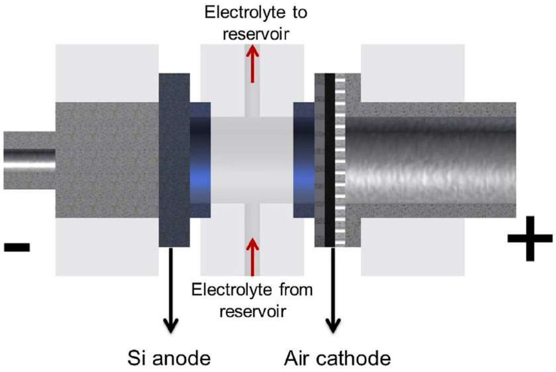

Figure 30: Schematic of a refill-type silicon-air battery cell. (Image taken from [30])

With this cell configuration it was shown by Durmus et al. that continuous discharge is possible for more than 1100 hours, until the entire anode is used up. The results for a 3.0 mm As-doped silicon wafer are shown below in Figure 31.

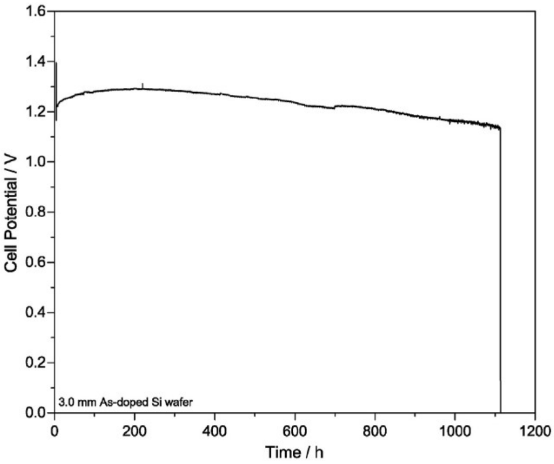

Figure 31: Galvanostatic discharge curve for a refill-type silicon-air battery cell with a 3.0 mm thick As-doped silicon wafer anode at 0.05 mA/cm^2 in 5 M KOH. (Image taken from [30])

In this experiment a specific capacity of 115 mAh/g was found.

Another problem that is identified in the study by Durmus et al. is the fact that water is being used up in the corrosion process, as can also be seen in the corrosion reaction discussed earlier. This problem is also addressed by using the refill-type silicon-air battery cell that Durmus et al use. By constantly refreshing the electrolyte, Durmus et al. prevent the electrolyte from drying out.

Unlike the crystalline silicon anodes used in the other studies, Garamoun et al. focus on amorphous silicon as anode material. The amorphous silicon anode is able to completely dissolve into the electrolyte, without silicon-oxide build-up on the surface. Nevertheless, the technology still suffers from very high corrosion rates. The results of the experiments by Garamoun et al. are summarized in Figure 32 and Table 3.

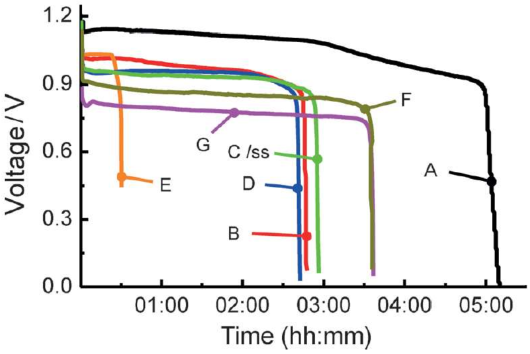

Figure 32: Galvanostatic discharge curves for different configurations of amorphous silicon anode battery cells. (Image taken from* [32]*)

Table 3: Results for different configurations of amorphous silicon anode battery cells. (Table taken from* [32]*)

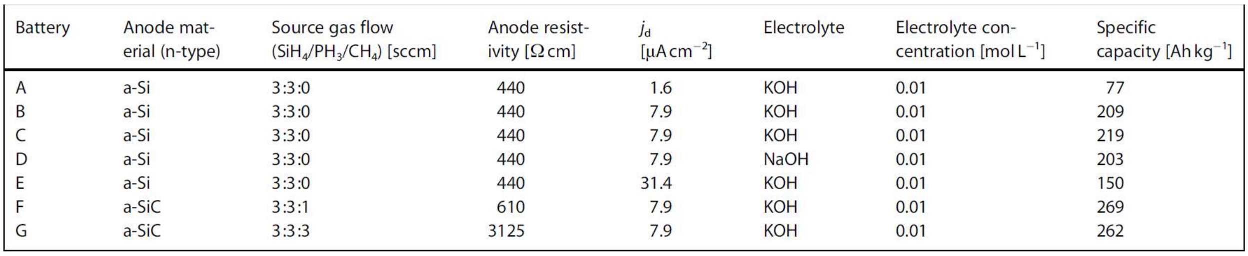

Battery	Anode material (n-type)	Source gas flow (SiH_4/PH_3/CH_4) [sccm]	Anode resistivity [Ω cm]	j_d [μA cm^{-2}]	Electrolyte	Electrolyte concentration [mol L^{-1}]	Specific capacity [Ah kg^{-1}]
A	a-Si	3:3:0	440	1.6	KOH	0.01	77
B	a-Si	3:3:0	440	7.9	KOH	0.01	209
C	a-Si	3:3:0	440	7.9	KOH	0.01	219
D	a-Si	3:3:0	440	7.9	NaOH	0.01	203
E	a-Si	3:3:0	440	31.4	KOH	0.01	150
F	a-SiC	3:3:1	610	7.9	KOH	0.01	269
G	a-SiC	3:3:3	3125	7.9	KOH	0.01	262

The amorphous silicon anodes were grown by plasma enhanced chemical vapour deposition (PECVD) at a temperature of 170 °C. The gases consisted of SiH_4, PH_3 and CH_4. By varying the ratio of these gases, different silicon and silicon carbide compositions were formed. A maximum specific capacity of 269 Ah/kg is achieved with an a-SiC anode, 0.01 M KOH electrolyte and a discharge current density of 7.9 μA/cm^2. The highest specific capacity achieved using silicon is 219 Ah/kg at the same electrolyte concentration and discharge current density.

4. Experimental methods

This chapter describes the experimental approach used to investigate the discharge behaviour of an aqueous, alkaline silicon-air battery. First, the design of the cell itself is shown and described. After that, the used electrolyte, anode and cathode materials are detailed and motivated. Finally, the equipment used for measuring and characterizing are mentioned.

4.1 Cell design

For the experimental investigation of a silicon-air battery, a custom battery cell was designed and manufactured. This battery cell consists of 3 separate parts. Two identical parts function as both sides of the battery cell. These parts hold the electrodes and ensure that these can make contact with the electrolyte on one side, while also allowing for electrical contact to be made on the other side. The opening through which the wire runs to make electrical contact also functions as the oxygen inlet for the air cathode. The middle part of the battery cell holds the electrolyte. An opening in the top of the part allows for it to be filled with electrolyte once the cell has been assembled. The design of the cell is shown schematically in Figure 33. Figure 34 shows the battery cell after it has been assembled.

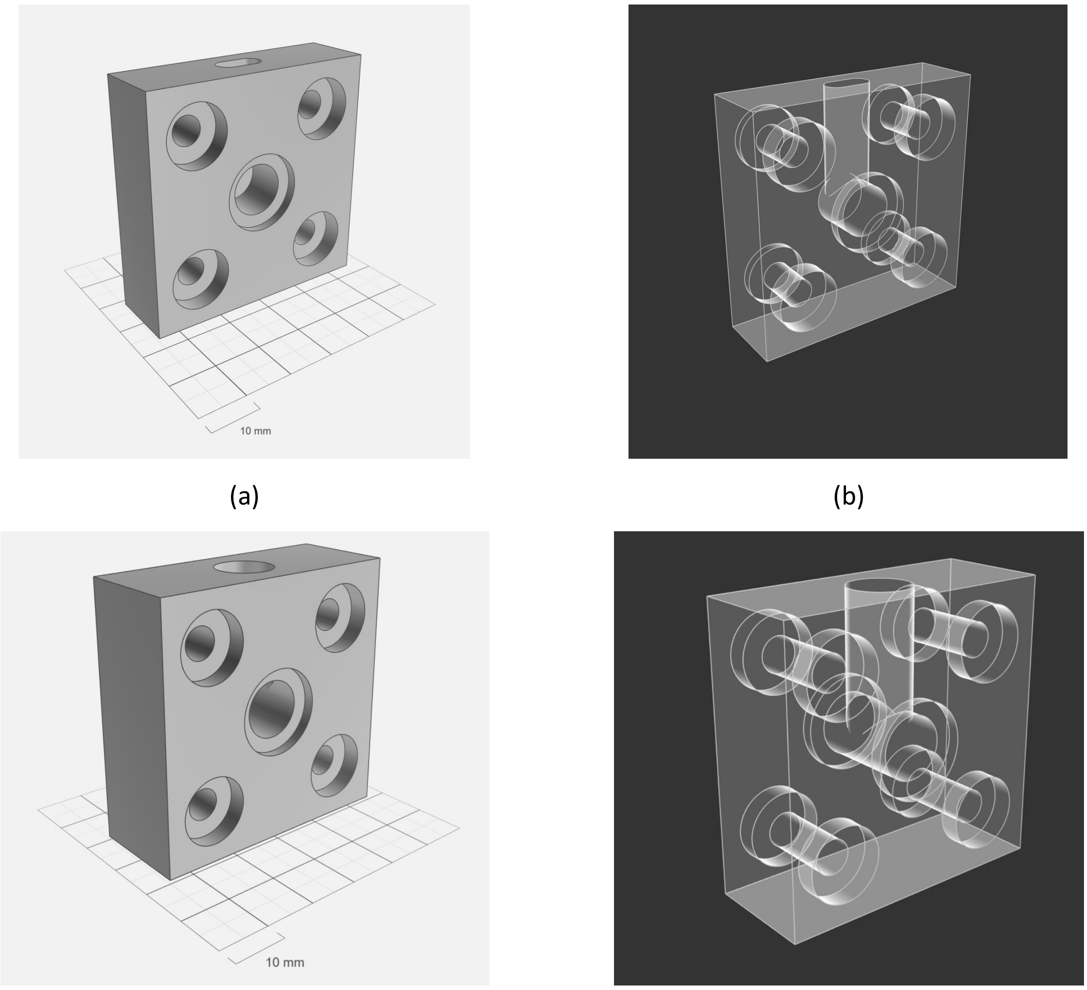

(a) (b)

(c) (d)

Figure 33: (a) Schematic representation of one of the side parts of the battery cell. (b) X-ray representation of one of the side parts of the battery cell. (c) Schematic representation of the middle part of the battery cell. (d) X-ray representation of the middle part of the battery cell.

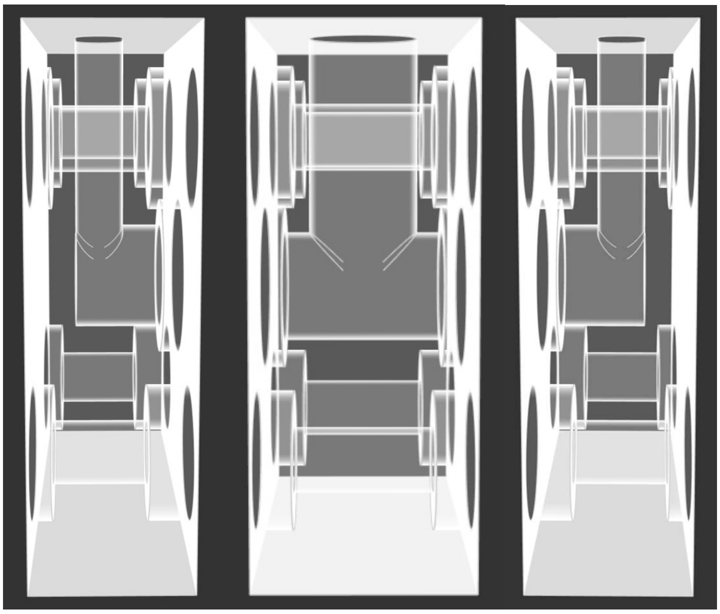

Figure 34: X-ray representation of all three battery parts after assembly of the battery cell. The electrodes are situated between each of the side parts and the middle part.

The three parts are made of polytetrafluoroethylene (PTFE), also known by its brand name Teflon. Both electrodes are lodged and squeezed between one of the outer parts and the middle part. PTFE O-rings are used to ensure a better seal on both sides of each electrode. Nevertheless, throughout the experiments, some minor leakage of the electrolyte could still be observed at the joints between each part. This was observed predominantly at the side of the air cathode. Nylon wires run through the four holes in each of the corners of the battery cell pieces. Nylon nuts are used to hold everything tightly together. Metal springs are used to directly contact each electrode electrically. Copper wires are soldered to the springs for easy electrical access.

The three battery parts are 50 mm by 50 mm in size. The thickness of the middle part is 20mm, which means the distance between the electrodes is also 20 mm. The circular openings on which the electrodes are placed as well as the cross-section of the electrolyte reservoir have a surface of exactly 1 cm^2. This allows for each experiment to test the performance of the battery for an active surface area of 1 cm^2. In this way, the found results can be compared easily with each other as well as with results from other publications.

4.2 Electrolyte

The electrolyte used in this work consists of potassium hydroxide (KOH) dissolved in water. As discussed in the previous chapter, the concentration of this KOH solution can have a very significant impact on the performance of the battery. In general, a more concentrated electrolyte allows for a higher discharge potential, possibly due to increased conductivity of the more concentrated electrolyte amongst other things. The cost of this improved discharge performance is an increase in silicon corrosion. As mentioned above, the length of the reservoir containing the electrolyte is 20 mm. This is larger than other separators typically used in batteries. Therefore, it can be expected the overpotential caused by the limited conductivity of the electrolyte plays a greater role. In order to minimize this effect, a concentrated electrolyte solution is used. The concentration of the KOH solution used is 30%, which corresponds to a molarity of 6.91 M. For consistency between experiments, the electrolyte used is taken from the same batch of KOH solution in each experiment. After each experiment, the used electrolyte is discarded and the battery is filled with a new portion of electrolyte from the same batch of KOH solution.

4.3 Anode

The anode used in this work consists of pure silicon. Like the electrolyte salt concentration, the type of doping of the silicon can impact the performance of the battery, as has been explained and demonstrated in the previous two chapters. N-type doping yields a higher discharge potential at low discharge current densities, while p-type doping results in higher discharge potentials at high discharge current densities. Furthermore, n-type doping is more heavily affected by corrosion than p-type doping. To counteract some of the increased corrosion caused by the high concentration of electrolyte salt, p-type doped silicon is used in these experiments.

4.3.1 Current collector

To further improve the performance of the developed battery, a current collector is used at the silicon anode side. This current collector consists of a 375 nm thick layer of aluminium containing 1% silicon (AlSi). This material is typically used in the production of certain types of solar cells, and was therefore readily available for use in these experiments. The AlSi layer is deposited on the back side of the silicon wafer using a Trikon Sigma 204 sputter coating machine.

4.3.2 Laser cutter

For the sputter coating machine, ten-inch silicon wafers are used. For use in the battery cell, these wafers need to be cut into smaller pieces. A laser cutter is used to etch lines into the wafer, forming squares of two cm by two cm. After this etching, the wafer can be easily broken manually. The two cm by two cm square samples can then be placed in the battery cell, where the PTFE O-rings ensure that exactly 1 cm^2 of silicon is involved in the discharge of the battery. Since in the production of solar cells the surface of the silicon needs to be very pristine and free of defects, the laser cutter is often used to etch lines into the back of the wafer, so as to keep the front free of defects. For use in a battery, the defects at the surface of the silicon are of less importance, especially at the edges of the two cm by two cm squares, since these will be located outside of the O-rings, and thus are not used in the battery. The laser cutter can therefore be used to etch lines either into the back or into the front of the silicon wafer, prior to manual breaking.

4.4 Cathode

The air electrode used in this experiment is a commercially available air cathode produced by ElectricFuel [67]. The electrode consists of activated carbon powder pressed onto a nickel mesh. Manganese oxides are used as a catalyst [68]. The electrode is specifically designed for use in metal-air batteries as well as fuel cells. Figure 35 shows the polarization of the air electrode versus a reference electrode at different current densities.

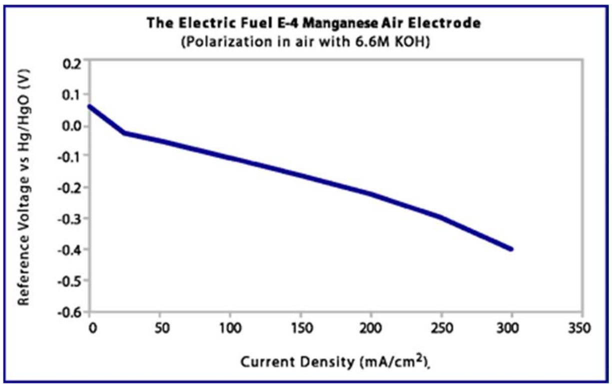

Figure 35: Polarization of the air electrode versus a reference electrode at different current densities, as provided by the manufacturer. (Image taken from [68]***)***

In these experiments, the influence of the air electrode on the discharge performance of the silicon-air battery is the main topic of interest. To investigate this influence, the air electrode is pre-treated by submerging it in KOH solution prior to the discharge tests. For this, the same 30% KOH solution is used that is also used as electrolyte in the battery. The air electrode is placed in the KOH solution for times between 0 and 110.75 hours. The air electrode is taken out of the KOH solution and placed in the battery. The KOH solution that was used for the pre-treatment is discarded. Fresh, unused KOH solution from the same batch is used as electrolyte in the battery.

4.5 Measurement and characterization

4.5.1 Galvanostatic discharge experiments

To test the performance of the developed battery cell, galvanostatic discharge experiments are carried out. In galvanostatic discharge experiments the discharge current density is kept constant and the output potential of the battery cell is evaluated. For this, a galvanostat is used in combination with Metrohm NOVA software from Autolab b.v.. The battery is discharged at discharge currents between 150 and 500 µA. Since the active surface area in the battery is 1 cm^2 in each experiment, this discharge current corresponds to a discharge current density of 150-500 µA/cm^2. In each experiment, the battery is kept at open circuit potential (OCP) for 3600 seconds (1 hour). After that, the specified discharge current is applied and the cell potential is registered every second. A stop condition is implemented that specifies to terminate the process after the measured cell potential is lower than zero for four consecutive measurements.

4.5.2 Scanning electron microscopy (SEM)

In order to visualize the effect of pre-treatment as well as the effects of discharging the battery on the air electrode, SEM images are taken. A Philips XL50 scanning electron microscope is used. The acceleration voltage used in the SEM varies between 2 kV and 15 kV. The spot size used is 2.0. The magnification is varied between 80x and 120 000x. These values are also specified in each SEM image in this report.

5. Experimental results

Using the battery cell described in the previous chapter, the influence of the air electrode on the discharge behaviour of the silicon-air battery is experimentally investigated. For the first set of experiments, the air electrode is pre-treated with KOH solution for different times. In the second experimental setup, the air electrode is pre-treated with water instead of KOH to compare the performance of a KOH pre-treated air electrode with a water pre-treated air electrode. Thirdly, the battery is discharged at several different discharge currents, to investigate the effect of discharge current on the discharge performance. The results of these experiments are presented in order in this chapter.

5.1 Air electrode pre-treatment

In the first set of discharge experiments, the battery cell was discharged at 150 µA, after an OCP period of one hour. These experiments were carried out after different durations of pre-treatment of the air electrode with alkaline solution. The discharge curves for these experiments are shown together below in Figure 36. Each individual discharge curve is also included in Appendix 1 to Appendix 9.

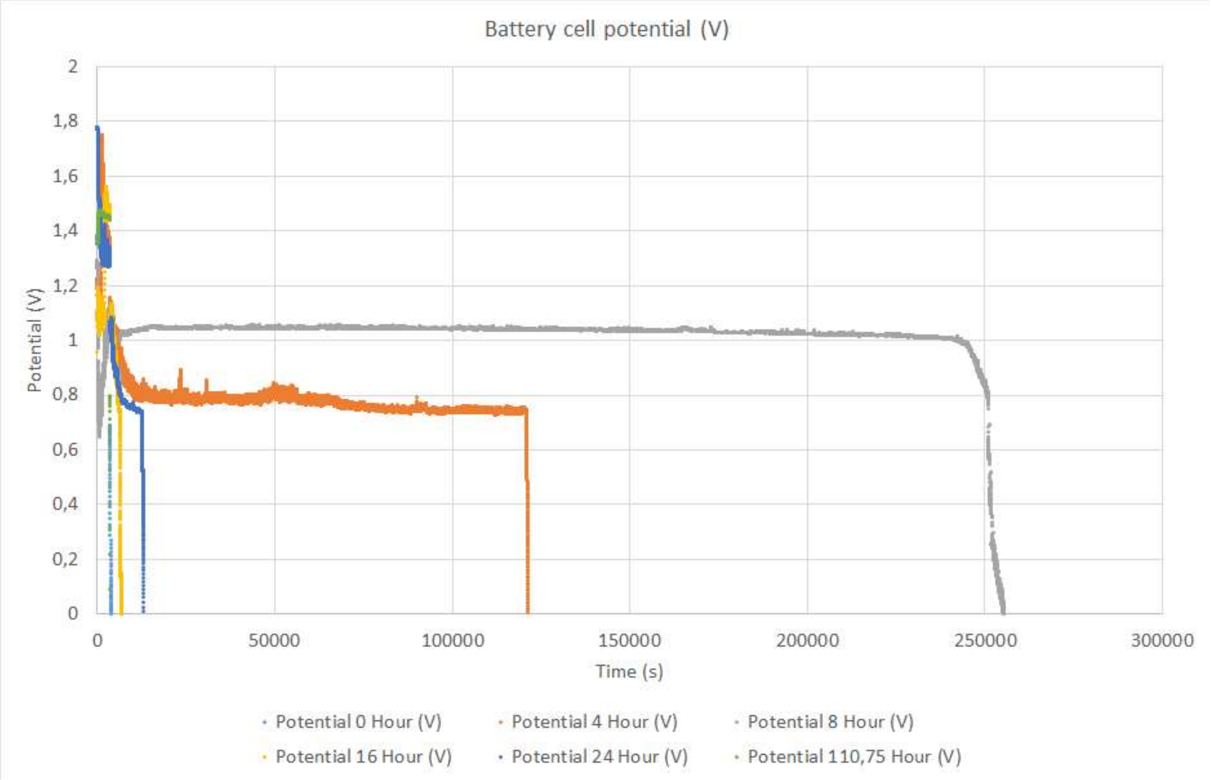

Figure 36: OCP measurements and discharge measurements at a discharge current of 150 µA for different pre-treatment times of the air electrode.

From this overview it can already be seen that both the time the battery can be discharged for and the potential at which the discharge takes place, vary significantly for the different pre-treatment times of the air electrode. To get a clearer view of these differences, the same discharge curves are also plotted without the OCP measurements and on a logarithmic time axis. This is shown in Figure 37.

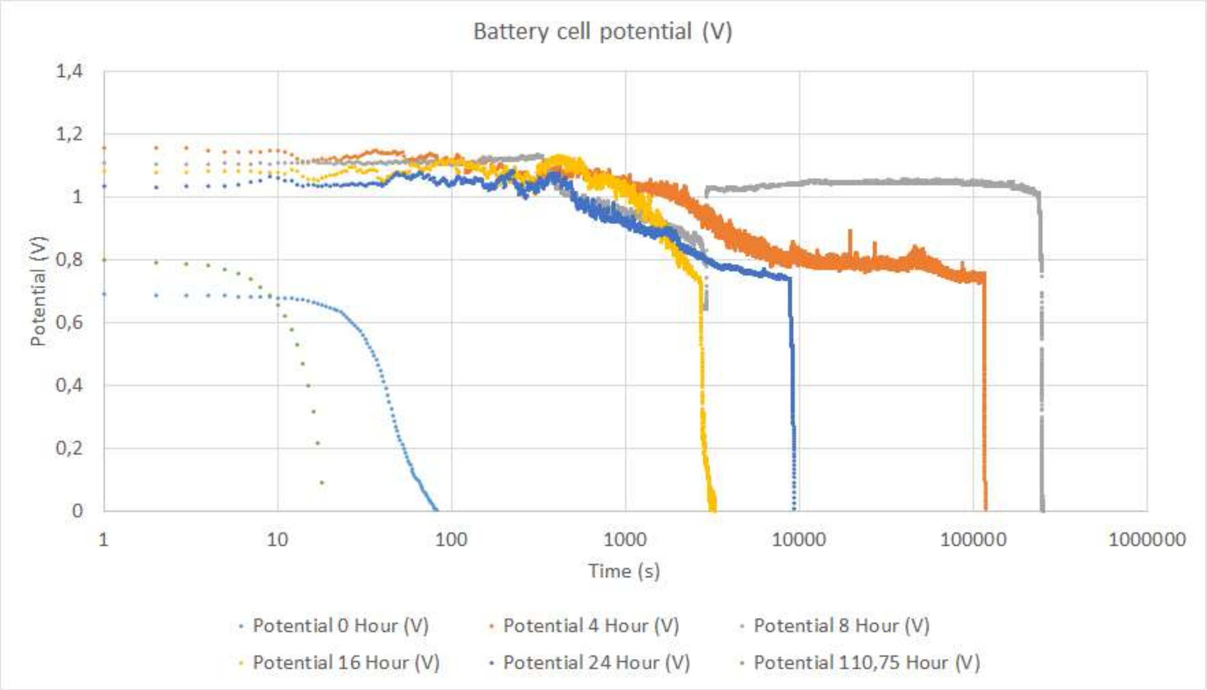

Figure 37: Discharge measurements at a discharge current of 150 µA for different pre-treatment times of the air electrode, plotted on a logarithmic time axis.

In this figure it can be seen that without pre-treatment of the air electrode, as well as for a very long pre-treatment of the air electrode (110.75 hours), the discharge potential starts at around 0.7-0.8 V and drops to 0 V within 100 seconds for both experiments. For pre-treatment times between four and 24 hours the discharge potential starts between 1 and 1.2 V and the discharge lasts between one and 71 hours depending on the pre-treatment time.

The time the battery can be discharged for and the discharge potential are the two most important indicators used in these experiments to measure the performance of the battery. The results of these experiments can therefore be summarized as shown in Figure 38.

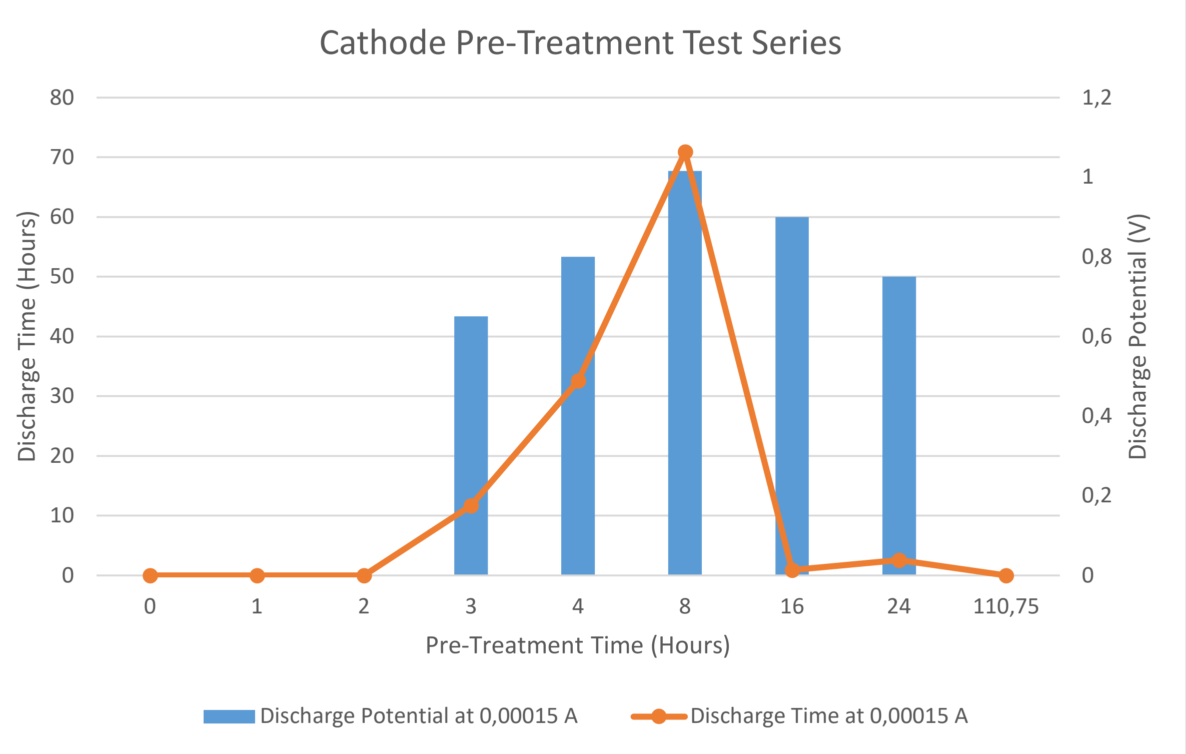

Figure 38: Discharge time and observed discharge potential of the silicon-air battery cell after different durations of pre-treatment of the air electrode.

The left-hand y-axis in this graph shows the discharge time of the battery before reaching a potential of 0 V. In the graph, the results are shown by the orange markers and line. On the right-hand y-axis, the measured discharge potential of the battery cell is shown. These results are represented in the graph by the blue bars. On the x-axis, the different pre-treatment times of the air electrode are shown. Note that the x-axis in this graph is not linear.

It can be seen that for pre-treatment times from zero up to two hours, discharging the battery is (almost) impossible. In these experiments, the potential of the battery cell starts to drop immediately after the OCP period and reaches 0 V within the first 30 seconds of the discharge. Since there is no observable, stable discharge potential, there are no results for the discharge potential for these pre-treatment times in the graph. Starting at three hours of pre-treatment and up to eight hours of pre-treatment, it can be seen that there is a very large increase in discharge time, with the discharge potential seemingly following a similar trend. For pre-treatments longer than 8 hours, the discharge time drops dramatically, with the discharge potential again following a similar trend. For a very long pre-treatment of over 110 hours, the potential drops to 0 V immediately after the OCP period, the same as in the experiments for zero to two hours of pre-treatment. Therefore, no discharge potential is shown in the graph for this experiment.

At a constant discharge current, the discharge time is directly related to the capacity of the battery. The best discharge performance found in this set of experiments lasted 255293 seconds, after eight hours of pre-treatment. This corresponds to a capacity of slightly over 10 mAh. For an area of 1 cm^2, a 500 nm thick silicon wafer and a density of 2,33 g/cm^3, this corresponds to a specific capacity of 9,13 mAh/g. The specific capacities found in each experiment are plotted in Figure 39.

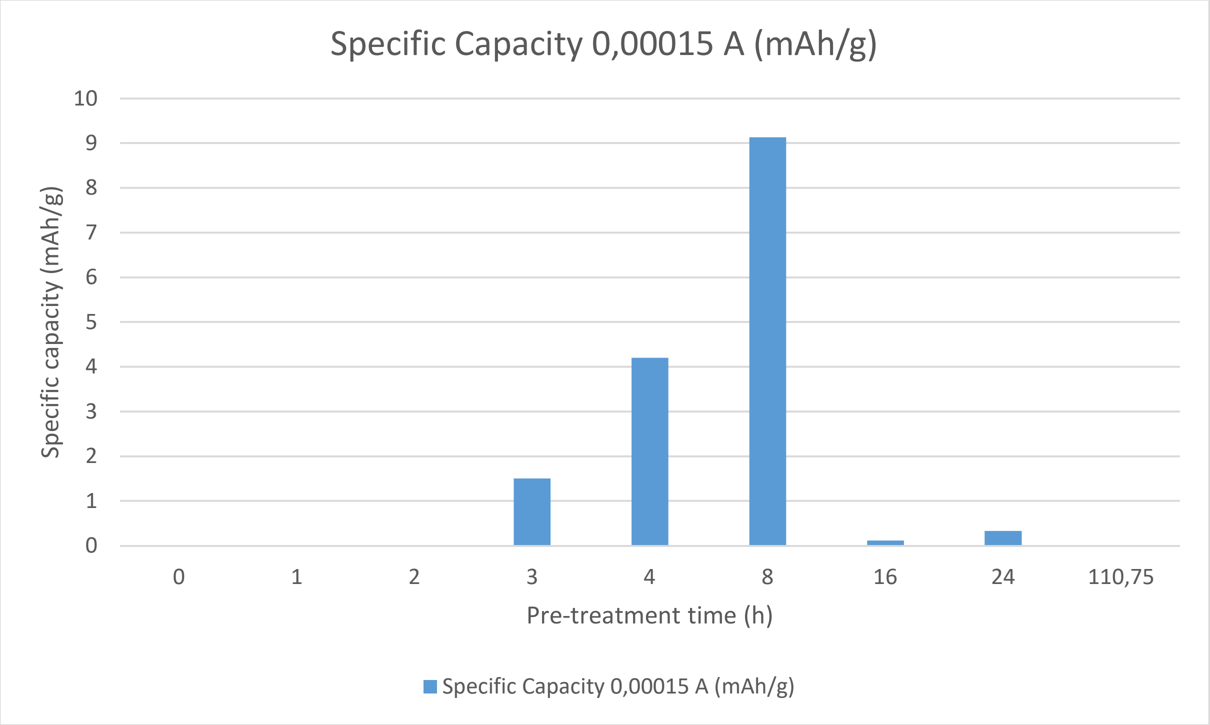

Figure 39: The calculated specific capacities for each discharge experiment.

The specific capacities found in these experiments are orders of magnitude lower than the specific capacities reported in prior literature. In the calculation of the specific capacities for these experiments, the weight of the full 500 nm thick silicon wafer is used. In the experiments, the battery operation is terminated pre-maturely due to other factors than the complete consumption of the silicon anode. This means that in reality, not all of the silicon is being consumed, resulting in low specific capacities.

A different way to approximate the specific capacity of the tested battery, is to calculate the amount of silicon consumed in the discharge process, as well as in the corrosion process. From the applied discharge current, the amount of charge extracted from the silicon can be calculated. The elemental charge of an electron can then be used to calculate the number of electrons extracted from the silicon. Equation 1 in section 2.2 shows that four electrons can be extracted from one silicon atom, which means the number of silicon atoms can be calculated. Using the molar mass of silicon and Avogadro's number, the number of atoms can be translated into a mass of silicon consumed during discharge.

Zhong et al. report an average corrosion rate of 1.34 µm/h for n-type doped silicon in 6 M KOH [27]. While the silicon used in the experiments in this work is p-type doped and the concentration of KOH is 6.91 M, the value found by Zhong et al. still provides a reasonable estimate for the corrosion rate in these experiments. This corrosion rate is used to determine the mass of silicon lost to corrosion in the experiments. The mass of silicon consumed in discharge is added to the mass of silicon lost to corrosion to find the total mass of silicon consumed in the discharge experiments. By multiplying the discharge current with the discharge time, the discharge capacity of the battery is calculated. Dividing this discharge capacity by the total mass of silicon consumed in the experiment, the specific capacity is calculated. The results of these calculations are shown in Table 4.

Table 4: Calculated specific capacity of the battery for different pre-treatment times of the air cathode.

Pre-treatment time (hours)	Discharge time 0.00015 A (seconds)	Si Mass consumed in discharge (gram)	Corroded Si (gram)	Battery capacity (mAh)	Specific capactiy (mAh/g)
0	30	4.15E-10	2.60E-05	1.25E-03	48.04
1	30	4.15E-10	2.60E-05	1.25E-03	48.04
2	30	4.15E-10	2.60E-05	1.25E-03	48.04
3	42000	5.81E-07	3.64E-02	1.75E+00	48.04
4	117400	1.62E-06	1.02E-01	4.89E+00	48.04
8	255293	3.53E-06	2.21E-01	1.06E+01	48.04
16	3295	4.56E-08	2.86E-03	1.37E-01	48.04
24	9306	1.29E-07	8.07E-03	3.88E-01	48.04
110.75	18	2.49E-10	1.56E-05	7.50E-04	48.04

In these calculations it is found that the mass of silicon consumed in corrosion is orders of magnitude larger than the mass of silicon consumed in the discharge process. The mass of silicon consumed in corrosion is directly dependant on the discharge time of the battery. The charge extracted from the battery, and thus the capacity of the battery, is also directly dependant on the discharge time. Therefore, the same specific capacity is found for each of the batteries. The specific capacity found for the battery in this way is 48.04 mAh/g, which is higher than the values shown in Figure 39, yet still significantly lower than the specific capacities found in previous publications.

From these experimental results, it can be expected that there is an optimal pre-treatment time for the air electrode at some point between eight and sixteen hours. However, it is not immediately clear what is causing this improvement in performance.

5.2 KOH vs water

In the previous set of experiments, a solution of KOH in water is used for the pre-treatment. Both the KOH and the water might thus be the reason for the improvement in performance of the battery after pre-treatment of the air electrode. As explained in chapter 2.2, in the cathodic half reaction (which takes place at the air electrode during discharge) water is consumed. Therefore, it seems a reasonable possibility that it takes some time for water from the electrolyte to diffuse fully throughout the air electrode, enabling the discharge half reaction. Pre-treatment would then ensure that water is already present in all parts of the air electrode, fully enabling discharge from the start. To test this hypothesis, the performance of a battery with air electrode pre-treated in KOH solution is compared to that of a battery with air electrode pre-treated in water. The results of these experiments are shown in Figure 40. The individual discharge curves are also shown in Appendix 1, Appendix 5 and Appendix 10 for no pre-treatment, four hours of KOH pre-treatment and four hours of water pre-treatment respectively.

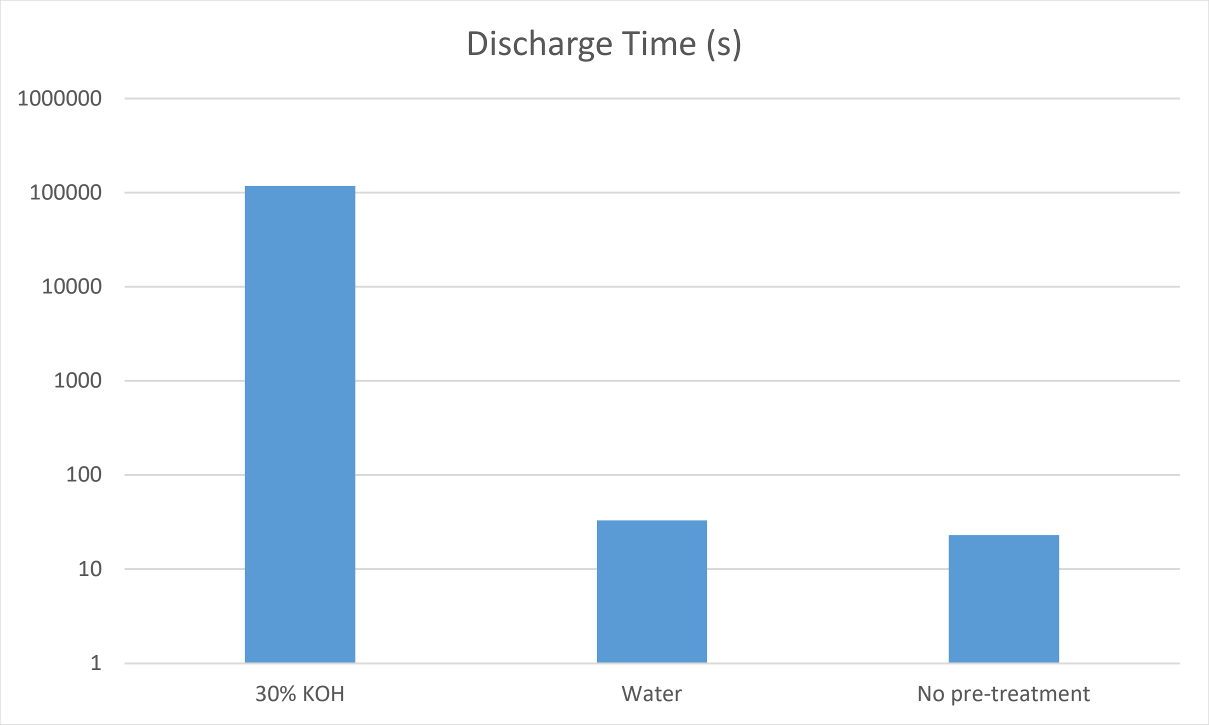

Figure 40: Discharge time at a discharge current of 150 µA after four hours of pre-treatment of the air electrode with KOH, four hours of pre-treatment of the air electrode with water and no pre-treatment of the air electrode.

It should be noted that the y-axis in this figure is plotted logarithmically in order to fit the large differences in a single figure. It can be seen that the battery could be discharged for more than 100 000 seconds after four hours of pre-treatment using a KOH solution. After four hours of pre-treatment using only water, the battery performs similarly to a battery with an air electrode that has not been pre-treated whatsoever. Water diffusing into the air electrode is therefore excluded as a possible cause for the differences in performance for different pre-treatment times.

5.3 Discharge current

As explained earlier, the air electrode being the limiting factor during the discharge of the silicon-air battery was also identified by Cohn and Ein-Eli in their study of a non-aqueous silicon-air battery [20]. In this study, a silicon-air battery using hydrophilic 1-ethyl-3-methylimidazolium oligofluorohydrogenate [EMI·(HF)2.3F] room temperature ionic liquid electrolyte was studied. It was found that battery operation was terminated early due to the deposition of reaction product in the micro-pores of the air electrode. At higher discharge currents, the reaction product formed in larger clusters, depositing on the macro-pores of the air electrode, but leaving the micro-pores available for reactions. This caused the battery to perform better at higher discharge currents. To investigate if a similar phenomenon might be at work in the alkaline silicon-air battery used in this study, higher discharge currents were used after pre-treating the air electrode for four hours in KOH solution. The results of these experiments are shown in Figure 41. The individual discharge curves are also shown in Appendix 5 and Appendix 11, Appendix 12 and Appendix 13 respectively.

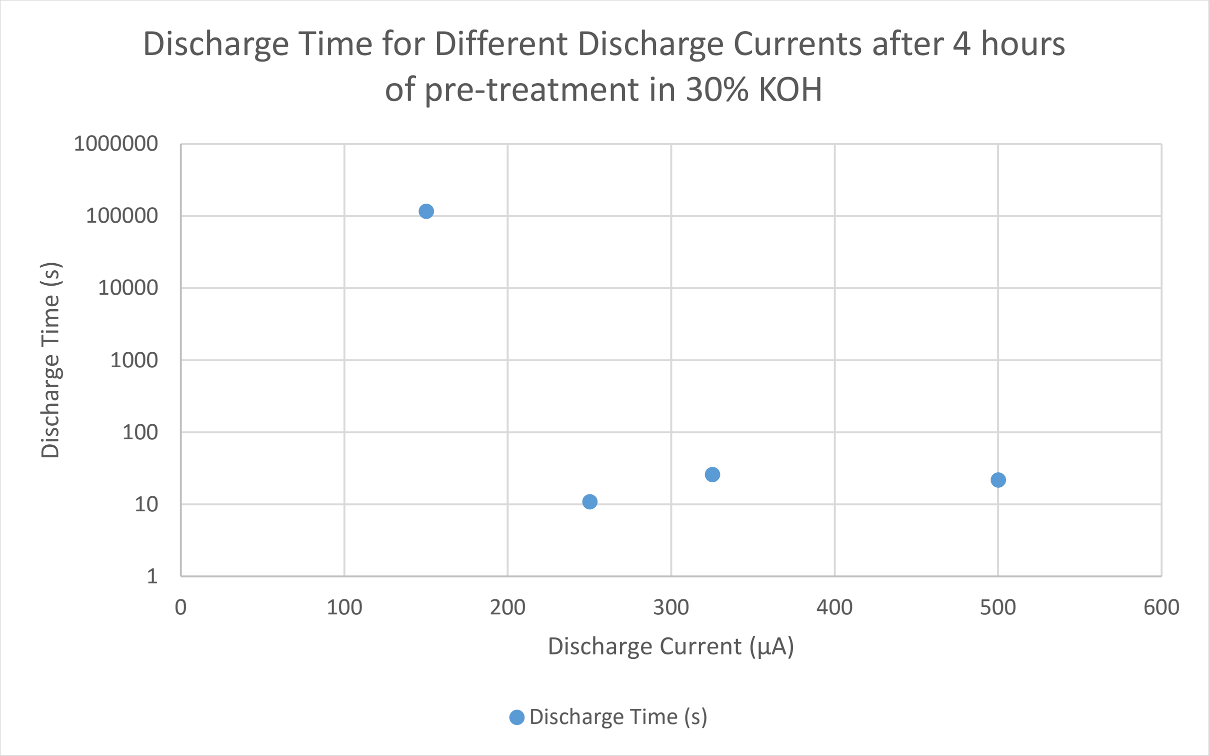

Figure 41: Discharge time after four hours of pre-treatment in KOH solution, at different discharge currents.

Again, it is important to note that the vertical time axis in this figure is logarithmic to account for the large differences in the results. It is found that at a discharge current of 150 µA the battery can be discharged for over 100 000 seconds. However, at any discharge current tested higher than 150 µA, the discharge lasts 30 seconds at the most. From these results it is concluded that reaction product depositing at the air electrode is not the mechanism at work in the alkaline silicon-air battery. Furthermore, it is noted that the battery does not support discharge currents over 150 µA after four hours of pre-treatment.

5.4 SEM images

In an attempt to gain a better understanding of the processes taking place at the air electrode, SEM images are taken both before and after pre-treatment as well as before and after being used in a discharge experiment. These SEM images are shown below in Figure 42.

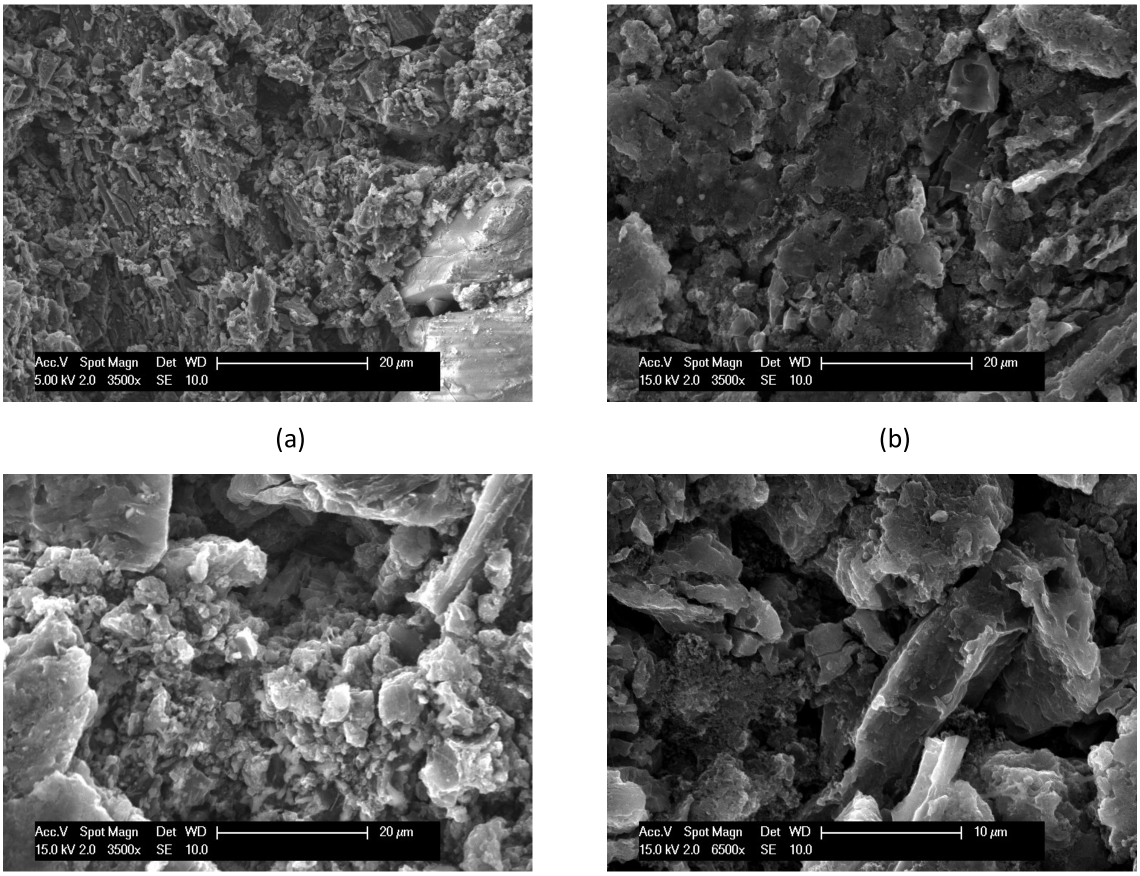

(a) (b)

(c) (d)

Figure 42: SEM images of the air electrode (a) before discharge, without pre-treatment (b) before discharge after sixteen hours of pre-treatment (c) after discharge at 150 µA without pre-treatment (d) after discharge at 150 µA after sixteen hours of pre-treatment.

From the SEM images it can be seen that structural changes occur in the air electrode both during pre-treatment and during discharge. These structural changes will be further investigated in the next chapters.

6. Discussion experimental results

From the first set of experiments it is found that the discharge performance of the battery can be improved significantly by pre-treating the air electrode with KOH solution prior to using it in the battery cell. For very short pre-treatment times (up to two hours) the effect is minimal and the battery discharge performance is similar to that of the battery without pre-treatment of the air electrode. Starting at four hours of pre-treatment, the discharge performance of the battery improves significantly, both in discharge time and in discharge potential. This improvement of discharge performance continues for pre-treatment times up to eight hours. Starting at sixteen hours and up to 24 hours of pre-treatment, the discharge performance of the battery reduces, with both a lower discharge potential and discharge time. For a very long pre-treatment time (110,75 hours) the pre-treatment even appears detrimental to the performance of the battery. From these results it might be expected that the optimal pre-treatment time for the air electrode is situated between eight and sixteen hours. It is important to point out that each of the results shown is from a single experiment. To improve the accuracy of the results, the experiments should be carried out multiple times to find an average performance indicator. Furthermore, additional measurements for pre-treatment times between eight and sixteen hours could shed more light on the optimal pre-treatment time.

The rest of the experiments are focused on identifying the cause of the improved discharge performance of the battery after pre-treatment of the air electrode. Water diffusing into the air electrode is excluded as a limiting factor by comparing the discharge performance of a battery with air electrode pre-treated in KOH solution with that of a battery with air electrode pre-treated in water. Therefore, it is reasonable to assume that the KOH is responsible for the higher discharge potential and longer discharge time after pre-treatment.

Reaction products depositing in the micro-pores of the air electrode is also excluded as a performance limiting factor in the battery, by performing experiments at higher discharge currents. It was found by Cohn and Ein-Eli in their investigation of a non-aqueous silicon-air battery using hydrophilic 1-ethyl-3-methylimidazolium oligofluorohydrogenate [EMI·(HF)2.3F] room temperature ionic liquid electrolyte that reaction product was depositing on the air electrode, clogging the micro-porous reaction sites [20]. When discharging the battery at higher discharge currents, the reaction product still deposits on the air electrode, however it forms larger clusters, depositing on the meso- and macro-pores rather than the micro-pores. Therefore, the micro-pores, which are the effective reaction sites in the air electrode, were still available for reactions to take place. This resulted in the battery achieving higher capacities at higher discharge currents. The increased discharge time and discharge potential of the battery found in the experiments in this work could be the result of increased micro-pore surface, resulting in slower clogging of all micro-pores in the air electrode by depositing reaction product. If this was indeed the case, the battery would also be expected to achieve higher capacities at higher discharge current densities, as was the case in the experiments by Cohn and Ein-Eli. However, experiments show that higher discharge current densities do not result in higher capacities in the alkaline silicon-air battery, meaning that reaction product depositing in the micro-pores of the air electrode is likely not the mechanism at work in the alkaline silicon-air battery.

However, an increase in micro-pore surface area in the air electrode is not fully discarded as an explanation for the increased discharge time and discharge potential found in the experiments. This will be discussed in the next chapters.

From SEM images it can be seen that structural changes do occur in the air electrode from pre-treatment as well as from discharging. However, to draw further conclusions based on the SEM images is difficult and might require additional image analysis software or alternative measurements such as atomic force microscopy (AFM).

Wang et al. have studied an air electrode of similar design for use in fuel cells [40]. It is found that the performance of the air electrode could be improved significantly by pre-treating it with an alkaline solution. In this study, the maximum supported power density of the air electrode was increased by 16% after alkaline pre-treatment. Several reasons for this improved performance are proposed in the study. First of all, the micro-pore area of the air electrode had increased after pre-treatment. Secondly, the charge transfer resistance decreased. Furthermore, the electrical conductivity of the air electrode had increased by 7%. Finally, adsorbed OH^- ions were found in the air electrode. These ions contribute to the oxygen reduction reaction activity of the air electrode.

To gain a further understanding of the effects of the parameters suggested by Wang et al., a computer model is developed to investigate some of these parameters. This computer model is discussed in the next chapters.

7. Modelling methods

This chapter describes the approach adopted for modelling a silicon-air battery within COMSOL. For this, COMSOL version 5.4, build 225 is used. The battery is modelled in one dimension (1D). Different parts of the silicon-air battery model are based on several other battery models provided within the COMSOL software [69]–[71]. The 1D silicon-air battery model consists of three domains: the anode, the separator, which is defined by the electrolyte properties, and the cathode. A schematic overview of the model is shown below in Figure 43.

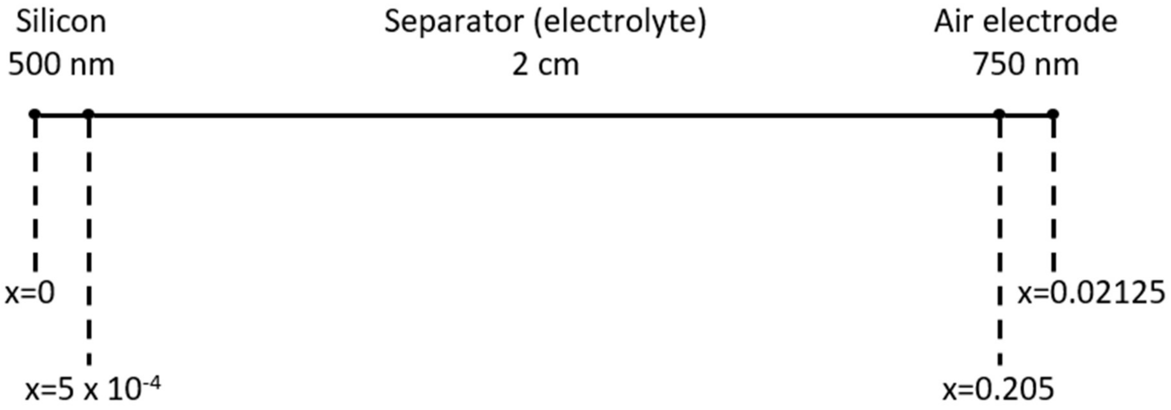

Figure 43: Schematic representation of the 1D COMSOL model.

FEM is used to solve differential equations; variables are calculated based on input parameters taken from literature as well as from other models present in the COMSOL software. In this chapter the modelling approach for each domain is discussed in detail.

7.1 Electrolyte

The electrolyte in the studied silicon-air battery consists of KOH dissolved in water. In COMSOL this can be modelled using the 'battery with binary electrolyte' (batbe) interface. A binary electrolyte is an electrolyte in which the electrolyte molecule dissociates into ions at a ratio of 1:1. When KOH dissolves into water, it dissociates into K^+ and OH^- at a ratio of 1:1. Therefore, it qualifies as a binary electrolyte.

The initial concentration of the electrolyte salt (KOH) is set to 6910 mol/m^3. This corresponds to 6.91 M, the same as used during the experiments. The cross section of the battery is set to 0.0001 m^2, while the length of the separator is set to 0.02 m. Both of these values also match the experimental setup. This ensures that the electrolyte volume is equal to the experimental value.

The molecular weights and densities of the involved species (potassium, hydroxide, water) are set to their empirical values where needed. The diffusion coefficients of potassium and hydroxide in the electrolyte are the same as used in the Zinc-Silver Oxide battery model provided within the COMSOL software [71]. The effective conductivity of the electrolyte is calculated in COMSOL based on the actual electrolyte salt concentration. This electrolyte salt concentration is being calculated by the 'domain ODE and DAE' interface in COMSOL. By tracking the amount of electrolyte salt being used in the anode and the amount being produced in the cathode, as well as the diffusion of electrolyte salt through the separator, the actual electrolyte salt is calculated for each computational domain.

7.1.1 Summary of parameters

In Table 5 below, an overview is shown of the parameters used to model the separator and electrolyte of the silicon-air battery in COMSOL.

Table 5: Summary of parameters used in modelling the separator of the silicon-air battery in COMSOL.

Parameter	Value	Physical interpretation	Reference
Lsep	0.02 [m]	Length of separator	
epsilonsep	0.87	Porosity of separator	[69]
D_OH	5.26e-9 [m^2/s]	Diffusion coefficient of OH^- ion	[71]
D_K	1.96e-9 [m^2/s]	Diffusion coefficient of K^+ ion	[71]
T_plus	0.22	Transport number	[71]
Dlnfdlnc_sep	-1.03	Activity dependence of separator	[69]
Cl_init	6910 [mol/m^3]	Initial electrolyte salt concentration	[71]
Rho_H2O	0.997 [g/cm^3]	Density of H_2O	
Rho	1500 [kg/m^3]	Electrolyte solution density	[71]
MW_H2O	18.01528 [g/mol]	Molecular weight of H_2O	[71]
MW_OH	17.008 [g/mol]	Molecular weight of OH^-	[71]
MW_K	39.1 [g/mol]	Molecular weight of K^+	[71]

7.2 Cathode

As a cathode, the silicon-air battery model uses an air electrode. In the COMSOL software a model for a lithium-air battery is readily available [69]. The air electrode in a lithium-air battery has the same function as the air electrode in a silicon-air battery. Therefore, the same modelling approach was used.

The air electrode is modelled as a porous material. It is set to an initial porosity of 0.73, meaning that 73% of the air electrode is modelled as pores filled with electrolyte, while the other 27% is modelled as solid material. The electrical conductivity of this solid material is set to 10 S/m. The length of the air electrode is set to 7.5 x 10^{-4} m. All of these values are based on the air electrode in the lithium-air battery model.

7.2.1 Electrode reaction

The equilibrium potential of the air electrode is set to 0.40 V [27]. The number of electrons involved in the reaction is set to 4 and the coefficient for the production of OH$^-$ ions is also set to 4 according to equation 2 in section 2.2. The electrode kinetics are governed by the extended Butler-Volmer equation, as shown below.

$$i_{loc} = i_0 \left[C_R \exp\left(\frac{\alpha_a F \eta}{RT}\right) - C_O \exp\left(\frac{-\alpha_c F \eta}{RT}\right) \right] \tag{9}$$

In this equation i_{loc} stands for the local current density. This local current density depends on the exchange current density i_0. α_a and α_c are the anodic and cathodic transfer coefficients. F stands for Faraday's constant, R for the gas constant and T for the temperature. The overpotential at the electrode is given by η. C_R and C_O are the reduced species and oxidized species expressions, respectively.

The values used for i_0 as well as α_a and α_c are taken from the lithium-air model. C_R and C_O are unitless expressions, which are calculated based on the actual concentrations of reaction species with respect to their equilibrium concentrations.

7.2.2 Oxygen dissolution and diffusion

Within COMSOL an interface called 'transport of diluted species (tds)' is used to model the dissolution of oxygen from the external atmosphere into the electrolyte that is present within the porous air electrode. From dissolving at the external edge of the electrode, the oxygen can then diffuse throughout the electrode. The concentration of oxygen throughout the air electrode over time is modelled by the tds interface. The concentration of oxygen outside the air electrode is set to 9.46 mol/m^3, which is the concentration of oxygen in atmospheric air at a pressure of 1 atm. The concentration of oxygen at the interface of the air electrode with the atmosphere (i.e. the boundary condition) is subsequently calculated by multiplying the external oxygen concentration with a solubility factor. This solubility factor is set to 0.4 in the base case, but is varied in one of the experiments to study its effect on the discharge performance of the battery. The consumption of oxygen at the air electrode interface with the electrolyte is modelled based on the applied current density.

7.2.3 Summary of parameters

All parameters related to the cathode of the battery model are summarized below in Table 6, as well as their physical interpretation.

Table 6: Summary of parameters used in modelling the cathode of the silicon-air battery in COMSOL.

Parameter	Value	Physical interpretation	Reference
Lpos	7.5e-4[m]	Length of positive electrode	[69]
Kpos	10 [S/m]	Conductivity of positive electrode	[69]
Epsilonl0_pos	0.73	Initial porosity of positive electrode	[69]
Epsilons0_pos	1-epsilonl0_pos	Initial active material solid fraction of positive electrode	[69]
Rpos0	25e-9 [m]	Particle radius in positive electrode	[69]

Apos	10 [cm^2/cm^3]	Specific surface area positive electrode	[69]
Alpha_a_pos	0.013	Anodic transfer coefficient positive electrode	[69]
Alpha_c_pos	0.054	Cathodic transfer coefficient positive electrode	[69]
i0_ref_pos	0.1 [A/m^2]	Reference exchange current density positive electrode	[69]
SolO2	0.4	Solubility factor oxygen in electrolyte	[69]
cO2ext	9.46 [mol/m^3]	External oxygen concentration in air at 1 atm	[69]
cO20	SolO2*cO2ext	Initial oxygen concentration in positive electrode	[69]
D_O2	7e-10 [m^2/s]	Oxygen diffusion coefficient	[69]
Eeq_pos	0.40 [V]	Equilibrium potential positive electrode	[27], [28]
n	4	Number of transferred electrons	[27]
Rho_carbon	2260 [kg/m^3]	Density of carbon	
Rho_O2	1.141 [g/cm^3]	Density of oxygen	
MW_O2	15.999 [g/mol]	Molecular weight of oxygen	

7.3 Anode

In the lithium-air battery model provided by COMSOL, the lithium anode is simply modelled as a boundary, set at the right equilibrium potential, with other parameters such as the electrical conductivity also set at the right values to represent lithium metal. For the lithium-air battery model, modelling the anode in this way is sufficient since most of the important processes the model simulates, take place at the cathode side of the battery. These processes include the dissolution and diffusion of oxygen, and the dissolution and deposition of reaction product into the electrolyte and in the micropores of the electrode material, respectively. However, from previous literature it is known that processes such as the dissolution and deposition of reaction product may also take place at the anode side of the battery in the case of a silicon-air battery. Therefore, a more detailed approach is needed to model the silicon anode. Such a detailed model of a silicon anode is not yet present in the COMSOL software. Therefore, a silicon anode model is developed based on values found in literature and in other COMSOL models. Several assumptions are made, as will be discussed in the following sections.

7.3.1 Porous electrode

Like the air cathode, the silicon anode is modelled as a porous electrode. Since the silicon used in experiments is often a solid silicon wafer, the initial porosity of the porous silicon modelled here should be very low. However, the initial porosity of the silicon anode has a very significant impact on the discharge potential and discharge time of the silicon-air battery. Empirically, this was already found by other studies, as discussed in chapter 3 [27], [28]. In the next chapter, the effect of the initial porosity of the silicon anode on the performance of the modelled battery is discussed in detail.

As is the case in the air cathode, the electrode kinetics of the silicon anode are governed by the extended Butler-Volmer equation, equation 9 shown in section 7.2.1. In the silicon anode, the equilibrium potential is set to -1.69 V [27]. According to equation 1 in section 2.2, the number of transferred electrons in this electrode is also set to 4. The coefficient for the consumption of OH^- ions is set to 4 as well. Additionally, a coefficient for the production of reaction product is introduced and set to 1. The production of reaction product will be discussed in the next section.

7.3.2 Deposition of reaction product and passivation

In chapters 2 and 3, the problem of passivation is silicon-air batteries has been discussed extensively. The main reaction product in the discharge process of silicon-air batteries is $Si(OH)_4$. This compound can dissolve into the electrolyte to a certain extent. Once the dissolution rate of this reaction product becomes insufficient, the passivation reaction starts, in which $Si(OH)_4$ is turned into SiO_2 with water as a by-product. The formed SiO_2 is a solid and will deposit on the silicon anode, forming a passivating layer on the surface. This passivation process is included in the COMSOL model in a simplified way. One assumption is made to simplify the modelling of this process: all $Si(OH)_4$ is directly turned into SiO_2 as soon as its produced. This is shown in equations 10-12.

Discharge: $Si + 4OH^- \rightarrow Si(OH)_4 + 4e^-$ (10)

Passivation: $Si(OH)_4 \rightarrow SiO_2 + 2H_2O$ (11)

Modelled reaction: $Si + 4OH^- \rightarrow SiO_2 + 2H_2O + 4e^-$ (12)

The reason for this assumption is that the used software interface is designed for redox-reactions. In redox-reactions electrons are transferred from one species to another, changing the oxidation state of the species involved in the reaction. As can be seen in equation 11, no charge is transferred in the passivation reaction. Therefore, implementing this reaction in the used software interface is difficult.

The made assumption has several implications. First of all, this means there is no dissolution of reaction product into the electrolyte, only deposition of reaction product on the silicon anode. Secondly, the rate at which the reaction from $Si(OH)_4$ to SiO_2 takes place in reality is not taken into account in the model. This means that the reaction rate of the passivation reaction could have an effect on the discharge performance of the battery, that will not be present in the model.

The deposition of SiO_2 is included in COMSOL by specifying the weight and density of the formed compound, and by relating the rate at which this reaction product is formed to the applied discharge current density. The deposited SiO_2 is added to the volume fraction of solid material and deducted from the liquid volume fraction. In that way, SiO_2 is replacing liquid electrolyte at the surface of the silicon anode, effectively passivating the surface.

To improve the accuracy and validity of the model in the future, the discharge reaction at the silicon anode should be split into two separate reactions. The first reaction for the formation of $Si(OH)_4$ from Si and OH^-

and a second reaction for the formation of SiO_2 from $Si(OH)_4$. By separating these two reactions, important physical processes such as the dissolution of $Si(OH)_4$ into the electrolyte can be included in the model.

7.3.3 Corrosion

The other main problem faced by alkaline silicon-air batteries that has been discussed in the early chapters of this work is corrosion of the silicon anode. In the current version of the COMSOL model, this process has not been included yet. The assumption is made that the silicon is infinite and does not run out. This allows for the investigation of other components of the battery besides the anode. The effect of this assumption and the assumption discussed in the previous section, will be explained extensively in chapter 9.

7.3.4 Summary of parameters

A summary of the parameters used in modelling the silicon anode in COMSOL is given in Table 7.

Table 7: Summary of parameters used in modelling the anode of the silicon-air battery in COMSOL.

Parameter	Value	Physical interpretation	Reference
Lneg	500e-6 [m]	Length of negative electrode	
Kneg	2.5e7 [S/m]	Conductivity of negative electrode	
Epsilonl0_neg	0.002	Initial porosity of negative electrode	
Epsilons0_neg	1-epsilonL0_neg	Initial active material solid fraction of negative electrode	
Aneg	10 [cm^2/cm^3]	Specific surface area negative electrode	[69]
Alpha_a_neg	0.025	Anodic transfer coefficient negative electrode	[70]
Alpha_c_neg	0.054	Cathodic transfer coefficient negative electrode	[70]
Rfilm	50 [ohm*m^2]	Film resistance over SiO_2 film	[69]
i0_ref_neg	0.8 [A/m^2]	Reference exchange current density negative electrode	[70]
Eeq_neg	-1.69 [V]	Equilibrium potential negative electrode	[27], [28]

n	4	Number of transferred electrons	[27]
Rho_SiO2	2.65 [g/cm^3]	Density of SiO_2	
MW_SiO2	60.08 [g/mol]	Molecular weight of SiO_2	

7.4 Mesh and solver

A fine mesh is used to divide the model into 44 separate computational domain elements. For each of these elements, differential equations are solved using a time-dependent solver. The time-dependent solver produces one solution per ten seconds. The decision to only calculate one solution every ten seconds is made to limit the computational burden as well as to minimize the time needed to find a solution. The model can also produce solutions at a much higher resolution if needed. However, to identify the trends presented in Chapter 8 a time resolution of ten seconds is sufficient. Parametric sweeps are executed for different values of several of the input parameters used in the model. The input parameter that is varied in the parametric sweep, as well as the values used for these input parameters, are specified in each of the results.

8. Model results

To gain a more comprehensive understanding of the different processes taking place in the silicon-air battery and their influence on the performance of the battery, the model as detailed in the previous chapter is used. In the first two sets of simulations, the performance of the model is evaluated and compared to the performance of different batteries in previous publications. This is done by varying the initial porosity of the silicon electrode, as this has been investigated in several different prior publications. Furthermore, the initial concentration of the electrolyte is varied, as this has also been studied previously. After the initial evaluation and calibration of the model, the influence of different parameters is investigated. These parameters are the electrical conductivity of the air electrode, the specific surface area in the air electrode and the solubility of oxygen in the electrolyte.

8.1 Experiments and simulations

In order to be able to draw reliable and valid conclusions based on simulations, it is desirable for the simulation results to match up with empirical data as closely as possible. This indicates proper functioning of the model, as well as proper calibration of the initial input values used in the model. In the case of silicon-air batteries, matching simulation results to empirical data is difficult due to the large differences in battery performance found in literature. Discharge times in literature range from several hundreds of seconds to over 1100 hours, depending on the materials and experimental setup [21], [27], [28], [30], [31]. Furthermore, discharge potentials in these experiments range from less than 0.6 V to approximately 1.4 V.

Similarly, in the experiments carried out in this work, the discharge time ranges from mere tens of seconds, to upwards of 70 hours. At the same time the potential ranges from approximately 0.7 V to almost 1.2 V.

In order to demonstrate the functioning of the model presented in this work, as well as to relate it to previous experimental work, the model accuracy is assessed qualitatively rather than quantitatively. Several trends have been identified in previous work, as extensively discussed in chapter 3. These trends include the dependence of the discharge time and discharge potential on the initial porosity of the silicon anode, as well as the dependence of the discharge potential on the electrolyte salt concentration. In the next two sections, these two trends are investigated thoroughly in the COMSOL model. Based on these two trends, the functioning of the model is shown and explained.

Each of the results presented in this chapter are produced by recomputing the model. All inputs for the model are kept constant at the values as detailed in the previous chapter. Only one parameter is changed per simulation. Which input parameter is varied and which values are used is specified for each of the presented results.

8.2 Initial porosity silicon electrode

In the first set of simulations, the initial porosity is varied between 5×10^{-4} and 0.002. This implies that at the start of the simulation 0.05% to 0.2% of the silicon electrode consists of voids filled with electrolyte. The other 99.95% to 99.8% consists of solid silicon. Such low values for the initial porosity are used to simulate the non-porous crystalline silicon wafer used in the experiments. However, since the silicon anode is modelled as a porous electrode, the initial porosity cannot be zero. The results of these simulations are shown in Figure 44.

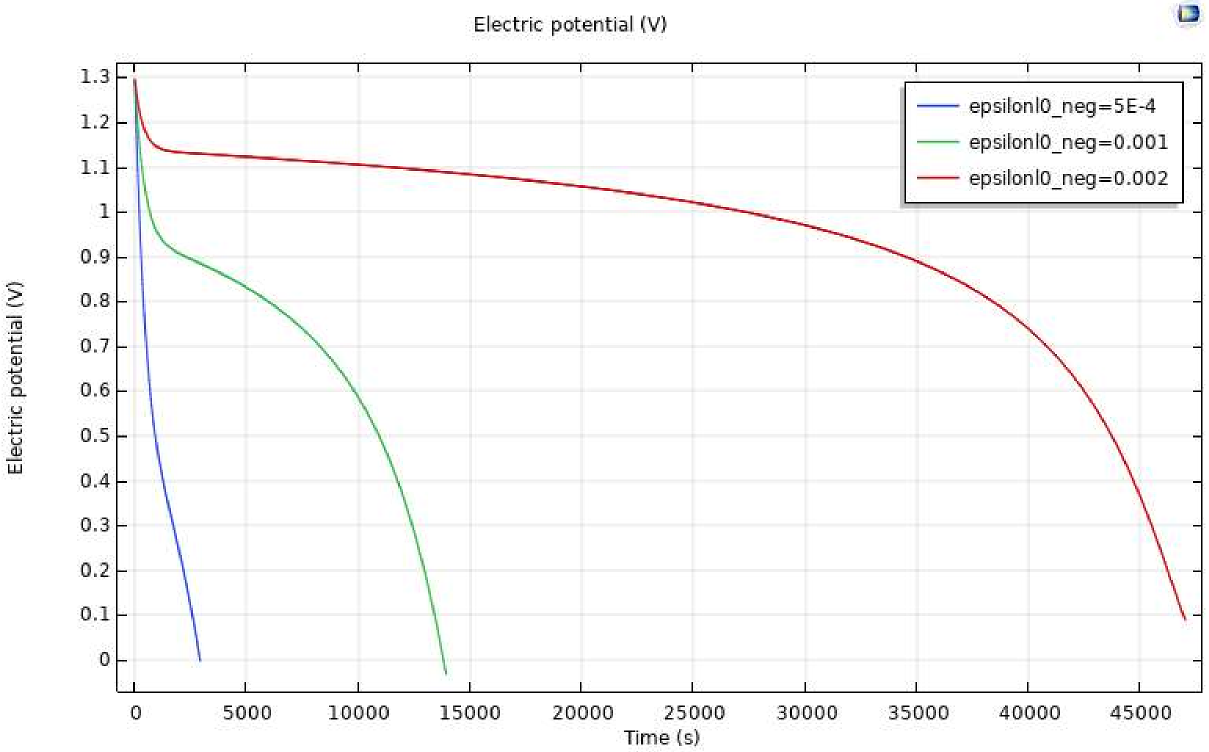

Figure 44: The battery cell potential simulated for different initial porosities of the silicon electrode between 5 x 10 $^{-4}$ and 0.002.

It can be seen that both the battery cell potential and the discharge time of the battery are greatly influenced by the initial porosity of the silicon electrode. For an initial porosity of 5 x 10^{-4}, the potential starts dropping from the start of the simulation and reaches zero in around 3000 seconds. For an initial porosity of 0.002, the potential starts above 1.1 V and gradually drops to zero over a period of more than 47000 seconds.

8.2.1 Electrolyte salt concentration

The difference in discharge time and discharge potential is caused mainly by the difference in pore electrolyte volume in the model. The anodic reaction taking place at the silicon electrode consumes OH$^-$ ions from the electrolyte in the pore. These OH$^-$ ions are regenerated at the air electrode, from where they diffuse through the bulk electrolyte and eventually into the pores at the silicon electrode. This process is limiting in this set of simulations. In Figure 45 the electrolyte salt concentration is shown as a function of the x-coordinate in the battery at the start of the simulation. Figure 46 shows the electrolyte salt concentration as a function of the x-coordinate in the battery by the end of battery operation for all three values for the initial porosity of the silicon electrode.

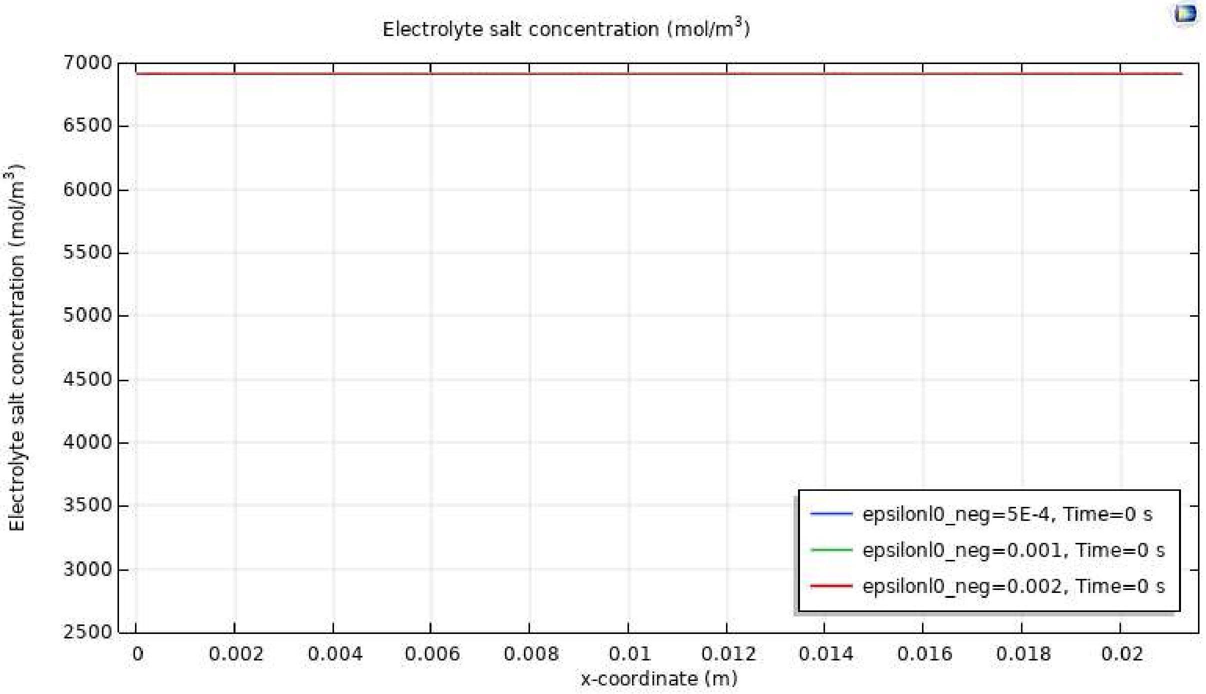

Figure 45: Electrolyte salt concentration as a function of x-coordinate in the battery cell for different initial porosities of the silicon electrode at the start of battery operation.

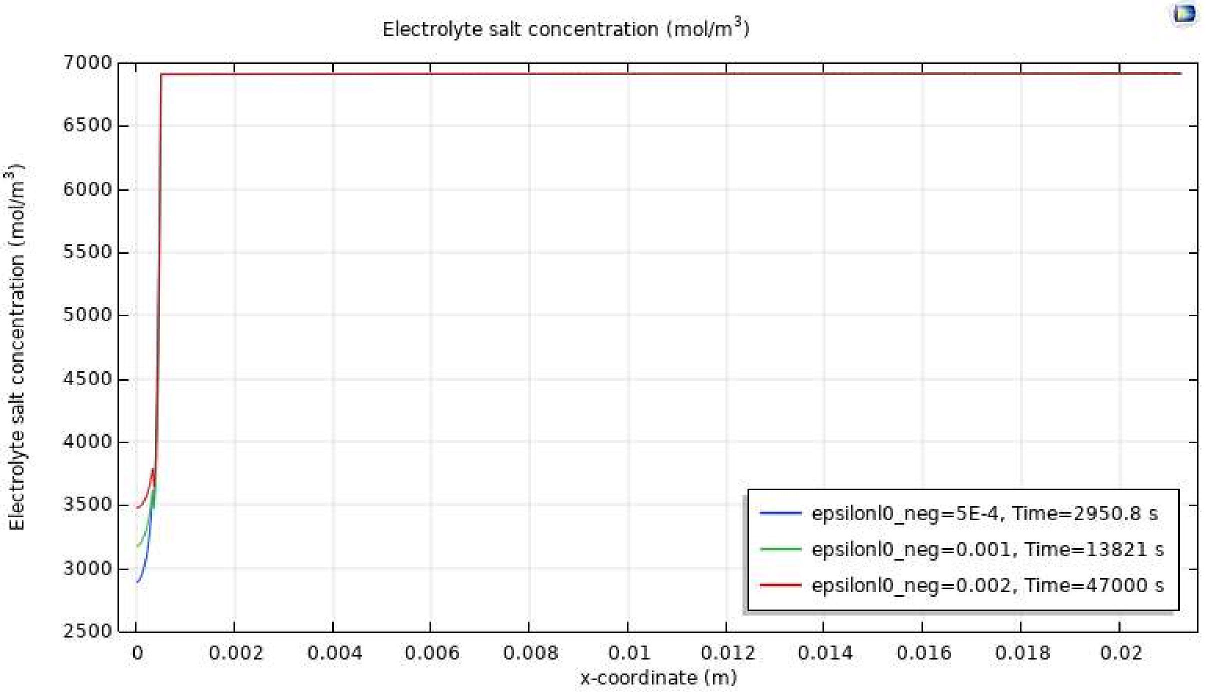

Figure 46: Electrolyte salt concentration as a function of x-coordinate in the battery cell for different initial porosities of the silicon electrode at the end of battery operation.

It can be seen in these two graphs that in the silicon anode, located from x=0 to x=5 x 10^{-4}, the concentration of electrolyte salt is decreased to around half of the initial value by the end of operation. Meanwhile, in the rest of the battery, no change in electrolyte salt is visible. The steep decrease in electrolyte salt concentration only occurs inside the silicon electrode, due to the low porosity of the silicon electrode. There is only little electrolyte present in the electrode pores. As a result, a small consumption of OH^- will already lead to a very significant reduction in concentration. In the separator as well as in the air electrode (situated on the right-hand side in this model, starting at x=5 x 10^{-4} and x=0.0205 respectively) the electrolyte volume is orders of magnitude larger, leading to a significantly smaller change in electrolyte salt concentration as a consequence of the same amount of consumption or production of OH^- ions.

Not only is the change in electrolyte salt concentration larger for a smaller porosity of the silicon anode, the change in electrolyte salt concentration also varies much quicker for smaller initial porosities. This effect can be seen in Figure 46. The legend shows the time-stamp at which the battery operation is terminated. It can be seen that for an initial porosity of 5 x 10^{-4} the change in electrolyte salt concentration already occurs within less than 3000 seconds, while for an initial porosity of 0.002, the change in electrolyte salt happens over a period of more than 47000 seconds. Thus, the initial porosity of the silicon anode not only affects the discharge potential of the battery, it also has a significant effect on the discharge time of the battery.

In comparison, Figure 47 shows the electrolyte salt concentration throughout the battery over time for an initial porosity of the silicon electrode of 0.1, closer to the initial porosity of the air electrode.

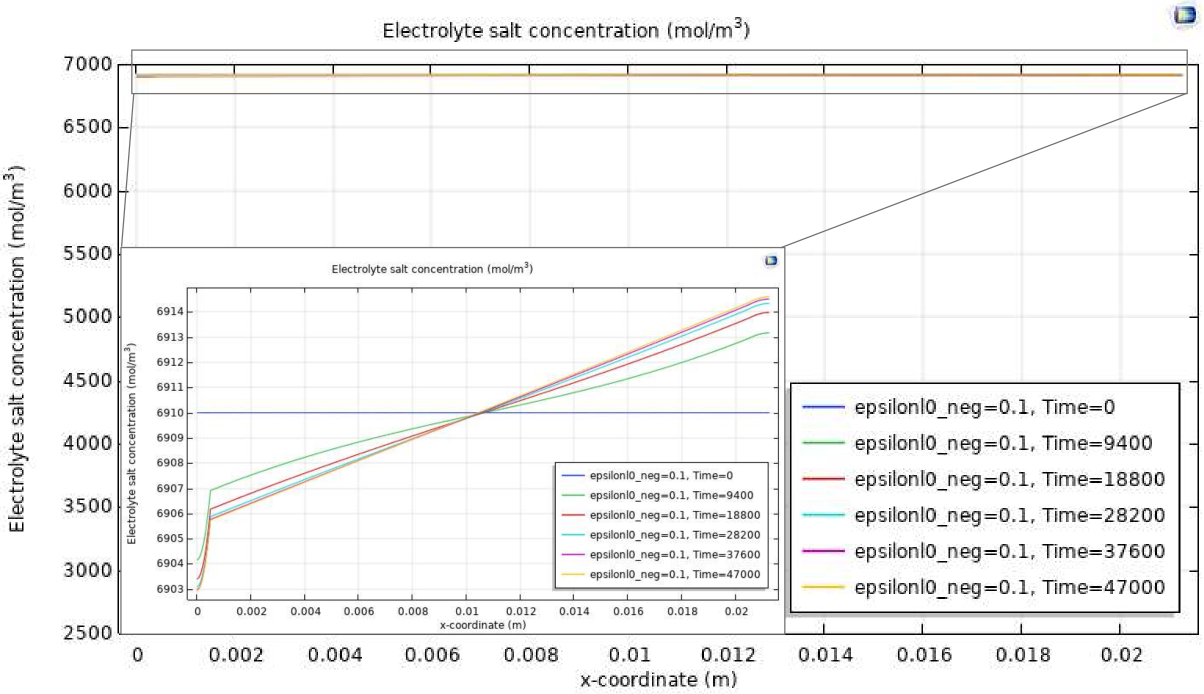

Figure 47: Electrolyte salt concentration as a function of x-coordinate in the battery cell for an initial porosity of 0.1 for different times during the simulation.

Here it can be seen that the concentration change in the silicon electrode due to the consumption of OH^- is much smaller (7 mol/m^3 in Figure 46 vs 3000 mol/m^3 in Figure 45). Furthermore, it can be noted in Figure 47 that the OH^- consumption at the silicon electrode and the OH^- production at the air electrode cause a gradient throughout the electrolyte, since the OH^- ions are unable to diffuse through the electrolyte quickly enough. This gradient also occurs for smaller values for the initial porosity of the silicon anode, such as in Figure 46. However, due to the very large change in concentration in the silicon anode, the smaller changes in concentration in the separator and the air cathode are not visible in this figure.

8.2.2 Silicon dioxide concentration and deposition

Besides changes in electrolyte salt concentration, another concentration change also influences the performance of the battery. Figure 48 shows how the concentration of silicon dioxide increases over time inside the silicon electrode, for an initial porosity of 0.002. This silicon dioxide does not dissolve into the electrolyte, instead it deposits as a solid film on the silicon electrode.

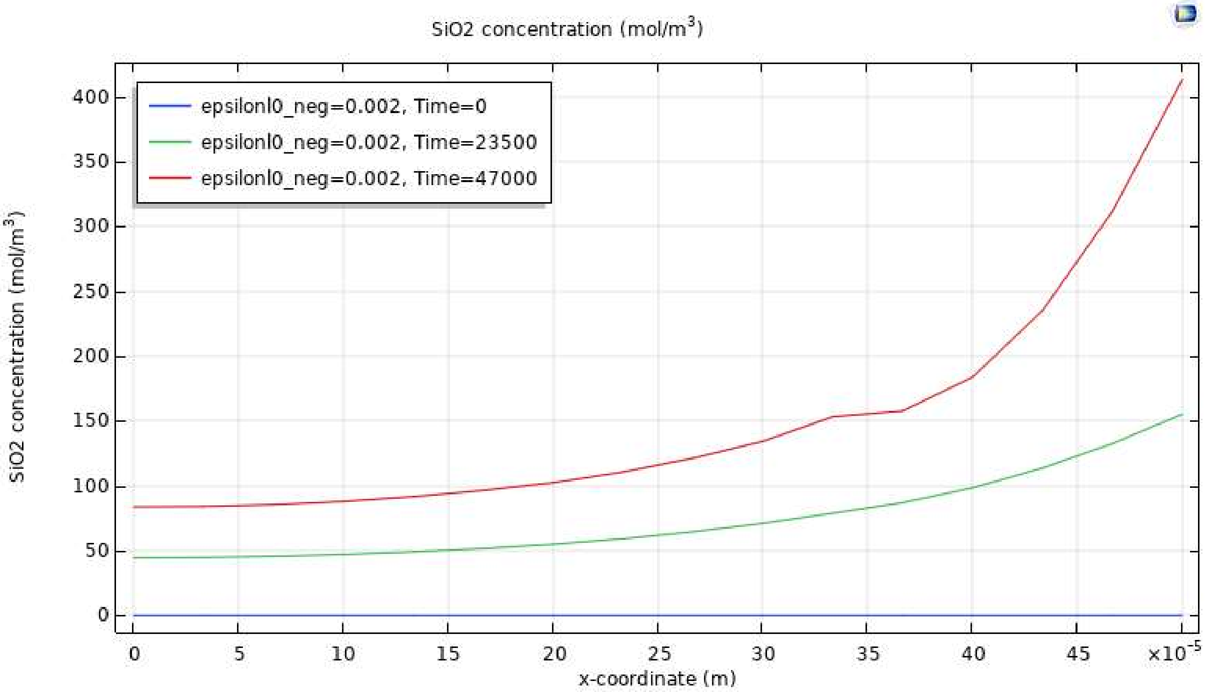

Figure 48: The concentration of silicon dioxide as a function of the x-coordinate in the battery cell. The initial porosity of the silicon electrode is 0.002. Silicon dioxide concentration shown at the beginning of the simulation, halfway through and at the end of the simulation. Silicon dioxide is formed and deposited in the silicon electrode; results are therefore only shown for x-coordinates situated in the silicon electrode. In this graph, x=0 is the outside edge of the silicon anode, x=5 x 10^{-4} is the interface of the silicon anode with the electrolyte.

It can be seen that the concentration of silicon dioxide increases the most near the interface of the silicon electrode with the bulk electrolyte, located at x=5 x 10^{-4} in the graphs. The further to the left of this interface, the smaller the increase in silicon dioxide concentration. Since OH^- from the electrolyte is needed in the reaction, it can be expected that the reaction takes place at a higher rate near the interface with the bulk electrolyte compared to deeper inside the silicon electrode. Therefore, the main formation and deposition of reaction product can also be expected near this interface.

Figure 49 shows how the silicon dioxide concentration differs for different initial porosities of the silicon anode. The results are shown at t=2490 s, which is close to the end of operation for the battery when the initial porosity of the silicon anode is equal to 5 x 10^{-4}. This time is the latest moment that can be used where each battery has discharged for an equal amount of time. After this time, the battery with an initial porosity of 5 x 10^{-4} stops working, while the other two continue. A moment as late as possible into the simulation is shown, to ensure that the silicon dioxide concentration has developed as much as possible.

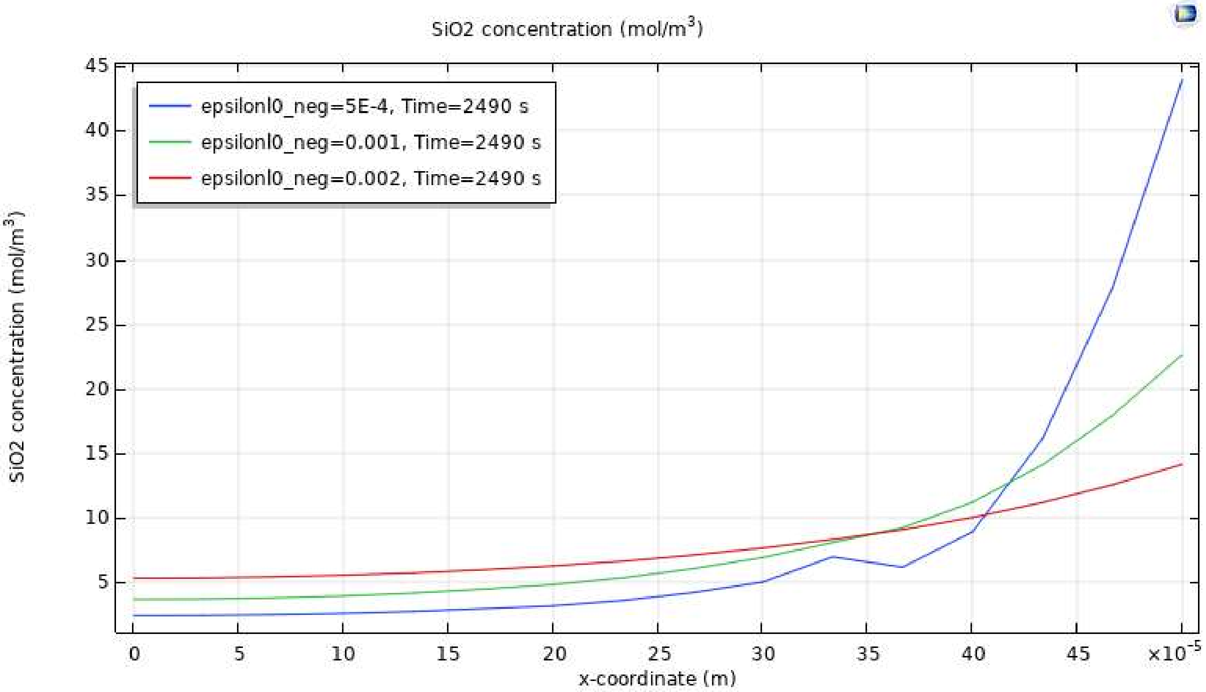

Figure 49: Silicon dioxide concentration in the silicon anode as a function of x-coordinate at time=2490 s.

In Figure 49 the silicon dioxide concentration is shown as a function of x-coordinate. X=0 represents the outside edge of the silicon anode, while x=5 x 10^{-4} represents the interface between the silicon anode and the bulk electrolyte. It can be seen that for each initial porosity of the silicon anode, the concentration of silicon dioxide is higher near the interface with the bulk electrolyte. As mentioned above, this is to be expected, since the majority of reactions will take place closer to the interface between the electrode and the bulk electrolyte. Furthermore, it can be seen that the highest silicon dioxide concentration occurs in the silicon anode with the lowest initial porosity. Like the decrease in electrolyte salt concentration discussed in the previous section, the higher silicon dioxide concentration is caused by the lower pore electrolyte volume. The electrode with the smallest initial porosity also has the smallest pore volume. The same change in amount of silicon dioxide will therefore result in a larger change in concentration, compared to electrodes with larger initial porosities and thus larger pore volumes.

Additionally, it can be seen that further away from the electrode-electrolyte interface (closer to x=0) the electrode with the larger initial porosity also has the larger silicon dioxide concentration. As the initial porosity of the electrode gets larger, more and more electrolyte will be able to reach further into the electrode, taking part in reactions there. In these reactions, silicon dioxide is formed. Furthermore, a larger porosity of the electrode allows silicon dioxide formed close to the electrode-electrolyte interface to diffuse into the electrode before depositing.

From this section as well as the previous section it can be concluded that the modelled battery benefits greatly from an increased initial porosity of the silicon anode. This corresponds well to empirical findings, where it was concluded that the surface texturing and porosity of the silicon anode is essential for sustained discharge of an alkaline silicon-air battery [27], [28].

8.3 Oxygen concentration

The final concentration playing a role in the discharge performance of the modelled silicon-air battery is the oxygen concentration. As explained, oxygen dissolves into the electrolyte inside the air electrode from the atmospheric air. The oxygen then diffuses through the air electrode, where it is consumed in the discharge reaction.

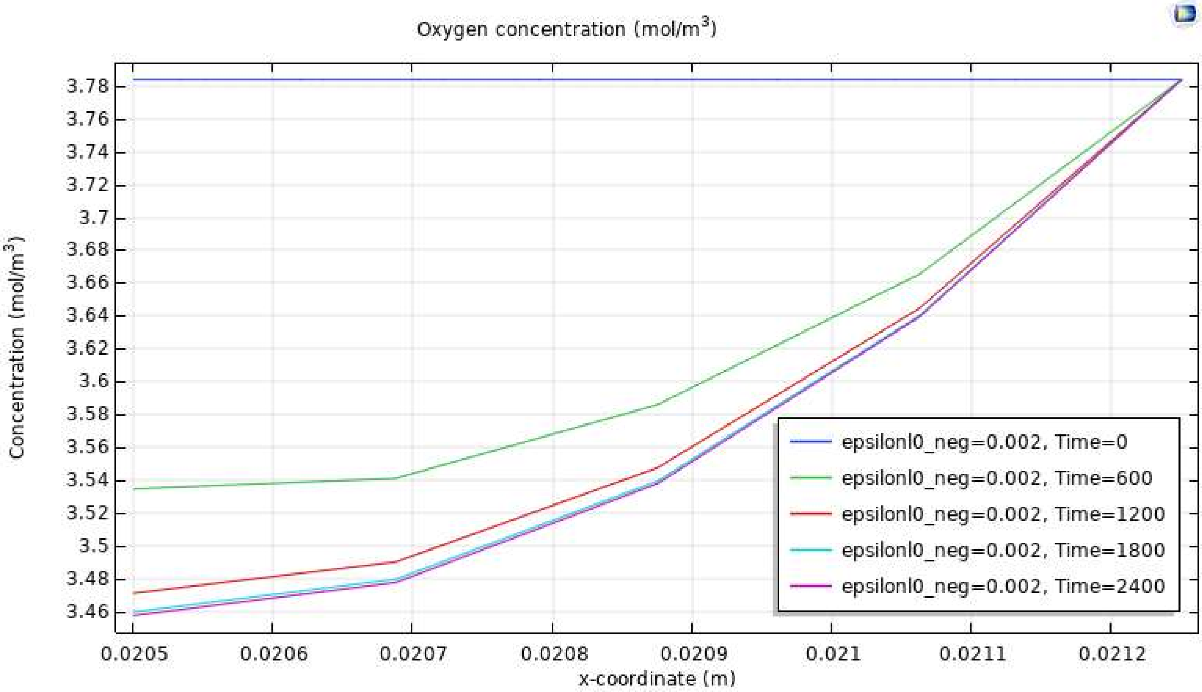

Figure 50: Oxygen concentration inside the air electrode for the first 2400 seconds of the simulation. After this time, the oxygen concentration stabilizes at 3.45 mol/m^3.

Figure 50 shows the development of the oxygen concentration in the first 2400 seconds of the simulation. It can be seen that the oxygen concentration is constant throughout the air electrode for t=0. As soon as the discharge starts, oxygen is consumed. Similar to the silicon electrode, the reaction takes place at a higher rate near the interface with the bulk electrolyte, which is at x=0.0205. Therefore, more oxygen is consumed in that region, compared to deeper inside the air electrode. After around 2400 seconds, the concentration of oxygen in the air electrode stabilizes at 3.45 mol/m^3. This indicates that the oxygen dissolves into and diffuses through the air electrode at the same rate as it is consumed. The air electrode and the oxygen concentration therein are the main focus of this research and will be discussed further in the last sections of this chapter.

8.4 Initial concentration of electrolyte

Another way in which the accuracy of the model is assessed, is by varying the initial concentration of the electrolyte. It is known from previous publications that a higher electrolyte salt concentration results in a higher discharge potential of the battery cell. The price paid for this increased discharge potential is the increased corrosion of the silicon electrode by the electrolyte. As can be seen in Figure 51 the model correctly displays the same behaviour. In this simulation, the initial porosity of the silicon anode is set to 0.1 in order to minimize the effects discussed in sections 8.2.1 and 8.2.2. The potential of the battery starts at around 1.3 V and immediately drops to a value between 1.26 V and 1.18 V depending on the electrolyte salt concentration. The discharge potential of the battery decreases slowly over time as a result of changes in concentration of electrolyte salt as well as reaction product, and the formation of a silicon dioxide film on the silicon anode. Since the corrosion of the silicon electrode is a side reaction that has not been implemented in this model yet, the discharge time of the battery is not influenced by the changed electrolyte salt concentration. In the figure, only the first 47000 seconds of the simulation are shown, however discharge of the battery continues, with the potential following the same slope as seen in the figure, until the potential reaches 0 V.

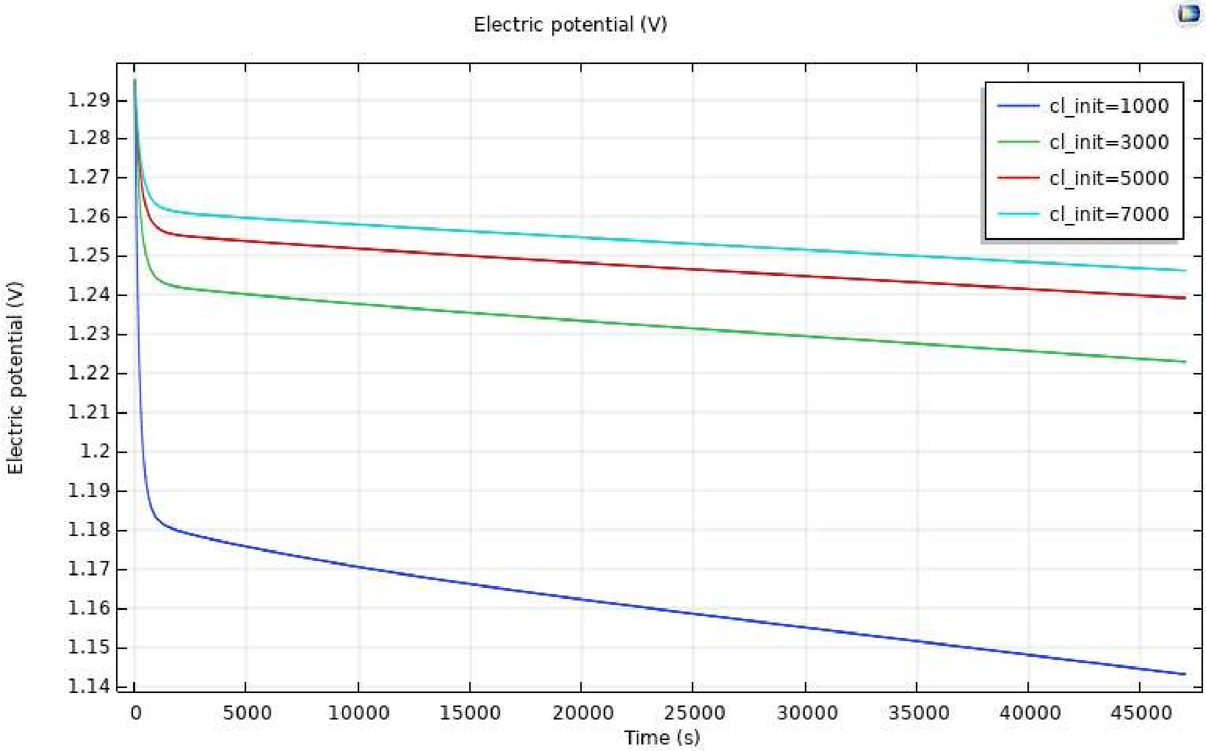

Figure 51: The battery cell potential simulated for different initial electrolyte salt concentrations between 1000 mol/m^3 and 7000 mol/m^3.

The lower discharge potential when using a lower electrolyte salt concentration corresponds to empirical findings [27], [30]. The discharge time is also lower for a lower electrolyte salt concentration. This does not correspond with empirical findings. Empirically it has been found that higher electrolyte salt concentration lead to higher corrosion rates, which in turn results in lower discharge times. However, the corrosion of silicon is not modelled in these simulations. Therefore, it may be expected that the higher electrolyte salt concentration does not reduce the discharge time of the battery. With the model displaying the same behaviour as the silicon-air batteries used in experiments in prior publications, it is used to assess several of the changes in the air electrode as a result of alkaline pre-treatment and their effects on the discharge performance of the battery cell.

8.5 Electrical conductivity air electrode

One of the reasons proposed by Wang et al. for the improved performance of the air electrode after alkaline pre-treatment, is the increased electrical conductivity of the air electrode [40]. To test this, the electrical conductivity of the air electrode in the model is varied between 0.01 S/m and 10000 S/m. The result of this test is shown in Figure 52. A closer inspection of the first 5000 seconds of the same result is also shown.

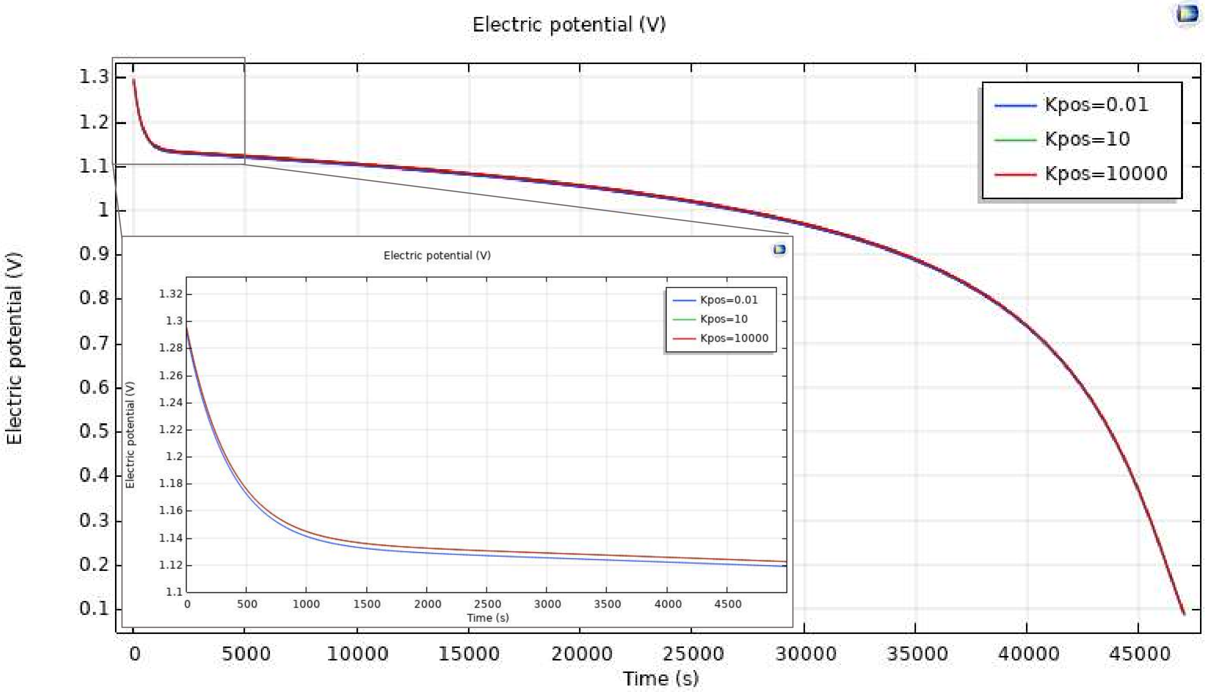

Figure 52: The battery cell potential simulated for different values of electrical conductivity of the air electrode between 0.01 S/m and 10000 S/m. (Close-up) The first 5000 seconds of the simulated battery cell potential for different values of electrical conductivity of the air electrode between 0.01 S/m and 10000 S/m.

From both graphs it can be seen that (even for large differences of) the electrical conductivity of the air electrode only minimally influences the discharge potential of the silicon-air battery, while it does not influence the discharge time at all. With the corrosion reaction not present in the model, the discharge time of the battery is determined mainly by the passivation at the silicon anode in these simulations. It has been shown in section 8.2 that this passivation can be postponed by increasing the initial porosity of the silicon anode. For an initial porosity of 0.002, passivation of the silicon anode terminates battery operation after approximately 47000 seconds. This can also be seen in the results in Figure 52. From these results, it seems unlikely that the increased electrical conductivity of the air electrode causes the large differences in discharge performance found in the experimental section of this work.

8.6 Increased micro-pore area

Another possible explanation offered by Wang et al. is an increased micro-pore area in the air electrode after alkaline pre-treatment [40]. This option is also tested, by varying the specific surface area in the air electrode between 1000 m^2/m^3 and 2000 m^2/m^3. From Figure 53 it can be seen that the impact of this parameter on the discharge potential of the battery cell is more noticeable than that of the electrical conductivity of the air electrode. However, similar to the electrical conductivity, the specific surface area of the air electrode does not appear to influence the discharge time of the battery. Again, in this case, the battery operation is terminated by passivation of the silicon anode after around 47000 seconds.

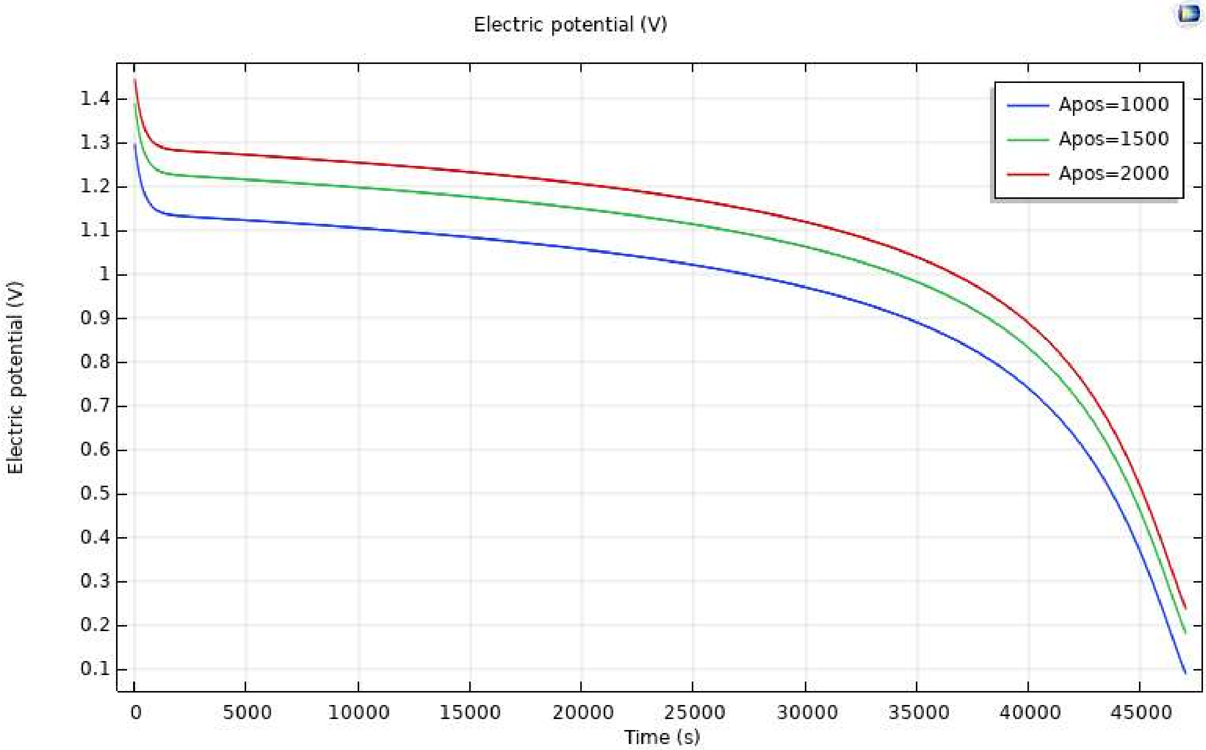

Figure 53: The battery cell potential simulated for different values of specific surface area of the air electrode between 1000 m^2/m^3 and 2000 m^2/m^3.

8.7 Oxygen solubility in electrolyte

A final parameter that is identified by this model to have an influence on the discharge performance of the silicon-air battery is the solubility of oxygen in the electrolyte. As mentioned before, the concentration of oxygen at the edge of the air electrode where it meets with the atmosphere, is modelled by multiplying the atmospheric oxygen concentration with a solubility factor. By changing this solubility factor, the concentration of oxygen throughout the air electrode is changed. This can be seen in Figure 54 below.

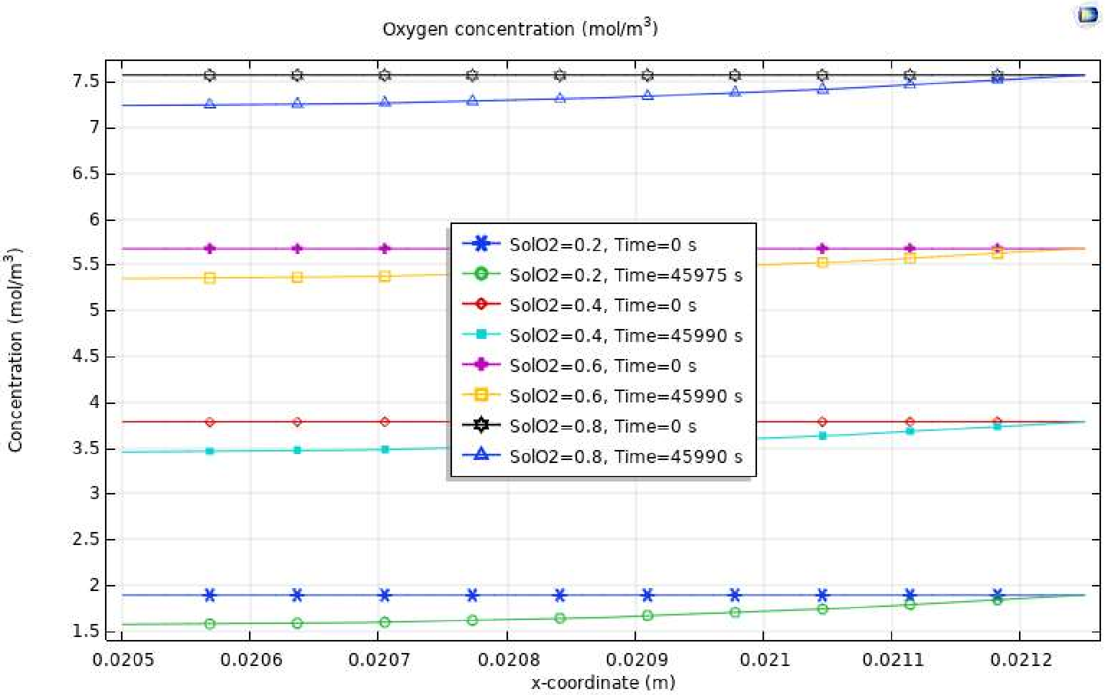

Figure 54: The oxygen concentration as a function of x-coordinate inside the air electrode for different solubility factors at the beginning and at the end of the simulation. X=0.0205 represents the interface between the air electrode and the bulk electrolyte. X=0.02125 represents the interface of the air electrode with the atmosphere.

As can be seen in the figure, the oxygen concentration at the interface of the air electrode with the atmosphere (x=0.02125) depends on the solubility factor. For a solubility factor of 0.8, the oxygen concentration in the air electrode starts slightly above 7.5 mol/m^3, while for a solubility factor of 0.2, the oxygen concentration in the air electrode starts at less than 2 mol/m^3. This in turn changes the value at which the oxygen concentration stabilizes during the simulation. For a solubility factor of 0.8 the oxygen concentration in the air electrode stabilizes around 7.3 mol/m^3 during discharge, while for a solubility factor of 0.2, the oxygen concentration stabilizes around 1.5 mol/m^3 during discharge. As can be clearly seen in Figure 54, a higher solubility factor for atmospheric oxygen results in a higher oxygen concentration in the air electrode, both at the start of the simulation and during discharge.

Due to the concentration dependent reaction kinetics at both electrodes, the oxygen concentration in the air electrode, which is directly influenced by the solubility factor as shown in Figure 54, influences the performance of the battery. This is shown below in Figure 55.

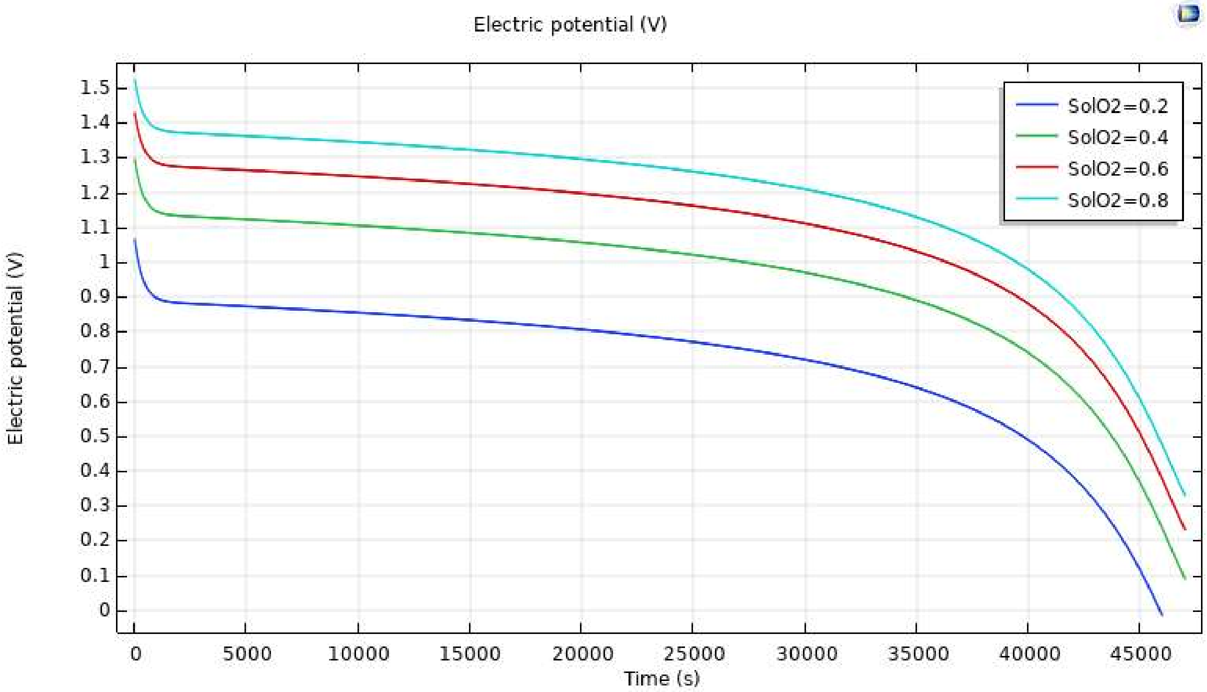

Figure 55: The battery cell potential simulated for different values of oxygen solubility in the electrolyte between 0.2 and 0.8.

From this figure it becomes clear that the discharge potential strongly depends on the amount of oxygen available in the air electrode. As a consequence, the solubility factor of oxygen has a strong influence on the discharge potential of the battery cell. A higher oxygen solubility factor leads to a higher oxygen concentration in the air electrode, which in turn results in a higher discharge potential.

Similar to the previous to parameters, the oxygen solubility mainly effects the discharge potential of the battery, while only minimally effecting the discharge time. Nevertheless, it can be seen that with a lower solubility factor, and thus a lower oxygen concentration in the air electrode, the discharge of the battery lasts slightly shorter than for a higher oxygen solubility factor.

9. Discussion model results

In the model, several different processes known to take place in alkaline silicon-air batteries are modelled. These include the dissolution and diffusion of oxygen at the air electrode and the deposition of reaction product at the silicon electrode. With these processes in place, it is shown that the battery model displays similar behaviour to the batteries used in experiments in prior publications.

The initial porosity of the silicon anode is shown to have a significant impact on both the discharge time and the discharge potential of the battery in the model. It was previously found by Zhong et al. and Park et al. that increasing the porosity of the silicon anode results in increased discharge potential as well as increased discharge time [27], [28]. This is the result of reduced passivation of the silicon anode. Increasing the porosity of the silicon anode increases the contact surface area between the silicon and the electrolyte. Because of this increased contact surface area, $Si(OH)_4$ is able to dissolve into the electrolyte at a higher rate, postponing the start of the passivation reaction. Furthermore, with the larger contact surface area, when the passivation reaction starts, it takes longer before the whole surface area of the silicon anode is covered by a passivation layer. Finally, a larger porosity of the silicon anode also results in a larger pore electrolyte volume. As a result of this, OH^- is more available and its concentration drops slower, compared to lower porosities with smaller pore electrolyte volumes.

As mentioned in chapter 7, the dissolution of $Si(OH)_4$ into the electrolyte is not modelled in the COMSOL model. Instead, SiO_2 is formed directly from the oxidation reaction. This SiO_2 directly forms a solid passivation layer on the silicon anode. Therefore, the increased dissolution of $Si(OH)_4$ into the electrolyte as a result of the increased contact surface area between the silicon anode and the electrolyte is not present in the model. However, the other consequences of an increased porosity, the longer time it takes for the silicon anode to be fully passivated and the increased availability of OH^-, are still demonstrated in the model. This allows the modelled battery to discharge for over 47000 seconds, for an initial porosity of the silicon anode of 0.002. This 47000 second discharge time is likely an underestimation of reality, since in reality the dissolution of $Si(OH)_4$ into the electrolyte will postpone the start of the passivation reaction. Especially with the relatively large electrolyte volume used in the experiments and simulations, it can be expected that dissolution of reaction product into the electrolyte will continue for a significant time before the passivation reaction starts. This was also shown in the experimental results in chapter 5, where the battery could be discharged for more than 70 hours without passivation of the silicon anode. Even though the model most likely underestimates the discharge time, due to the absence of reaction product dissolution, over 47000 seconds of discharge is enough to investigate the discharge behaviour. By keeping the initial porosity of the silicon anode constant throughout simulations, passivation of the silicon anode occurs identically in each simulation. This allows for the effect of changes in the air cathode to be isolated and studied. Especially changes in the discharge potential of the battery as a result of changes in the air cathode are unrelated to the passivation occurring in the silicon anode. These changes can therefore be studied using the model, despite the absence of reaction product dissolution. Additionally, the experimental results in chapter 5 clearly show that without pre-treatment of the air cathode, as well as for short pre-treatment times of up to three hours, the battery stops operating in less than 47000 seconds as a result of processes taking place at the air cathode. In these experiments, passivation of the silicon anode was not observed. The model being able to simulate over 47000 seconds of discharge is therefore deemed sufficient to study different processes at the air cathode taking place in the first 47000 seconds of discharge.

Another relation found in previous publications on alkaline silicon-air batteries is the relation between electrolyte salt concentration and battery potential. It has been found in multiple studies that a higher electrolyte salt concentration results in higher battery potentials [27], [30]. This relation has also been demonstrated in the model in section 8.2.1. As explained in chapters 2 and 3, the drawback of using a higher concentration of electrolyte salt is the increased corrosion of the silicon anode that results from it. In the experiments, this increased corrosion as a result of a high electrolyte salt concentration was countered by using p-type doped silicon rather than n-type doped silicon. As has been explained in chapters 2 and 3 p-type doped silicon is generally less affected by corrosion than n-type doped silicon. In the model, corrosion of the silicon anode by the electrolyte has not been implemented yet. The effect of this assumption however, is minimal. Zhong et al. have found an average corrosion rate of 1.34 µm/h for n-type doped silicon in 6 M KOH [27]. In this work 6.91 M KOH solution is used, which is expected to increase the corrosion rate somewhat. However, p-type doped silicon is used instead of n-type, which compensates for this higher electrolyte salt concentration. It was found by Cohn and Ein-Eli that the corrosion rate of n-type silicon can be up to 16 times as high as the corrosion rate for p-type silicon [20], [21]. This was found however for silicon in RTIL electrolyte, not in alkaline electrolyte. While the corrosion rate for p-type silicon will be lower than the corrosion rate for n-type silicon in alkaline electrolyte, no quantitative data is available. 1.34 µm/h is therefore used as a reasonable estimate for the corrosion rate in this work. Based on this corrosion rate, it can be expected that a 500 nm thick silicon wafer will last almost 375 hours before being fully etched away. Furthermore, in section 5.1 it has been shown that the amount of silicon used in the discharge reaction is many orders of magnitude smaller than the amount of silicon lost to corrosion, when discharging at 150 µA. Therefore, even when discharging the battery at 150 µA, a 500 nm thick silicon wafer can be expected to last over 350 hours before being fully etched away due to corrosion. In the experiments, the longest achieved discharge lasts almost 71 hours, while in the simulations, discharge stops after 47000 seconds (around 13 hours). It can therefore be concluded that the absence of the corrosion in the model will have little to no effect on the obtained results.

With the model demonstrated to show similar behaviour to silicon-air batteries studied in previous publications as well as the silicon-air battery used in the experimental section of this work, and with the assumptions as explained above, the model is then used to evaluate the impact of several changes in the air electrode on the discharge performance of the battery.

First of all, the electrical conductivity of the air electrode is investigated. Wang et al. have found that alkaline pre-treatment of the air electrode resulted in a decrease of ohmic resistance of the air electrode of 7%. Using the model, the electrical conductivity of the air electrode is varied between 0.01 S/m and 10000 S/m. This difference is much larger than what could realistically be achieved by alkaline pre-treatment of the air electrode alone. Nevertheless, such a large change in electrical conductivity of the air cathode was needed in the model to result in a change in discharge potential of the battery. With such a large change in electrical conductivity resulting in such a small change in battery cell potential, it is deemed unlikely that a change in electrical conductivity of the air cathode explains the significant impact of air cathode pre-treatment found in the experimental section of this work.

Secondly, the effect of the micro-pore surface area in the air cathode was investigated. It was found by Wang et al. that the micro-pore surface area in the air cathode was increased after alkaline pre-treatment [40]. In the model, the micro-pore surface area in the air cathode was varied between 1000 cm^2/cm^3 and 2000 cm^2/cm^3. This change had a more noticeable effect on the discharge potential of the battery, with an average discharge potential of around 1.2 V for 2000 cm^2/cm^3, compared to approximately 1 V for 1000 cm^2/cm^3.

A final parameter that was identified by the model to have an impact on the discharge potential of the battery is the solubility of oxygen in the electrolyte. By varying the solubility factor for oxygen between 0.2 and 0.8, the concentration of oxygen present in the air cathode was strongly affected. This in turn had an impact on the discharge potential of the battery. A higher solubility factor results in higher oxygen concentrations, leading to a higher discharge potential.

However, none of the parameters investigated in the model had a significant effect on the discharge time of the battery. Nevertheless, the experimental section of this work has shown clearly that the discharge time of the battery cell can be increased by multiple orders of magnitude by pre-treating the air electrode with an alkaline solution. From this it can be expected that the change in discharge time found in the experiments, has to be attributed to a process that is not yet included in the model.

One possible explanation might be related to other atmospheric gases. In the experiments, atmospheric oxygen is used, as opposed to pure oxygen. This means that around 21% of the gas arriving at the air electrode is oxygen, with the other 79% consisting of other atmospheric gases. It might be that these other atmospheric gases can dissolve and diffuse into the air electrode as well. Here they could settle in the micro-pores of the active carbon material of the air electrode. Pre-treatment of the air cathode has been shown to increase the micro-pore area in the air cathode. This could explain why pre-treatment of the air cathode prolongs the discharge of the battery. An increased micro-pore area in the air cathode would take longer to be fully clogged by other atmospheric gases, and would thus allow for oxygen reduction reactions to take place for a longer time before suffocating.

Another phenomenon observed by Wang et al. after alkaline pre-treatment of the air cathode was the presence of adsorbed OH^- ions in the air cathode. These ions increase the oxygen reduction reaction activity of the air cathode. It is possible that the presence of these adsorbed ions is essential for the proper functioning of the air cathode. This would also explain why no sustained discharge was possible without alkaline pre-treatment of the air cathode.

10. Conclusions and outlook

The main objective of this research is to evaluate the impact of different qualities of the air electrode on the discharge performance of an alkaline silicon-air battery. Based on theory and prior publications, the mechanisms of passivation and corrosion are explained. It is also explained how by making certain design choices, considering dopant type, electrolyte concentration and electrolyte volume, passivation and corrosion can be prevented from being the limiting factor in the discharge performance of an alkaline silicon-air battery. With the processes at the silicon electrode no longer being the limiting factor, the air electrode becomes limiting in the silicon-air battery. This allows for the investigation of different qualities of the air electrode and their influence on the discharge performance of the battery.

In the experimental section of this work, it is shown that the discharge performance of an alkaline silicon-air battery can be improved by pre-treating the air electrode with an alkaline solution. Both the discharge potential and the discharge time, which is directly related to the discharge capacity, are increased after pre-treatments of up to eight hours. For longer pre-treatments, the discharge time and discharge potential of the battery are lower with respect to eight hours of pre-treatment. For very long pre-treatments, the battery performs similarly to one without pre-treatment whatsoever. By comparing pre-treatments with alkaline solution and water, it is shown that the increase in discharge time and potential can be attributed to the hydroxide ions in the alkaline solution and not to the water. Furthermore, it is found that the discharge time is very short when discharging the battery at current densities higher than 150 $\mu A/cm^2$.

From literature on air electrodes for use in fuel cells, several different causes are suggested for the improved performance of the air electrode after alkaline pre-treatment. First of all, higher electrical conductivity of the air electrode is found in literature as a result of alkaline pre-treatment. Secondly, it is found that the specific surface area in the air electrode micro-pores is increased by the alkaline pre-treatment. Thirdly, hydroxide ions are found adsorbed to the air electrode material. These hydroxide ions contribute to increased oxygen reduction reaction activity.

In the modelling section of this work, some of the reasons suggested in literature are put to the test. It is found that the electrical conductivity of the air electrode only has a very limited effect on the discharge performance of the battery. While a higher electrical conductivity does result in a higher discharge potential, a very large increase in electrical conductivity is required for a very small increase in discharge potential. Meanwhile, the discharge time of the battery is not affected at all by the electrical conductivity of the air electrode. The specific surface area of micro-pores in the air electrode is found to have a more significant effect on the discharge potential of the battery. Still, a relatively large increase in specific surface area only results in an increase of around 0.2 V in discharge potential. For this parameter, the discharge time also remains unchanged.

From these findings it is concluded that the higher electrical conductivity and increased specific micro-pore area as a result of the alkaline pre-treatment could indeed contribute to the improved discharge performance of the battery cell, specifically by increasing the discharge potential. However, the impact of these qualities on the discharge potential of the battery is very limited, even for large variations of these parameters. Therefore, they do not explain the drastic increase in discharge time and discharge potential found in the experimental section. This means that the process causing this increase in discharge time and discharge potential in the experiments, is most likely not yet modelled in the COMSOL model.

10.1 Outlook

A careful suggestion is made in this work that the increase in discharge time and discharge potential found in the experiments might be related to the use of atmospheric oxygen instead of pure oxygen in the experiments, compared to the model. With oxygen making up only 21% of the atmospheric air, other gases might dissolve and diffuse into the air electrode besides oxygen. These gases could then settle in the micro-pores of the air electrode, blocking these sites for further reactions. Pre-treatment of the air electrode would increase the number of micro-porous sites in the material. In that way, it would take longer for other atmospheric gases to fully suffocate the air electrode. This could explain the increase in discharge time and discharge potential after pre-treatment of the air electrode. This hypothesis can be tested experimentally by discharging the battery using pure oxygen instead of atmospheric oxygen. Alternatively, adding other atmospheric gases besides oxygen in the model could give more insight into the accuracy of this hypothesis.

Another change that occurs in the air electrode as a result of alkaline pre-treatment that has not been investigated in this work yet, it the presence of adsorbed OH^- ions in the air electrode. These adsorbed ions increase the oxygen reduction reaction activity of the air electrode material. It could be that these ions are essential for the proper functioning of the air electrode. This would also explain why sustained discharge of the battery was only found possible after three or more hours of alkaline pre-treatment in the experimental section of this work. To test this hypothesis experimentally, the air electrode could be pre-treated with a different solution, using a different species. If the ions from this different solution do not adsorb on the air electrode, the air electrode can be tested again without adsorbed OH^- ions. Alternatively, the adsorption of molecules on the air electrode could be added to the model, to investigate its effect in simulations.

Additionally, the experiments could be expanded by pre-treating the air electrode with alkaline pre-treatments of different concentrations, and for durations that have not been studied in this work. The model can be expanded by adding the dissolution of reaction product into the electrolyte at a certain concentration dependent rate. Also, the chemical reaction in which silicon dioxide is formed from the silicate reaction product and its reaction rate are yet to be added. Another chemical reaction that is still to be added to the model is the corrosion of the silicon electrode by the alkaline electrolyte. This corrosion is dependent on factors such as the concentration of the electrolyte and the type of doping of the silicon. Even though it has been shown in chapter 9 that the absence of these chemical reactions in the model do not prevent the model from being a useful tool in evaluating the effect of changes in the air electrode on the discharge performance of the battery, any addition to the model to make it more accurate and realistic would of course only contribute to the accuracy and validity of the results found.

11. References

[1] S. A. Montzka, E. J. Dlugokencky, and J. H. Butler, "Non-CO 2 greenhouse gases and climate change," *Nature*, vol. 476, no. 7358. Nature Publishing Group, pp. 43–50, 04-Aug-2011.

[2] UNFCCC, "Kyoto Protocol to the United Nations Framework Convention on Climate Change." Kyoto, Japan, 1997.

[3] UNFCCC, "The Paris Agreement." Paris, France, 2015.

[4] Rijksoverheid, "Nationale Klimaatadaptatiestrategie (NAS)." Den Haag, 2016.

[5] Rijksoverheid, "Klimaatwet - BWBR0042394." 2020.

[6] D. Larcher and J.-M. Tarascon, "Towards greener and more sustainable batteries for electrical energy storage," *Nat. Chem.*, vol. 7, no. 1, pp. 19–29, Jan. 2015.

[7] K. Schmidt-Rohr, "How Batteries Store and Release Energy: Explaining Basic Electrochemistry," *J. Chem. Educ.*, vol. 95, no. 10, pp. 1801–1810, 2018.

[8] R. Kortlever, "Basic Electrochemistry I," 2019.

[9] K. C. Divya and J. Østergaard, "Battery energy storage technology for power systems—An overview," *Electr. Power Syst. Res.*, vol. 79, no. 4, pp. 511–520, Apr. 2009.

[10] K. T. Chau, Y. S. Wong, and C. C. Chan, "Overview of energy sources for electric vehicles," *Energy Convers. Manag.*, vol. 40, no. 10, pp. 1021–1039, 1999.

[11] F. Cheng and J. Chen, "Metal–air batteries: From oxygen reduction electrochemistry to cathode catalysts," *Chem. Soc. Rev.*, vol. 41, no. 6, pp. 2172–2192, 2012.

[12] G. Girishkumar, B. McCloskey, A. C. Luntz, S. Swanson, and W. Wilcke, "Lithium-air battery: Promise and challenges," *J. Phys. Chem. Lett.*, vol. 1, no. 14, pp. 2193–2203, Jul. 2010.

[13] S. Müller, F. Holzer, and O. Haas, "Optimized zinc electrode for the rechargeable zinc-air battery," *J. Appl. Electrochem.*, vol. 28, no. 9, pp. 895–898, 1998.

[14] J. S. Lee *et al.*, "Metal-air batteries with high energy density: Li-air versus Zn-air," *Adv. Energy Mater.*, vol. 1, no. 1, pp. 34–50, 2011.

[15] S. Yang and H. Knickle, "Design and analysis of aluminum/air battery system for electric vehicles," *J. Power Sources*, vol. 112, no. 1, pp. 162–173, 2002.

[16] G. E. Blomgren, "The Development and Future of Lithium Ion Batteries," *J. Electrochem. Soc.*, vol. 164, no. 1, pp. A5019–A5025, Dec. 2017.

[17] A. A. Mohamad, "Zn/gelled 6 M KOH/O2 zinc-air battery," *J. Power Sources*, vol. 159, no. 1 SPEC. ISS., pp. 752–757, 2006.

[18] T. R. Crompton, *Batteries Reference Book*, 2nd ed. Newnes, 2000.

[19] S. F. Bender, J. W. Cretzmeyer, and T. F. Reise, *Handbook of Batteries (2nd ed.)*. New York, NY: McGraw-Hill, 1994.

[20] G. Cohn and Y. Ein-Eli, "Study and development of non-aqueous silicon-air battery," *J. Power Sources*, vol. 195, no. 15, pp. 4963–4970, 2010.

[21] G. Cohn, D. Starosvetsky, R. Hagiwara, D. D. Macdonald, and Y. Ein-Eli, "Silicon-air batteries," *Electrochem. commun.*, vol. 11, no. 10, pp. 1916–1918, 2009.

[22] B. Shvartsev, G. Cohn, H. Shasha, R. A. Eichel, and Y. Ein-Eli, "Reference electrode assembly and its use in the study of fluorohydrogenate ionic liquid silicon electrochemistry," *Phys. Chem. Chem. Phys.*, vol. 15, no. 41, pp. 17837–17845, 2013.

[23] G. Cohn, R. A. Eichel, and Y. Ein-Eli, "New insight into the discharge mechanism of silicon-air batteries using electrochemical impedance spectroscopy," *Phys. Chem. Chem. Phys.*, vol. 15, no. 9, pp. 3256–3263, 2013.

[24] G. Cohn, D. D. MacDonald, and Y. Ein-Eli, “Remarkable impact of water on the discharge performance of a silicon-air battery,” *ChemSusChem*, vol. 4, no. 8, pp. 1124–1129, 2011.

[25] G. Cohn, A. Altberg, D. D. MacDonald, and Y. Ein-Eli, “A silicon-air battery utilizing a composite polymer electrolyte,” *Electrochim. Acta*, vol. 58, no. 1, pp. 161–164, 2011.

[26] Y. Ein-Eli, “2011/061728 Al,” 2011.

[27] X. Zhong *et al.*, “High-capacity silicon-air battery in alkaline solution,” *ChemSusChem*, vol. 5, no. 1, pp. 177–180, 2012.

[28] D. W. Park, S. Kim, J. D. Ocon, G. H. A. Abrenica, J. K. Lee, and J. Lee, “Controlled electrochemical etching of nanoporous si anodes and its discharge behavior in alkaline si - Air batteries,” *ACS Appl. Mater. Interfaces*, vol. 7, no. 5, pp. 3126–3132, 2015.

[29] Y. E. Durmus, “Modeling of Silicon-Air Batteries,” 2013.

[30] Y. E. Durmus *et al.*, “Long run discharge, performance and efficiency of primary Silicon–air cells with alkaline electrolyte,” *Electrochim. Acta*, vol. 225, pp. 215–224, 2017.

[31] H. Weinrich, Y. E. Durmus, H. Tempel, H. Kungl, and R. A. Eichel, “Silicon and iron as resource-efficient anode materials for ambient-temperature metal-air batteries: A review,” *Materials (Basel).*, vol. 12, no. 13, 2019.

[32] A. Garamoun, M. B. Schubert, and J. H. Werner, “Thin-film silicon for flexible metal-air batteries,” *ChemSusChem*, vol. 7, no. 12, pp. 3272–3274, 2014.

[33] S. Wu *et al.*, “A long-life lithium ion oxygen battery based on commercial silicon particles as the anode,” *Energy Environ. Sci.*, vol. 9, no. 10, pp. 3262–3271, 2016.

[34] H. Wu *et al.*, “Stable cycling of double-walled silicon nanotube battery anodes through solid-electrolyte interphase control,” *Nat. Nanotechnol.*, vol. 7, no. 5, pp. 310–315, 2012.

[35] H. Lin *et al.*, “Twisted aligned carbon nanotube/silicon composite fiber anode for flexible wire-shaped lithium-ion battery,” *Adv. Mater.*, vol. 26, no. 8, pp. 1217–1222, 2014.

[36] C. (John) Zhang *et al.*, “High capacity silicon anodes enabled by MXene viscous aqueous ink,” *Nat. Commun.*, vol. 10, no. 1, 2019.

[37] Y. E. Durmus *et al.*, “Investigation of the corrosion behavior of highly As-doped crystalline Si in alkaline Si–air batteries,” *Electrochim. Acta*, vol. 265, pp. 292–302, 2018.

[38] P. Jakes, G. Cohn, Y. Ein-Eli, F. Scheiba, H. Ehrenberg, and R. A. Eichel, “Limitation of discharge capacity and mechanisms of air-electrode deactivation in silicon-air batteries,” *ChemSusChem*, vol. 5, no. 11, pp. 2278–2285, 2012.

[39] A. Kraytsberg and Y. Ein-Eli, “Review on Li-air batteries - Opportunities, limitations and perspective,” *Journal of Power Sources*, vol. 196, no. 3. Elsevier B.V., pp. 886–893, 01-Feb-2011.

[40] X. Wang, N. Gao, Q. Zhou, H. Dong, H. Yu, and Y. Feng, “Acidic and alkaline pretreatments of activated carbon and their effects on the performance of air-cathodes in microbial fuel cells,” *Bioresour. Technol.*, vol. 144, pp. 632–636, 2013.

[41] R. Hofffmann, “C&EN: IT’S ELEMENTAL: THE PERIODIC TABLE - SILICON,” *Chemical & Engineering News*, 2003. [Online]. Available: http://pubsapp.acs.org/cen/80th/silicon.html? [Accessed: 14-Nov-2019].

[42] M. Fleischer, *Recent estimates of the abundances of the elements in the earth’s crust*, Vol. 285. United States Department of the Interior, Geological Survey, 1953.

[43] M. Wagemaker, “Energy Storage in Batteries Basic Principles and Developments CH3222SET,” 2018.

[44] A. J. Bard and L. R. Faulkner, *Electrochemical Methods - Fundamentals and Applications*, 2nd ed. Austin, Texas: Wiley and Sons, 2001.

[45] J. B. Goodenough and Y. Kim, “Challenges for rechargeable Li batteries,” *Chem. Mater.*, vol. 22, no. 3, pp. 587–603, 2010.

[46] M. Pourbaix, *Atlas of electrochemical equilibria in aqueous solutions*. Oxford: Pergamon Press Ltd., 1966.

[47] P. A. Nikolaychuk, “The Revised Pourbaix Diagram for Silicon,” *Silicon*, vol. 6, no. 2, pp. 109–116, 2014.

[48] H. Kazimierczak, P. Bobrowski, G. Kulesza, J. Poplewska, M. Gajewska, and K. Stan, “Electrochemical Phase Diagrams,” 2006.

[49] T. Nohira, K. Yasuda, and Y. Ito, “Pinpoint and bulk electrochemical reduction of insulating silicon dioxide to silicon,” *Nat. Mater.*, vol. 2, no. 6, pp. 397–401, May 2003.

[50] K. Yasuda, T. Nohira, and Y. Ito, “Effect of electrolysis potential on reduction of solid silicon dioxide in molten CaCl2,” in *Journal of Physics and Chemistry of Solids*, 2005, vol. 66, no. 2–4, pp. 443–447.

[51] M. Zeman, “Semiconductors Introduction,” 2018.

[52] O. Tobail, “Porous Silicon for Thin Solar Cell Fabrication,” *Elektrotechnik Und Informationstechnik*, no. January, p. 147, 2008.

[53] C. A. Koval and J. N. Howard, “Electron Transfer at Semiconductor Electrode-Liquid Electrolyte Interfaces,” *Chem. Rev.*, vol. 92, no. 3, pp. 411–433, 1992.

[54] V. A. Myamlin and Y. V. Pleskov, “The Electrochemistry of Semiconductors,” *Russ. Chem. Rev.*, vol. 32, no. 4, pp. 208–220, 1963.

[55] X. G. Zhang, *Electrochemistry of Silicon and its Oxide*. New York, NY: Kluwer Acedemic Publishers, 2001.

[56] R. Memming, *Semiconductor Electrochemistry*. Weinheim, Germany: WILEY-VCH, 2001.

[57] H. Reiss, “The Fermi level and the redox potential,” *J. Phys. Chem.*, vol. 89, no. 18, pp. 3783–3791, 1985.

[58] J. D. Ocon, J. W. Kim, G. H. A. Abrenica, J. K. Lee, and J. Lee, “Quasi-perpetual discharge behaviour in p-type Ge-air batteries,” *Phys. Chem. Chem. Phys.*, vol. 16, no. 41, pp. 22487–22494, 2014.

[59] Y. E. Durmus *et al.*, “ Influence of Dopant Type and Orientation of Silicon Anodes on Performance, Efficiency and Corrosion of Silicon–Air Cells with EMIm(HF) 2.3 F Electrolyte ,” *J. Electrochem. Soc.*, vol. 164, no. 12, pp. A2310–A2320, 2017.

[60] G. R. De Guel and D. L. Kendall, “Hydration Model for the Molarity Dependence of the Etch Rate of Si in Aqueous Alkali Hydroxides,” *J. Electrochem. Soc.*, vol. 138, no. 4, pp. 1055–1063, 1991.

[61] H. Seidel, L. Csepregi, A. Heuberger, and H. Baumgörtel, “Anisotropic Etching of Crystalline Silicon in Alkaline Solutions: I. Orientation Dependence and Behavior of Passivation Layers,” *J. Electrochem. Soc.*, vol. 137, no. 11, pp. 3612–3626, 1990.

[62] S. Cattarin and M. M. Musiani, “Electrodissolution and passivation of silicon in aqueous alkaline media: A voltammetric and impedance investigation,” *J. Phys. Chem. B*, vol. 103, no. 16, pp. 3162–3169, 1999.

[63] R. Hagiwara, T. Hirashige, T. Tsuda, and Y. Ito, “Acidic 1-ethyl-3-methylimidazolium fluoride: A new room temperature ionic liquid,” *J. Fluor. Chem.*, vol. 99, no. 1, pp. 1–3, 1999.

[64] H. Nakagawa *et al.*, “Application of nonflammable electrolyte with room temperature ionic liquids (RTILs) for lithium-ion cells,” *J. Power Sources*, vol. 174, no. 2, pp. 1021–1026, 2007.

[65] H. Sakaebe, H. Matsumoto, and K. Tatsumi, “Application of room temperature ionic liquids to Li batteries,” *Electrochim. Acta*, vol. 53, no. 3 SPEC. ISS., pp. 1048–1054, 2007.

[66] H. Ye and J. J. Xu, “Polymer Electrolytes Based on Ionic Liquids and Their Application to Solid-state Thin-film Li-Oxygen Batteries,” *ESC Trans.*, pp. 73–81, 2008.

[67] “Electric Fuel.” [Online]. Available: https://electric-fuel.com/. [Accessed: 09-Jun-2020].

[68] “Air Electrode – Electric Fuel.” [Online]. Available: https://electric-fuel.com/rd/zinc-air/air-electrode/#1447180412349-3562cb2c-6397508c-247ec9e5-1a86. [Accessed: 09-Jun-2020].

[69] COMSOL, “1D Isothermal Lithium-Air Battery.” [Online]. Available: https://www.comsol.com/model/1d-isothermal-lithium-air-battery-20023. [Accessed: 10-Jun-2020].

[70] COMSOL, “1D Isothermal Nickel-Metal Hydride Battery.” [Online]. Available: https://www.comsol.com/model/1d-isothermal-nickel-metal-hydride-battery-9435. [Accessed: 07-Jul-2020].

[71] COMSOL, "1D Isothermal Zinc-Silver Oxide Battery." [Online]. Available: https://www.comsol.com/model/1d-isothermal-zinc-silver-oxide-battery-17229. [Accessed: 16-Jun-2020].

12. Appendix

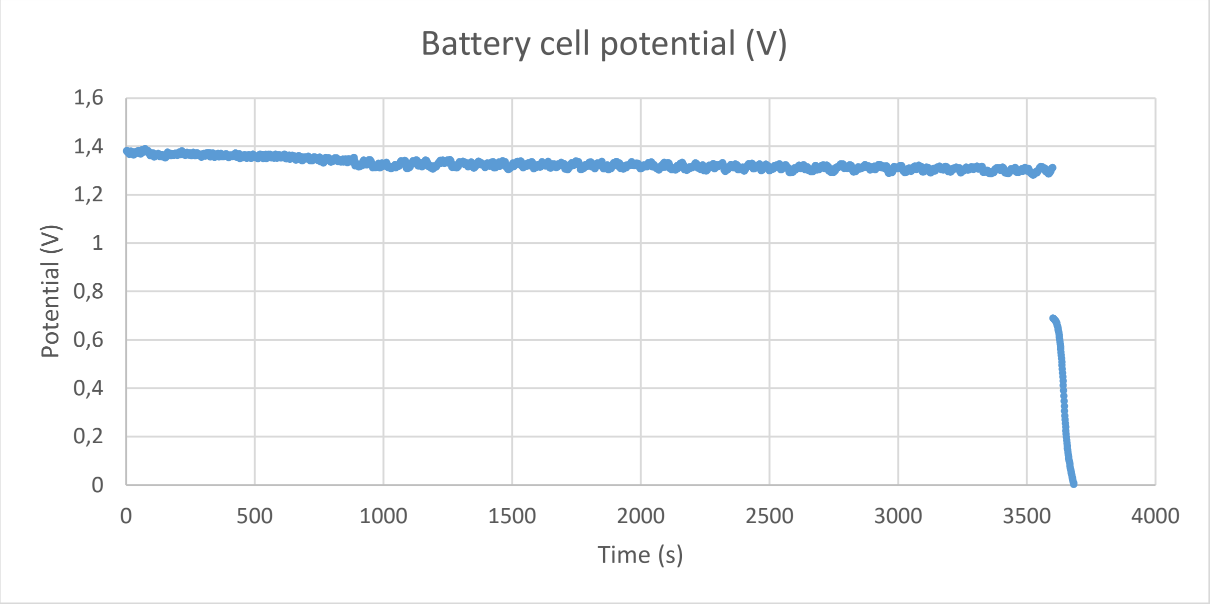

Appendix 1: Discharge curve of the silicon-air battery without pre-treatment of the air electrode. One hour of open circuit potential, followed by discharge at 150 µA/cm².

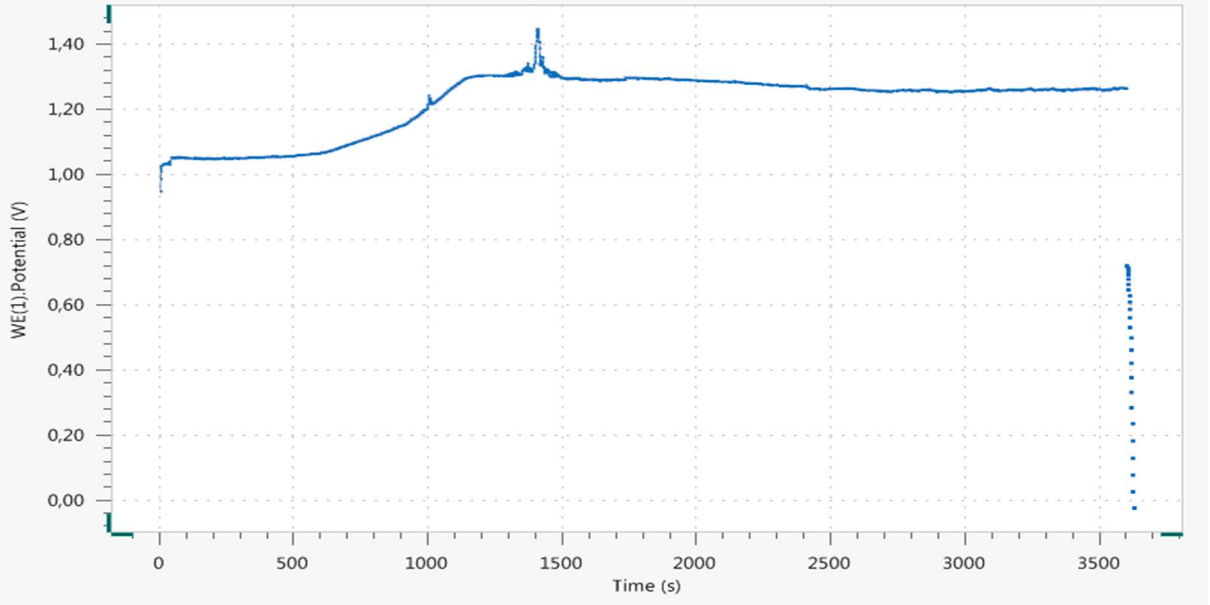

Appendix 2: Discharge curve of the silicon-air battery after one hour of pre-treatment of the air electrode. One hour of open circuit potential, followed by discharge at 150 µA/cm².

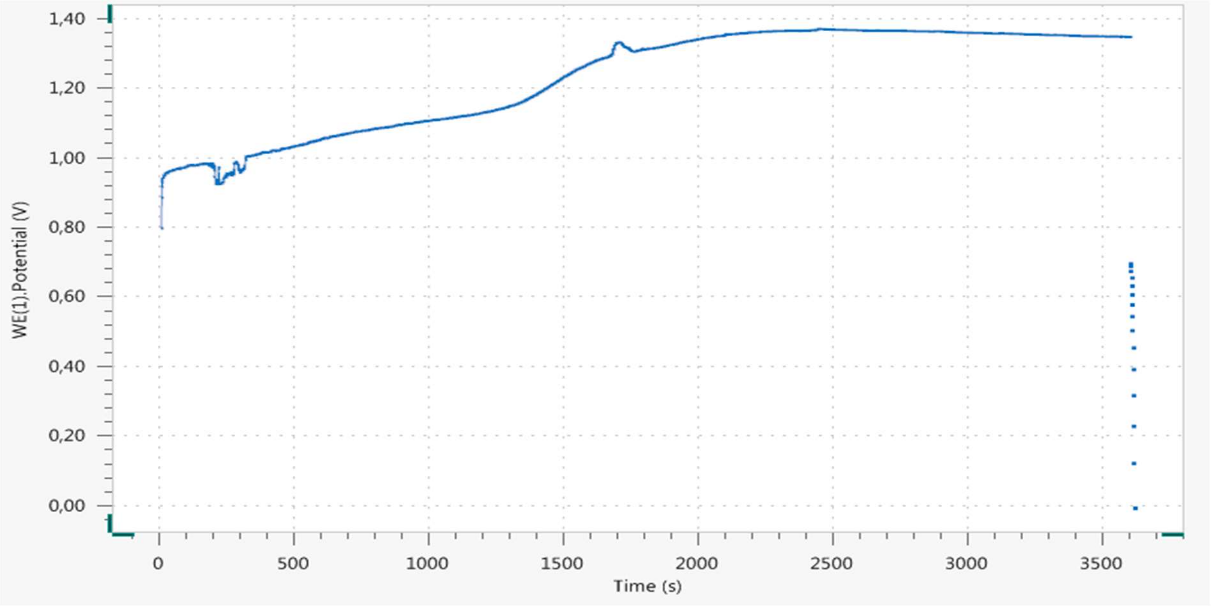

Appendix 3: Discharge curve of the silicon-air battery after two hours of pre-treatment of the air electrode. One hour of open circuit potential, followed by discharge at 150 µA/cm^2.

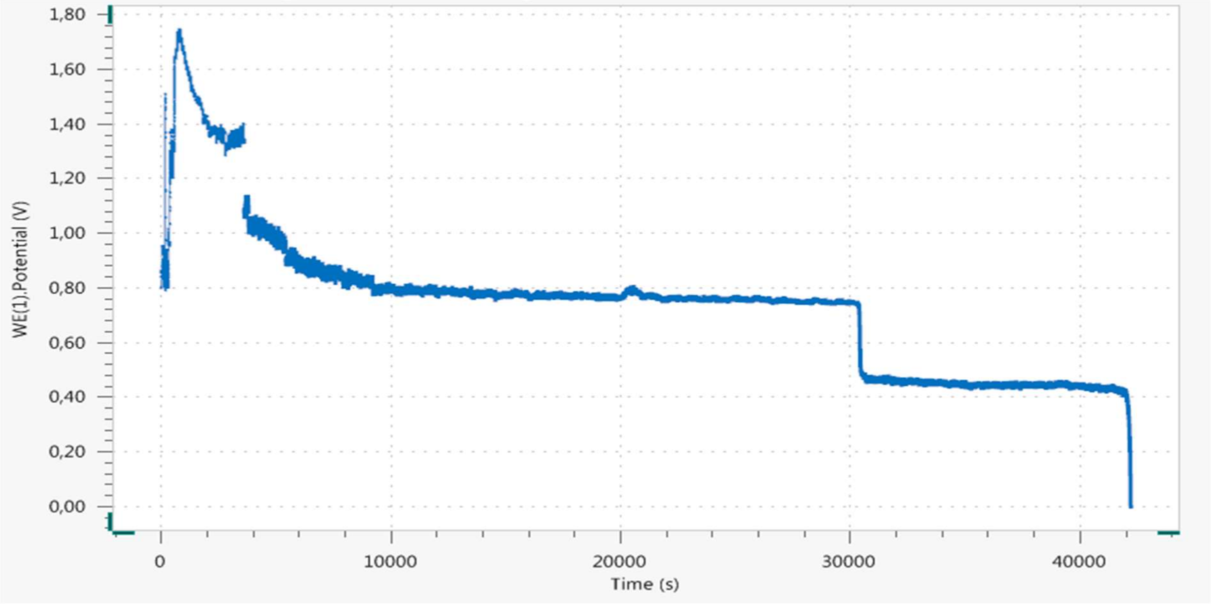

Appendix 4: Discharge curve of the silicon-air battery after three hours of pre-treatment of the air electrode. One hour of open circuit potential, followed by discharge at 150 µA/cm^2.

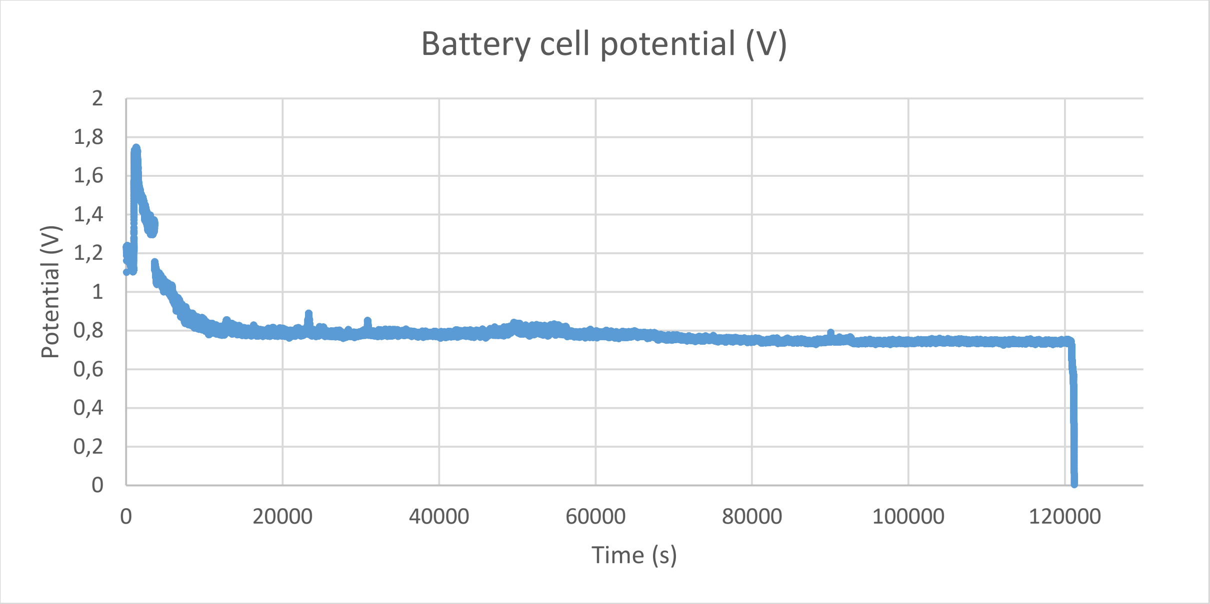

Appendix 5: Discharge curve of the silicon-air battery after four hours of pre-treatment of the air electrode. One hour of open circuit potential, followed by discharge at 150 µA/cm².

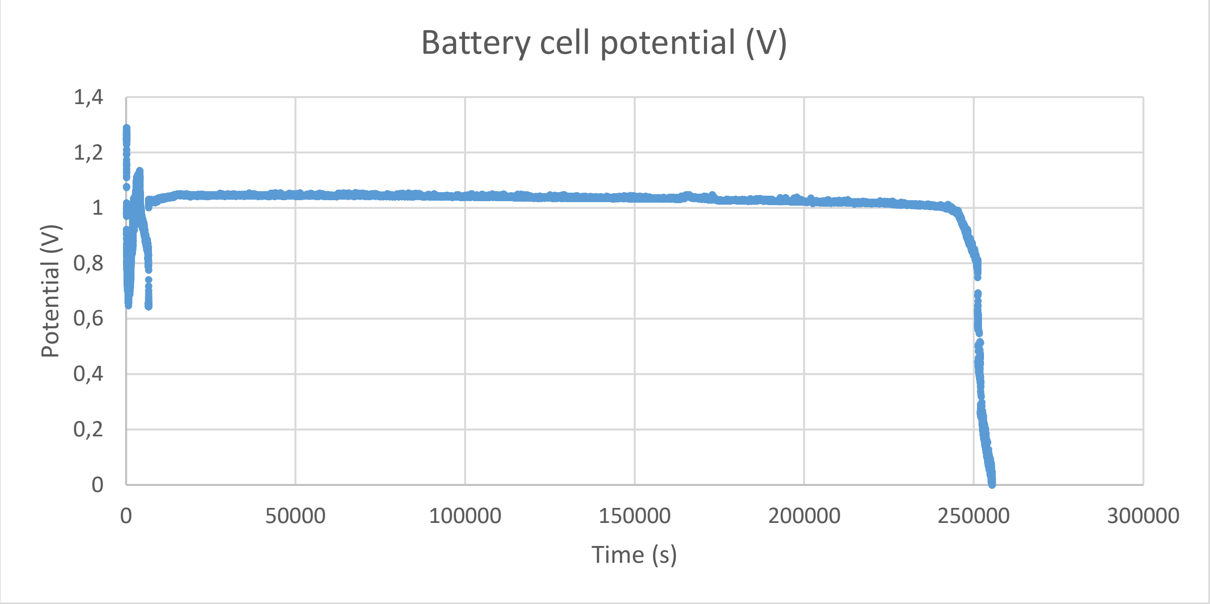

Appendix 6: Discharge curve of the silicon-air battery after eight hours of pre-treatment of the air electrode. One hour of open circuit potential, followed by discharge at 150 µA/cm².

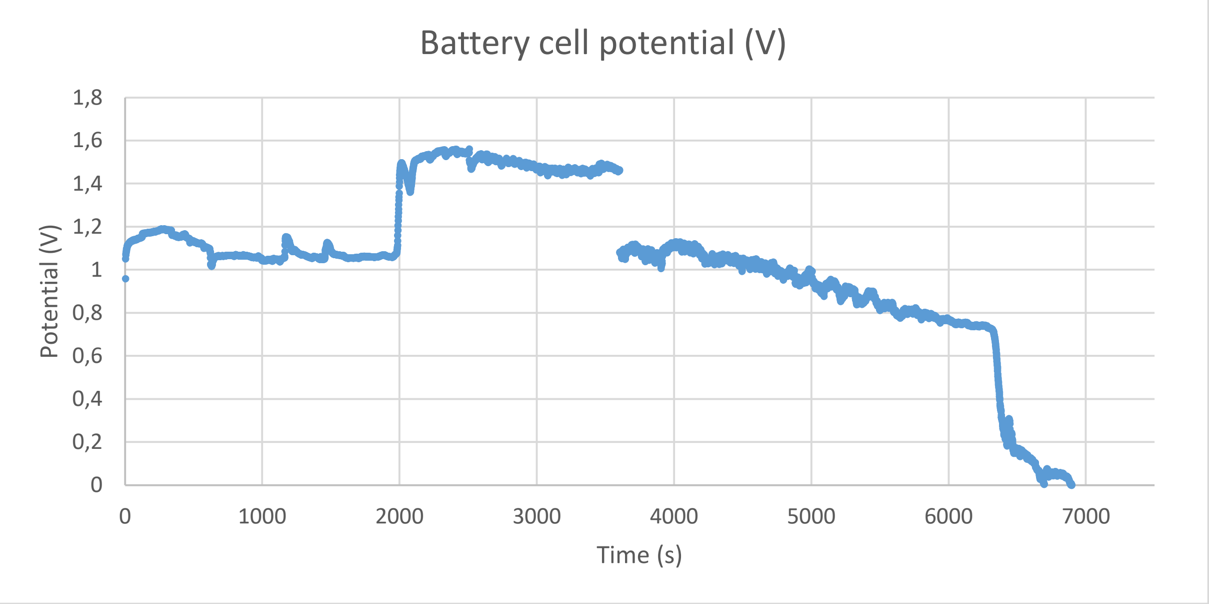

Appendix 7: Discharge curve of the silicon-air battery after sixteen hours of pre-treatment of the air electrode. One hour of open circuit potential, followed by discharge at 150 µA/cm²^2.

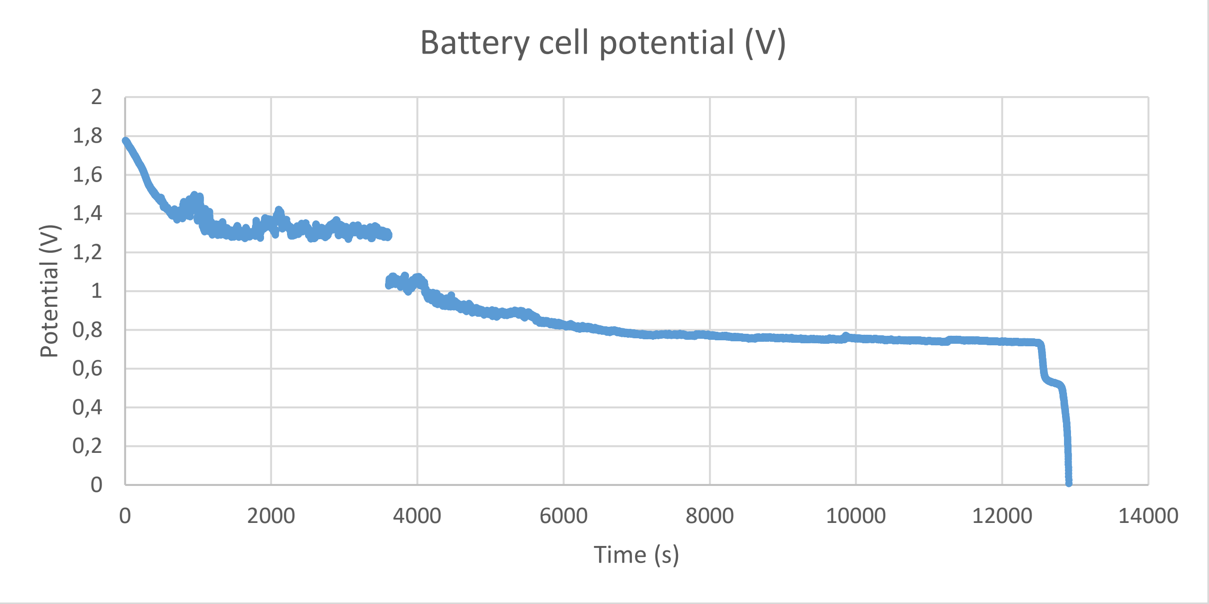

Appendix 8: Discharge curve of the silicon-air battery after 24 hours of pre-treatment of the air electrode. One hour of open circuit potential, followed by discharge at 150 µA/cm^2.

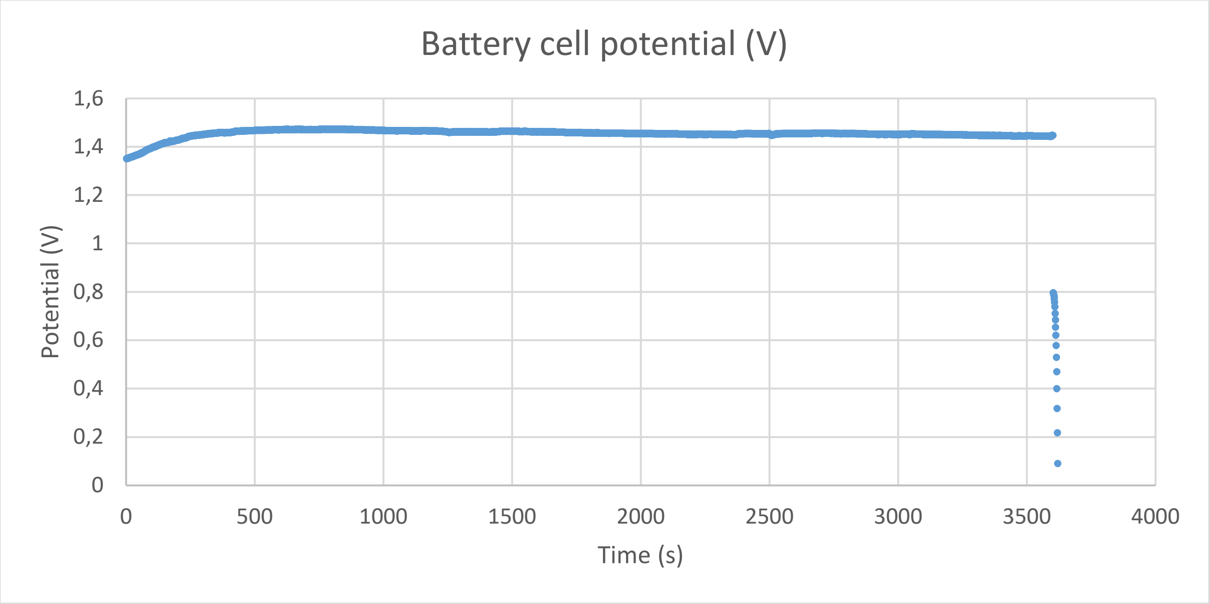

Appendix 9: Discharge curve of the silicon-air battery after 110.75 hours of pre-treatment of the air electrode. One hour of open circuit potential, followed by discharge at 150 µA/cm²^2***.***

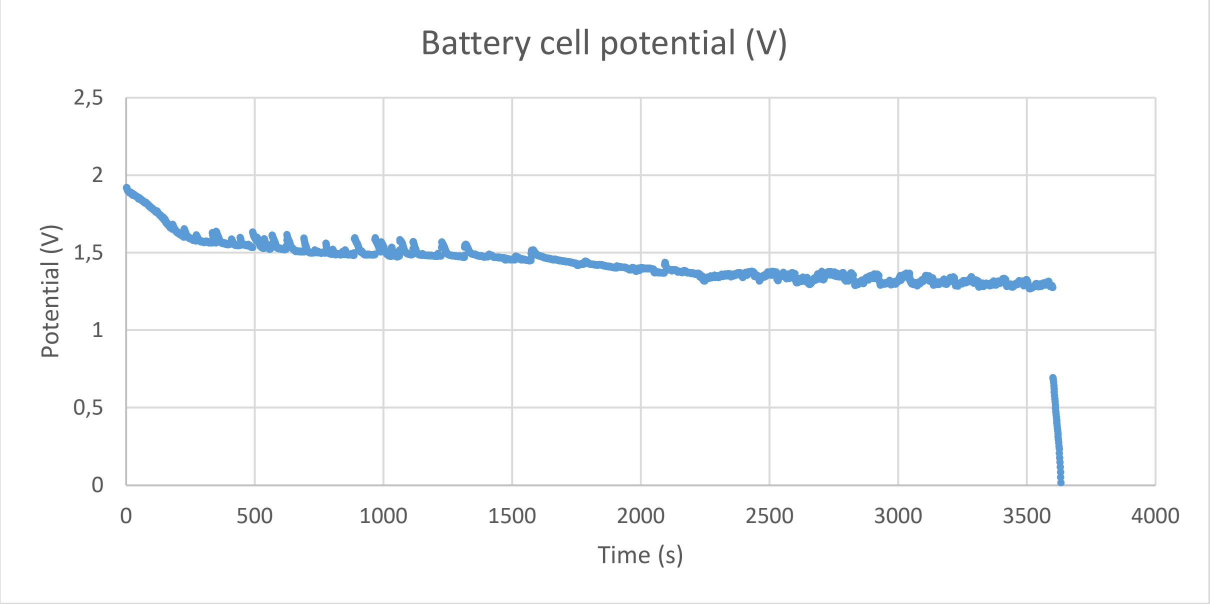

Appendix 10: Discharge curve of the silicon-air battery after four hours of pre-treatment of the air electrode in water. One hour of open circuit potential, followed by discharge at 150 µA/cm^2***.***

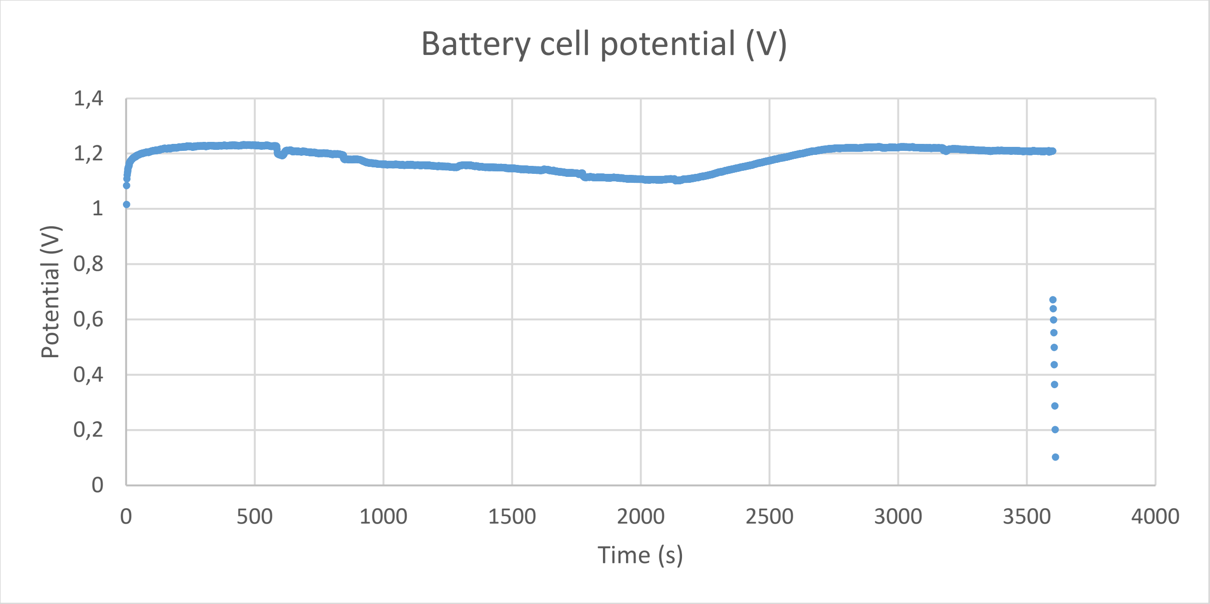

Appendix 11: Discharge curve of the silicon-air battery after four hours of pre-treatment of the air electrode. One hour of open circuit potential, followed by discharge at 250 µA/cm²^{2}.

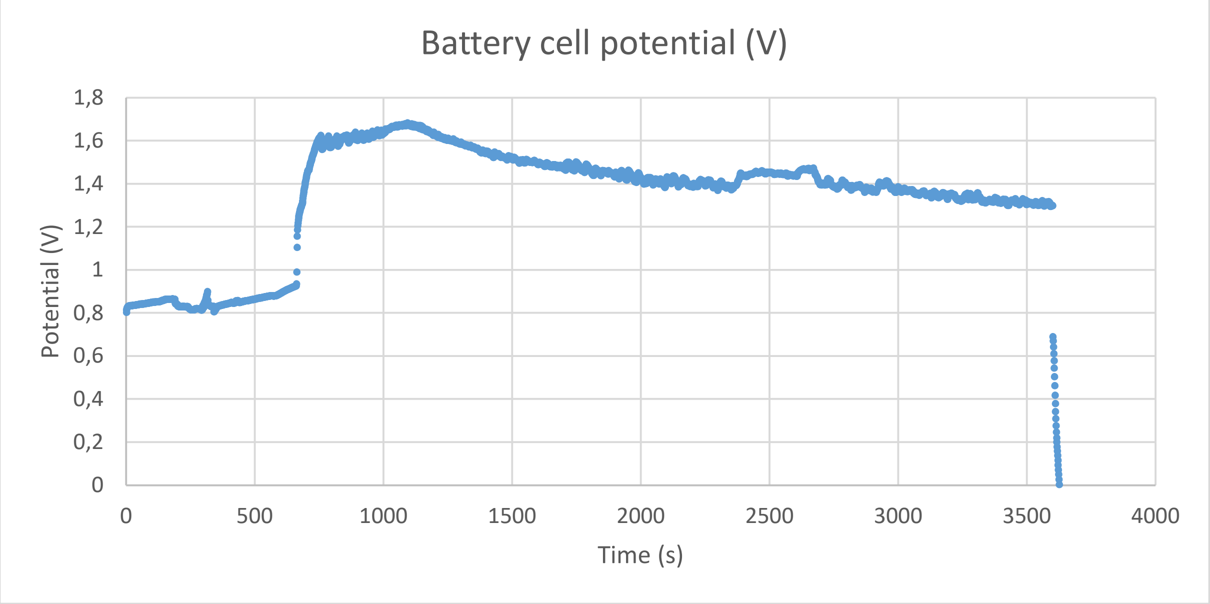

Appendix 12: Discharge curve of the silicon-air battery after four hours of pre-treatment of the air electrode. One hour of open circuit potential, followed by discharge at 325 µA/cm^{2}.

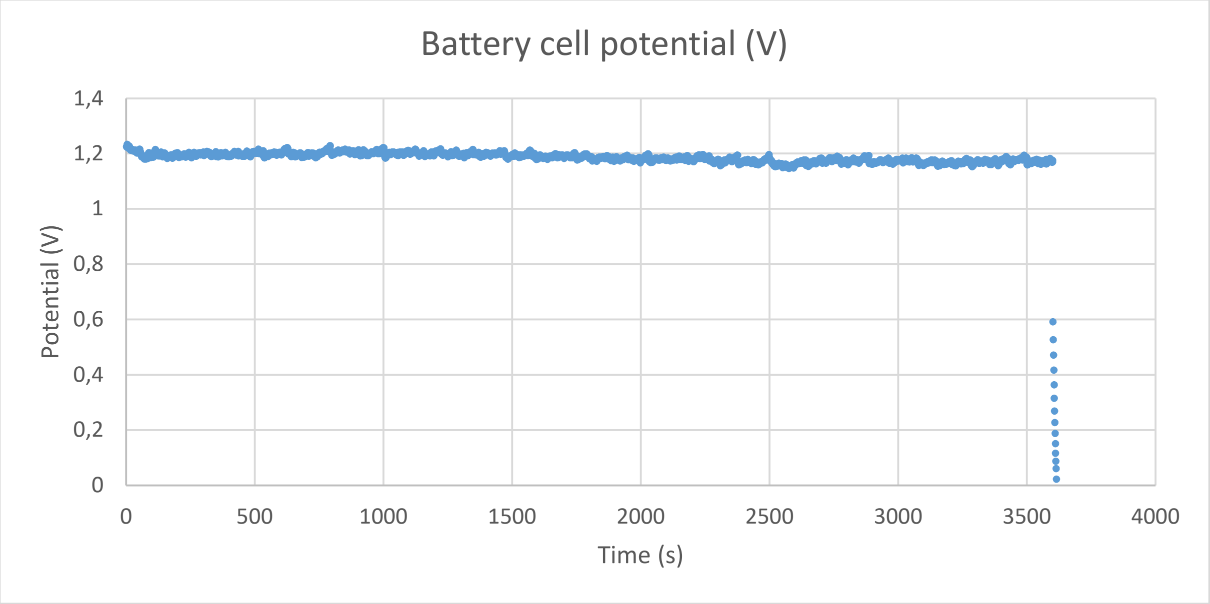

Appendix 13: Discharge curve of the silicon-air battery after four hours of pre-treatment of the air electrode. One hour of open circuit potential, followed by discharge at 500 µA/cm²^{2}.